Lii
881 10/6

Indian J. pure appl. Phys., Vol. 18 No. 5 pp. 307-382
May 1980
CODEN : IJOPAU ISSN : 0019-5596
18 (5) 307-382 (1980)

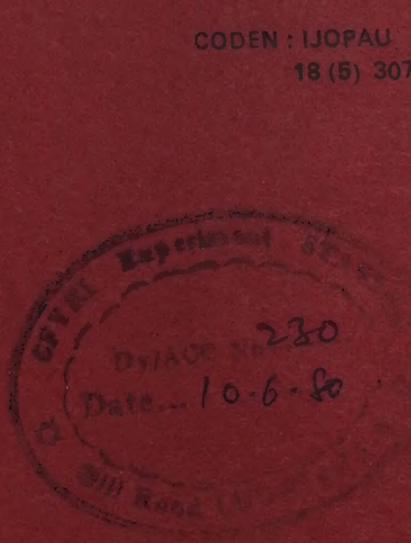

INDIAN JOURNAL OF PURE & APPLIED PHYSICS

Published by
PUBLICATIONS & INFORMATION DIRECTORATE, CSIR, NEW DELHI
in association with
THE INDIAN NATIONAL SCIENCE ACADEMY, NEW DELHI

Now here's a new slant on SEM automated analysis.

It's inside the SEM 501B.

Optimised X-ray geometry. A Philips "analytical +". What does it mean? We'll tell you.

In the wavelength-dispersive mode, you work with a full 35-degree take-off angle. You get optimum performance when analysing for the lighter elements. Full quantification is possible because the sample remains normal to the beam.

In the energy-dispersive mode, you can incline the spectrometer to either 16 or 26 degrees in a few minutes. This gives you the ability to look at both eucentric working positions with fully variable collection geometry.

The fact is, with the SEM 501B, you can optimise the geometry to suit the application. You use the same take-off angle for WDS and EDS at the same time, with the same beam current. And what does **this** mean?

It means you can use EDS with some elements. WDS with other elements. Use them in the one ZAF program. At the same time. Without waiting. Without wasting time. And you can have SEM with fully-automated WEDAX!

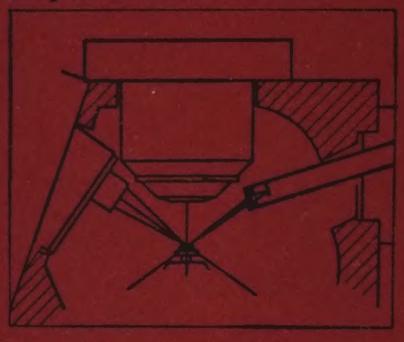

Optimised EDS/WDS geometry of the SEM 501 B.

For further details contact:
Peico Electronics & Electricals Limited
Product Division, Science & Industry
Shivsagar Estate, Block 'A'
Worli, Bombay 400 018

PHILIPS

Philips in Professional Electronics

PHILIPS

PE.SI.5463

Indian Journal of Pure & Applied Physics

VOLUME 18 No. 5 MAY 1980

EDITORIAL BOARD

Dr B A Dasannacharya
Bhabha Atomic Research Centre
Bombay

Prof. B M Deb
Indian Institute of Technology
Bombay

Prof. P Krishna
Banaras Hindu University
Varanasi

Prof. Krishnaji
Allahabad University
Allahabad

Prof. K V Ramanathan
Tata Institute of Fundamental Research
Bombay

Dr S Chandrasekhar
Indian National Science Academy
New Delhi/Raman Research
Institute Bangalore

Prof. A K Saha
Saha Institute of Nuclear Physics
Calcutta

Prof. N C Sil
Indian Association for
Cultivation of Science
Calcutta

Prof. R Srinivasan
Indian Institute of Science
Bangalore

Prof. K Venkataramiah
Osmania University
Hyderabad

Dr K L Chopra
Indian National Science Academy
New Delhi/Indian Institute of
Technology New Delhi

Shri Y R Chadha, *Ex-officio* Secretary & Chief Editor

EDITORIAL STAFF

Editors
D S Sastry & K S Rangarajan

Assistant Editors
G N Sarma, J B Dhawan & Tarun Banerjee

Published by the Publications & Information Directorate, CSIR, Hillside Road, New Delhi 110 012

Chief Editor : Y R Chadha

The Indian Journal of Pure & Applied Physics is issued monthly. The Directorate assumes no responsibility for the statements and opinions advanced by contributors. The editorial staff in its work of examining papers received for publication is assisted, in an honorary capacity, by a large number of distinguished scientists, working in various parts of India.

Communications regarding contributions for publication in the journal should be addressed to the Editor, Indian Journal of Pure & Applied Physics, Publications & Information Directorate, Hillside Road, New Delhi 110 012.

Correspondence regarding subscriptions and advertisements should be addressed to the Sales & Distribution Officer, Publications & Information Directorate, New Delhi 110 012.

Annual Subscription	**Single Copy**
Rs. 100.00 £ 16.50 $ 42.00	Rs. 10.00 £ 1.80 $ 4.50

50% Discount is admissible to research workers and students and 25 % discount to non-research individuals, on annual subscription. Payments in respect of subscriptions and advertisements may be sent by cheque, bank draft, money order or postal order marked payable *only* to **Publications & Information Directorate, New Delhi 110 012.** Claims for missing numbers of the journal will be allowed only if received within 3 months of the date of issue of the journal plus the time normally required for postal delivery of the journal and the claim.

© 1980 The Council of Scientific & Industrial Research, New Delhi.

CSIR SCIENTIFIC PERIODICALS

JOURNAL OF SCIENTIFIC & INDUSTRIAL RESEARCH (monthly)

With a fine record of over 35 years' service to the scientific community, this Journal has grown into India's leading general science periodical. Intended to fulfil the responsibility of helping the research workers to keep themselves abreast of current developments in various fields of science and technology, the Journal carries editorial features highlighting important scientific events in India and abroad; articles on science policy and management of science; review articles on topics of current research interest; technical reports on international and national conferences; reviews of scientific and technical publications; and notes on major advances in various fields.

Annual subscription	**Rs 60.00**	**£ 10.00**	**$ 25.00**
Single copy	**6.00**	**1.00**	**2.50**

INDIAN JOURNAL OF CHEMISTRY (monthly)

This Journal which is running the 18th year of its publication, Consists of the following two sections.

Section A : This section is devoted to papers in Inorganic, Physical, Theoretical and Analytical Chemistry.

Annual subscription	**Rs 70.00**	**£ 12.00**	**$ 30.00**
Single copy	**7.00**	**1.20**	**3.00**

Section B : This section is devoted to papers in Organic Chemistry including Medicinal Chemistry.

Annual subscription	**Rs 70.00**	**£ 12.00**	**$ 30.00**
Single copy	**7.00**	**1.20**	**3.00**

INDIAN JOURNAL OF PURE & APPLIED PHYSICS (monthly)

This Journal, which is running the 18th year of its publication, is devoted to original research communications (full papers and short communications) in all conventional branches of physics (except radio and space physics).

Annual subscription	**Rs 100.00**	**£ 16.50**	**$ 42.00**
Single copy	**10.00**	**1.80**	**4.50**

INDIAN JOURNAL OF RADIO & SPACE PHYSICS (bimonthly)

This Journal serves as a medium for the publication of original rearch work (full papers and communications) in various areas of radio and space physics.

Annual subscription	**Rs 60.00**	**£ 10.00**	**$ 25.00**
Single copy	**12.00**	**2.00**	**5.00**

INDIAN JOURNAL OF TECHNOLOGY (INCLUDING ENGINEERING) (monthly)

This Journal publishes papers reporting results of original research of applied nature pertaining to unit operations, heat and mass transfer, products, processes, instruments, and appliances, etc. The Journal is of special interest to research workers in the departments of applied sciences in universities, institutes of higher technology, commodity research laboratories, industrial cooperative research institutes, and industrial research laboratories.

Annual subscription	**Rs 60.00**	**£ 10.00**	**$ 25.00**
Single copy	**6.00**	**1.00**	**2.50**

INDIAN JOURNAL OF EXPERIMENTAL BIOLOGY (monthly)

This Journal, devoted to the publication of research communications in the fields of experimental botany, zoology, microbiology, pharmacology, endocrinology, nutrition, etc., is the only one in India with such a wide coverage and scope.

Annual subscription	**Rs 120.00**	**£ 20.00**	**$ 50.00**
Single copy	**12.00**	**2.00**	**5.00**

INDIAN JOURNAL OF BIOCHEMISTRY & BIOPHYSICS (bimonthly)

This Journal, published in association with the Society of Biological Chemists (India), Bangalore, is the only research Journal in India devoted exclusively to original research communications in biochemistry and biophysics.

Annual subscription	**Rs 40.00**	**£ 7.00**	**$ 17.00**
Single copy	**8.00**	**1.40**	**3.50**

INDIAN JOURNAL OF MARINE SCIENCES (quarterly)

Commencing publication from June 1972, this Journal is devoted to research communications (full papers and short communications) pertaining to various facets of marine research, viz. biological, physical, geological and chemical oceanography.

Annual subscription	**Rs 40.00**	**£ 7.00**	**$ 17.00**
Single copy	**12.00**	**2.00**	**5.00**

RESEARCH & INDUSTRY (quarterly)

Intended to serve as a link between science and industry, this Journal is addressed primarily to technologists, engineers, executives and others in industry and trade. It publishes informative original articles containing practical details of processes and products developed in India, which show promise of ready utilization, and technical digests on new processes, products, instruments and testing methods which are of interest to industry. Developments in Indian industry are regularly reported.

Annual subscription	**Rs 24.00**	**£ 4.00**	**$ 10.00**
Single copy	**7.25**	**1.30**	**3.50**

INDIAN JOURNAL OF TEXTILE RESEARCH (quarterly)

Commencing publication from March 1976, this Journal is devoted to the publication of papers reporting results of fundamental and applied researches in the field of textiles.

Annual subscription	**Rs 36.00**	**£ 6.00**	**$ 15.00**
Single copy	**12.00**	**2.00**	**5.00**

Please contact

THE SALES & DISTRIBUTION OFFICER
PUBLICATIONS & INFORMATION DIRECTORATE, CSIR
HILLSIDE ROAD, NEW DELHI 110 012

Indian Journal of Pure & Applied Physics

VOLUME 18 No. 5 MAY 1980

CONTENTS

Solid State Physics

The Plastic Deformation of Copper-Beryllium Alloy 307
AFAF A GADALLA

Variation of Electrical Conductivity of Ferric Hydroxide Films with Temperature ... 311
NIRMALA PAUL, M G KRISHA PILLAI & K BABU JOSEPH

Analysis of Crystal Binding Energies of Alkali Halides 314
JAI SHANKER, V C JAIN & L P SHARMA

Electrical Conductivity & Dielectric Constant of Semiconducting Glasses : As-Ge-Te & Se-Ge-Te Alloy Systems 318
A KUMAR, K N LAKSHMINARAYAN & K K SRIVASTAVA

Chemical Physics

Calculation of Multiplet Splittings of $A^2\Pi$ States of Some Diatomic Alkaline-earth Halides by Extended Hückel Approach 324
D P NANDA & B S MOHANTY

Semi-Empirical Π-Electron Calculations on Some Mono Substituted Acetophenones 327
DEVINDER GUPTA & R M P JAISWAL

Π^*—Π Systems in the Quartz Ultraviolet Electronic Absorption Spectra of Some Di-& Trisubstituted Acetophenones 332
DEVINDER GUPTA & R M P JAISWAL

Resonance Phenomena

EPR Studies on N, N′-Ethylenebis (Salicylaldiminato) Copper (II)-Thiourea & N, N′-*o*-Phenylenebis (Salicylaldiminato) Copper (II)-Thiourea 337
B A SASTRY, S MD ASADULLAH, ANITA DEB & C PELIZZI

Lasers, Masers & Holography

Dispersion Effects in the FM Mode-Locked Laser 342
K P JAGANNATHA REDDY

Optics

Effect of Field & Detector Temperatures on Photon Count Statistics 348
J P DUDEJA

Instrumentation

Sensor Design for an Electromagnetic Flow-Meter 351
S E DESA & E DESA

Electronics

Injection Synchronization in the Face of Heavy Interference 354
S K RAY, (Miss) K PRAMANIK & S KARMAKAR

CONTENTS

NOTES

Crystal Field Stabilization Energies of Second-row Transition-Metal Oxides & Halides 360

LAMBODAR THAKUR & B B SANDWAR

Relation between Microhardness & Atomic Vibration Frequency in Alkali Halides ... 362

B SUBRAMANIAM

Application of Hagemark's Theory to Multicomponent Systems ZnTe : Li, O & Na-implanted CdS 363

P D EKBOTE & J K ZOPE

Variation of Hardness with Load for Quenched KBr Single Crystals 365

R S CHAURE & R N SHRIVASTAVA

Electrochemically Deposited Schottky Contacts On *n*-Epitaxial Silicon 368

B K SINGH, R N MITRA & A N DAW

Electrical Properties of Vacuum-evaporated PbS-PbO Films 369

R KUMAR, S K AGARWAL & V C SETHI

Rotational Analysis of the (2, 0) Band of $^{13}C^{16}O^{+}$ Molecule of Commet-tail System 370

B R VUJISIC, D S PESIC, S WENIGER & D RAKOTORIJIMY

Influence of Vibration Rotation Interaction On Franck-Condon Factors 372

R TRIPATHI & S B RAI

Dielectric Dispersion in Certain Binary Mixtures & Solutions 374

B S RAJYAM, C V RAMA SASTRY & C R K MURTY

Annealing Effects on dc Current Gain (β) of Silicon Planar Transistors 377

S C SOOD, K L JASUJA & A VENKATARAMANI

Spectral Studies of Some Uranyl Complexes 379

V K RASTOGI, A N PANDEY, S L GUPTA & R C SAXENA

Papers Accepted for Publication 382

Indian Journal of Pure & Applied Physics
Vol. 18, May 1980, pp. 307-310

The Plastic Deformation of Copper-Beryllium Alloy

AFAF A GADALLA
Physics Department, Faculty of Science, Assiut University, Assiut, Egypt

Received 16 *September* 1978; *revised received* 26 *March* 1979

Copper-2 at. % Be alloy specimens containing coherent and/or incoherent spherical beryllium precipitates have been tested at different temperatures. The precipitation process and dislocation substructure were examined by electron microscopy. The yielding process is consistent with Orwan mechanism, and the work-hardening of the alloy is parabolic in nature for smaller particles but changes to three-stage hardening for larger particles. The extent of stage I deformation is temperature dependent, and the rate of work-hardening is quite steep and may be described by either the Ashby or the Hirsch parabolic models. There is a noticeable softening during this stage which may be attributed to shearing of particles during deformation. The dislocation substructure shows a uniform distribution of fine dislocations as well as propagation of cracks across grains. The precipitates are a mixture of semi-coherent and incoherent particles.

1. Introduction

Several investigations have been undertaken on the mechanism of precipitation in Cu-Be alloys.[1-4] Second-phase precipitates in a metallic matrix act as a barrier to the movement of dislocations, forcing them to behave in one of two ways: either to cut through the particles or to take a circuitous path around the obstacles. Since the precipitates are non-deformable, the yield stress is controlled by the Orwan mechanism, and the work-hardening rate is interpreted by the interaction of primary dislocations and geometrically necessary dislocations. The geometrically necessary dislocations as defined by Ashby,[5] are those formed at the non-deforming particle interfaces by cross slip, secondary slip and prismatic punching to accommodate the different deformations of the particle and matrix.

Recently, some investigations have been made on the mechanism of precipitation hardening in Cu-Be alloys by transmission electron microscopy. On the basis of these results the mechanism of precipitation is considered to follow a sequence flat zone→γ′b.s. tetragonal coherent precipitates or Gp zones→ equilibrim γ phase. Gp zones were found by X-ray diffraction in Cu-Be alloy aged at 200°C for 1/2 hr (Ref. 1).

The main purpose of the present work is to study the work hardening of the Cu-2 at. % beryllium alloy and to understand the mechanism of precipitation by transmission electron microscopy.

2. Experimental Procedure

The copper-2 at. % beryllium alloys were prepared by melting and casting in high vacuum from 99·98 % copper and 99·8% beryllium. The ingot was homogenized at 800°C for 4hr, then fast-quenched in water. The precipitation treatment was done under argon for various times ranging from 30 min to 2 days in the temperature range 120-350°C. The samples were later machined into tensile specimens of 20 mm gauge length either by spark erosion or by electrochemical thinning; in all cases the last treatment was electrochemical polishing down to 3mm diameter in a mixture of 500 ml phosphoric acid, 500 ml of glycerine and 125 ml of water. Tensile tests were carried out using a hydraulic fatigue testing machine at 100-300 K and a strain rate in the range 2×10^{-4} - 5×10^{-4} sec^{-1}. Samples for electron microscopy were prepared by a modified Window method.[6] The polishing voltage was 6 V at −30°C and the electrolyte used was as mentioned above. The thin foil samples were examined in an electron microscope operated at 100 kV.

3. Results and Discussion

3.1 Effect of Ageing

Fig. 1(a) shows a transmission electron micrograph of Cu-Be alloy homogenized at 800°C and quenched in water. This micrograph shows a very low dislocation density and lack of precipitates in grain and at grain boundaries.

In Cu-Be binary alloy, coherent particles were visible due to diffraction contrast effects associated with the strain field around the particle. Incoherent particles were also visible due to absorption and orientation contrast difference relative to the matrix. The particles were seen to be nearly spherical in shape. Some of the precipitates were relatively

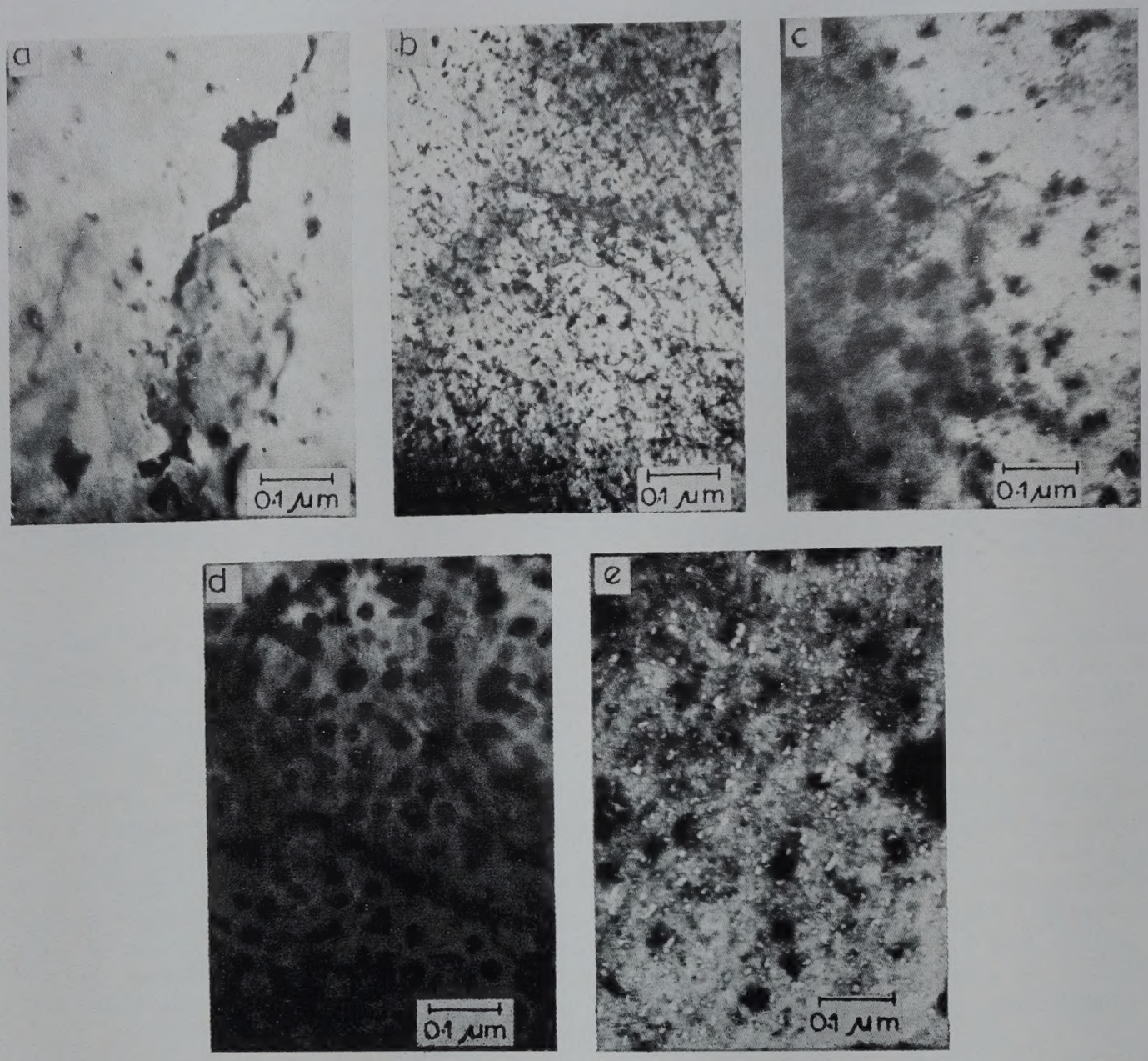

Fig. 1—Effect of ageing time at 200°C on transmission electron micrographs after different ageing treatments [(a) no ageing, homogenized at 800°C and quenched in water ; single phase structure, (b) ageing for 1 hr, resolvable coherent spherical particles, (c) ageing for 3 hr, particles are till mostly coherent, and the foil planes are (112), (d) ageing for 10 hr, incoherent particles start to form at longer annealing times and (e) ageing for 20 hr, showing elongated incoherent particles (these particles which showed no strain-field contrast were considered incoherent)]

etched away during thinning, leaving white holes. The nature of these particles has been discussed in detail earlier by Hermi.[7] The sizes were determined from the particles visible in the electron micrographs while their volume fraction was obtained from equilibrium phase diagram.[8] The particle radius R was estimated from the following equation[9]:

$$R=(3\ t\ f_v\ /\ 4\ \pi\ N_a)^{1/3}$$

where t is the foil thickness, N_a the number of particles per unit area and f_v the volume fraction.

Ageing up to 3 hr at 200°C gives particles still mostly coherent [Fig. 1 (c)]. Incoherent particles start to form at longer annealing times [Fig. 1 (d)]. The micrographs show no further evidence for coherency after 20 hr treatment at 200°C [Fig. 1 (e)]. It is to be noted that in the present work those particles which showed no strain field contrast were considered incoherent. Based on the present observations, Livingston's idea[10] that overageing is principally due to the spontaneous loss of coherency when particles reach the critical diameter appears to be invalid.

3.2 Fine Striations and Dislocation Twins

Fig. 2 (a) shows that fine striations were formed in the grain of Cu-2 at. % Be alloy aged at 300°C

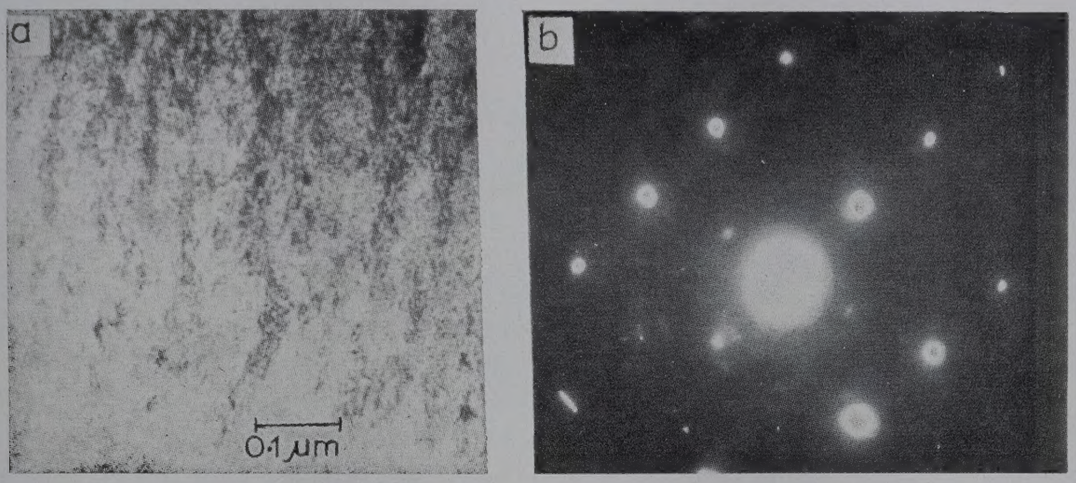

Fig. 2 – (a) Fine striations formed in the grain of Cu-2 at. % Be alloy, aged at 300°C for 30 min; (b) the electron diffraction pattern showing maximum density points of γ' phase. The plane of the foil is $\langle 211 \rangle$

for 30 min and Fig. 2(b) shows the maximum density points. Murakami and his coworkers[11] explained that these maximum density points were caused by the intermediate phase γ'. Since the G p zone and the γ' phase which were caused by ageing had a large strain, the strain of dislocations was cancelled out by that of the intermediate phase.

Figs. 3(a) and (b) show deformation twins indicating that Cu-Be alloy is a low stacking-fault-energy alloy. Due to the low stacking-fault-energy in Cu-Be alloy,[12] dislocation in the deformed specimen did not form the cell structure, but formed a structure similar to a Ag [Ref. 13] and Cu-Zn alloy (Ref. 14). In the specimens, cracks were initiated and propagated along grain boundaries [Fig. 4], but with the general direction of crack propagation coinciding with the plane perpendicular to the direction of the applied stress.

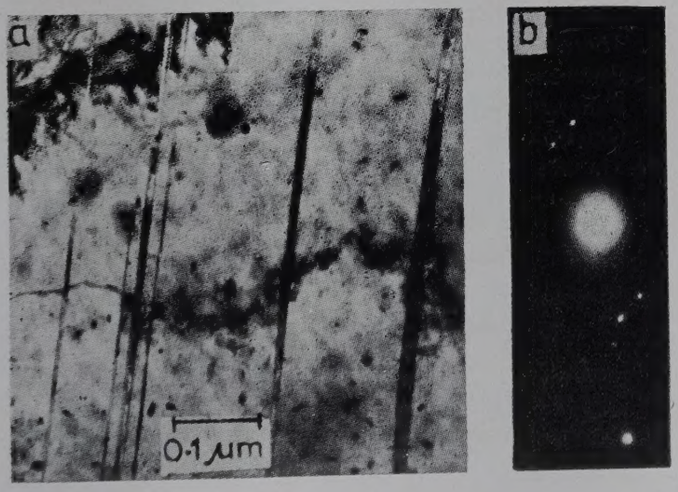

Fig. 3—(a) Deformation twins indicating that Cu-Be alloy is a low-stacking fault energy.
(b) Electron diffraction pattern showing the deformation twins.

Fig. 4—Photomicrograph showing plastic deformation in narrow slip zone which is associated with propagation of cracks.

3.3 Tensile Shear Stress-Shear Strain Curves

Fig. 5 shows some characteristic stress-strain curves for particle sizes from 80 to 350 Å radius. All experimental curves show a temperature dependent first stage of quasiparabolic work-hardening which extends up to about 70% shear strain. At particle sizes, about 160Å this stage is less steep and is followed by a second stage and the stress-strain curve becomes similar to that of a single phase crystal. Negligible serrations have been observed immediately following yielding for specimens aged for periods less then 16 hr at 573 K, and in most cases the serrations did not go beyond 1-2% shear

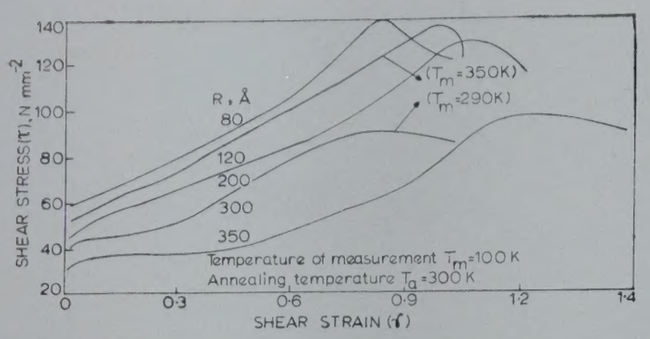

Fig. 5—Representative stress-strain curves for Cu-Be alloy.

strain. The smaller particles are more easily sheared during deformation.

3.4 Work-hardening and Parabolic Range

It is generally agreed that strain-hardening in alloys with non-sheared particles is a consequence of the formation of Orwan or Hirsch loops at dispersed particles. The high concentration of stress around the particles tends to induce relaxation processes. Ashby[5] in his secondary slip theory assumed that the geometrically necessary dislocations formed by these processes control the work-hardening of the specimen. They contribute to work-hardening in two ways: individually by acting as obstacles to slip and collectively by creating a long range back-stress with the wavelength equal to the particle spacing. His derivation gives the flow-stress as:

$$\tau - \tau_0 = c'u\,(b\,f\,\gamma/R)^{1/2}$$

where $(\tau - \tau_0)$ is the increase in the flow stress with strain γ, c' a constant with a value of 0·14 to 0·29, μ the shear modulus, b the Burger's vector and R and f are the precipitate radius and volume fraction respectively. This equation is almost independent of the details of dislocation model adopted. The precise mechanism by which scondary dislocations abstract primary ones is defined only by the constant c'. Representative data from the present experiments if plotted as $(\tau - \tau_0/\mu)$ versus $(b\,f\,\gamma/R)^{1/2}$ give a straight line with a slope between 0·05 and 0·1. These slopes are well below those observed experimentally for $Cu\text{-}Al_2O_3$ [Ref. 15] ($c' = 0{\cdot}17$).

4. Conclusion

The shape of the stress-strain curves varies systematically with temperature and the particle size. For small particles, the shape is parabolic with only slight indication of a second work-hardening stage before fracture. The experimental data of the parabolic stress-strain stage can be fitted to either the Ashby or the Hirsch equations for parabolic work-hardening due to undeformable particles. However, the lower work-hardening rates observed and the electron microscopic studies suggest that the particles are sheared. This shearing process may occur by the initially formed Orwan rings being pushed through the particles by the stress fields of the following dislocations.

Acknowledgement

This work was supported by a generous grant from Max-Planck Institut fur Metallkunde, Stuttgart, West Germany, to whom the author is greatly indebted.

References

1. Guy A S, Bareft S S & Mehl R F, *Trans. AIME*, **175** (1948),216.
2. Geisler A H, Hallery J N & Steigest F M, *J. Metals*, **4** (1952), 307.
3. Tyapkin Yu D, *Soviet Phys. Crystallogr.*, **10** (1966), 418.
4. Thomas H E, *Metallk.*, **52** (1961), 750; **56** (1966), 31.
5. Ashby R F, *Phil. Mag.*, **21** (1970), 399.
6. Nagashima S & Matsue Y, *Metal Phys.*, **6** (1960), 161.
7. Henmi Z & Nagai T, *Trans. JIM*, **10** (1939), 166.
8. Hansen M, *Constitution of binary alloys*, (McGraw-Hill, New York, Toronto, London), 1958, 470.
9. Hilliard J E, *Trans. Met. Soc. AIME*, (1948), 224.
10. Livingstone S D, *Trans. Met. Soc. AIME*, (1959), 566.
11. Murakami Y & Kawano T, Paper submitted to the Conference at Tokyo University, 4 April 1968.
12. Thomas G, *Electron microscopy and strength of crystals* (Interscience, New York), 1963, 793.
13. Bailey J E, *Electron microscopy and strength of crystals* (Interscience, New York) 1963, 535.
14. Thomas G J, *Aust. Inst. Metals*, **8** (1963), 80.
15. Shelling R & Ashby M F, *Phil. Mag.*, **13** (1966), 805.

Indian Journal of Pure & Applied Physics
Vol. 18, May 1980, pp. 311-313

Variation of Electrical Conductivity of Ferric Hydroxide Films with Temperature

Nirmala Paul, M G Krishna Pillai & K Babu Joseph
Department of Physics, Cochin University, Cochin 682 022

Received 14 *May* 1979; *revised received* 25 *September* 1979

Semiconducting thin films of $Fe(OH)_3$ have been successfully grown by a chemical deposition method. Structural, stoichiometric and electrical studies are carried out. An attempt has been made to explain the variation of conductivity with temperature in terms of the predominance of intrinsic conduction and impurity conduction in different temperature regions.

1. Introduction

Compound thin films are of great interest on account of their semiconducting and insulating properties. The chemical deposition method is one way of preparing these films. However, the non-availability of the exact chemical reaction restricts to a large extent this type of film deposition. Recently compound thin films of CdS, ZnO, etc. have been prepared by the interfacial chemical reaction of a solution and a gas.[1] In the present study, a similar method is used to prepare ferric hydroxide thin films by a chemical reaction involving ferrous sulphate solution and ammonia gas. The electrical properties of these films are discussed taking into consideration their dependence on factors such as thickness, temperature and possible chemical change.

2. Experimental Details

2.1 Preparation of Films

The experimental set-up used for preparing these films is similar to the one employed by Sathye and Sinha.[1] The ferrous sulphate and ammonia used are of BDH AnalaR grade. When the dish containing 1% ferrous sulphate solution with a glass slide dipped in it is kept in the ammonia atmosphere for about 1-3 min, a thin uniform layer of ferrous hydroxide having a light green colour is formed at the surface of the ferrous sulphate solution. The enclosure is removed, and the glass plate is lifted carefully to protect the film from cracking. The glass substrate is dipped in distilled water to get the soluble impurities dissolved. It is taken out, dried and kept in a desiccator.

The thickness of the film produced will depend upon the exposure of ferrous sulphate solution to the ammonia atmosphere. When the ferrous hydroxide film is taken out of the ammonia atmosphere it absorbs oxygen with great avidity and turns into yellowish brown ferric hydroxide by atmospheric contact.

In this method of film preparation, it is noted that due to the formation of a precipitate in the ferrous sulphate solution, on longer exposure to the ammonia atmosphere the thickness of the film cannot be increased beyond a limit. Also in the case of thick films there is a tendency for them to peel off from the substrate. To get good films free from these defects proper care is taken to see that the environment and substrate are clean and the exposure time is small. It is also noted that large concentrations of ammonia do not give any film because the OH^- ion concentration cannot, in these circumstances, rise above a very low value.[2]

2.2 Nature of film

The film prepared is found to be uniform throughout. Colorimetric tests show that the specimen lacks the correct percentage of Fe^{3+}, possibly because of the presence of Fe^{2+} in it. So it cannot be an ionic conductor. Even though $Fe(OH)_3$ is usually considered crystalline, the X-ray diffraction study carried out by us reveals an amorphous structure for the film (Fig. 1).

2.3 Resistance Measurement

The electrical resistance of the film is measured by means of a million megohmmeter. The electrical contacts are given by copper blocks used as electrodes. The film is heated to the desired temperature by external heaters and the temperature is noted by a chromel-alumel thermocouple. The

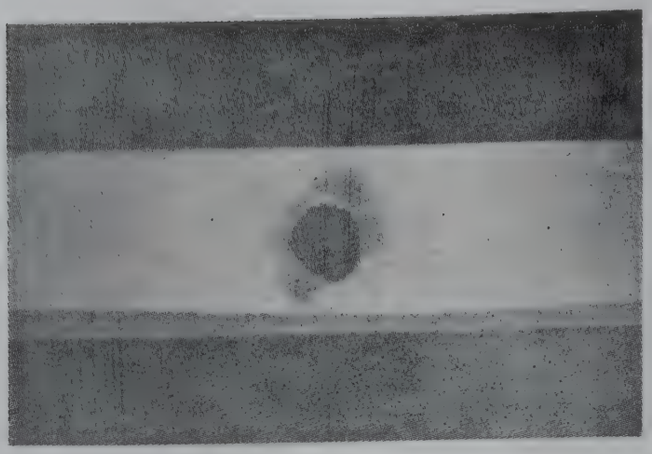

Fig. 1—X-ray photograph of $Fe(OH)_3$ film

whole system is kept in a copper box which acts as a shield to eliminate external effects of resistance measurement. The variation of resistance with temperature of the film is measured up to 473 K in three heating-cooling cycles, starting from room temperature, in all cases, keeping air as the ambient atmosphere. Above 473 K, the specimen starts to decompose into ferric-oxide and this region is not studied.

The thickness of the film is determined by the interference fringe method.

3. Results and Discussion

The variation of resistance with temperature of the film is as shown in Fig. 2. For films having a wide range of thicknesses (180-1200 Å) the shape of the curve is found to be the same The temperature dependence of conductivity is studied in two regions. The increase in resistance is pronounced in the first heating up to about 363-373 K. This may be regarded as a moisture effect,[3] because as the film is heated, moisture is gradually removed and the resistance increases. However, the resistance begins to decrease when a considerable portion of moisture has been removed In the cooling course as well as in all subsequent heating-cooling cycles, the resistance monotonically increases up to 308-313 K. In this region, impurities may be the controlling factor determining the conductivity. Also non-stoichiometry of the film[4,5] may be another factor. The second region extends from 313-473 K where heating and cooling curves are almost linear, especially in the case of very thin films. Conduction in this region is apparently dominated by intrinsic defects. At high temperatures, a certain number of ions will get released from their normal positions and will be free to cause an increase in conductivity.[6,7] Since the heating is done in ambient air, the specimen chemisorbs oxygen, which gets ionized and the electrons

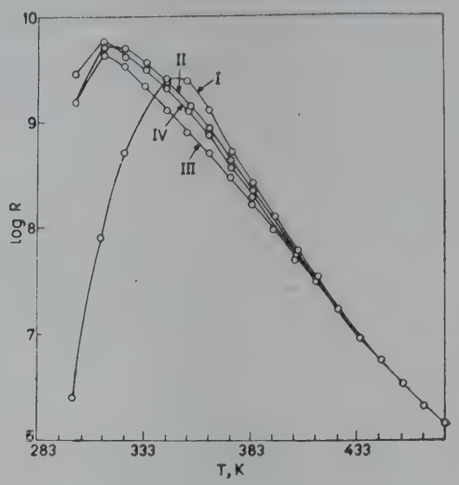

Fig. 2—Plot of log R versus temperature of $Fe(OH)_3$ films [I. First heating; II. cooling; III. Second heating; IV. cooling]

thus liberated tend to enhance the conductivity. During the cooling process the recombination may be assumed to dominate over ionization resulting in a decrease in conductivity up to the point where impurity conduction starts.

The log resistivity (ρ) versus $\frac{1}{T \times 10^{-4}}$ plot shown in Fig. 3 consists of two distinct branches each of which is approximately linear. The activation energy ΔE is calculated for each region assuming the formula

$$\rho = \rho_0 \exp \frac{-\Delta E}{k T}$$

The absolute value of ΔE in the impurity conduction region is 0·27 eV as against the value 0·36 eV in

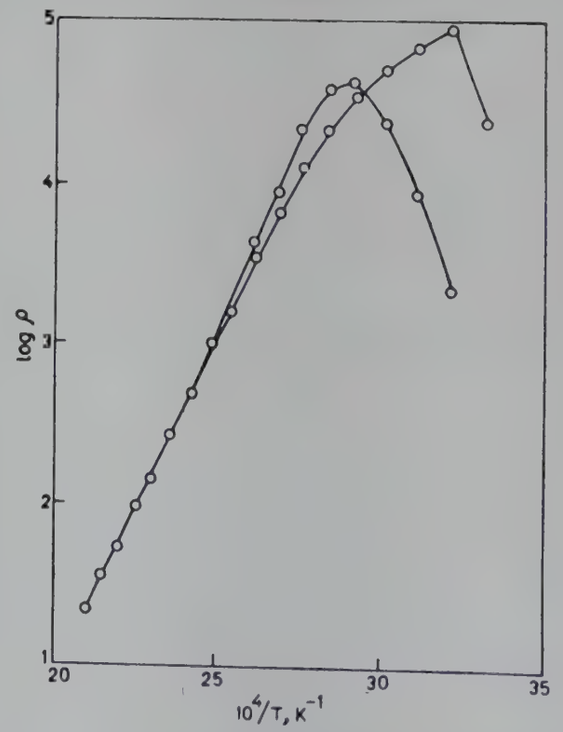

Fig. 3—Plot of log ρ versus $\frac{1}{(T \times 10^{-4})}$ of $Fe(OH)_3$ film

the region of intrinsic conduction. The low activation energy in the region of impurity conduction indicates a higher probability of the carriers hopping to a more distant centre.[8] A graph plotted between log thickness (t) and activation energy (ΔE) of the film indicated that the activation energy decreases with increase of film thickness. This may be due to the possibility of impurity charge carriers giving rise to various energy levels in the band gap and various defects which are not removed by heating as pointed out by Goswami *et al.*, in their study of MnTe film.[9]

4. Conclusion

The $Fe(OH)_3$ film produced by the chemical deposition method is amorphous and non-stoichiometric. The plot showing the variation of conductivity with temperature of the film consists of two linear branches which join at a point below which the conduction is mainly of the impurity type and above which the conduction is intrinsic.

Acknowledgement

We thank Prof. Joy George for the cooperation he extended in carrying out this investigation. One of us (NP) is grateful to the University Grants Commission, New Delhi, for the award of a junior research fellowship.

References

1. Sathye S D & Sinha A P B, *Thin Solid Films*, 37 (1976), 15.
2. Remy H, *Treatise on Inorganic Chemistry*, Vol. 2 (Elsevier, Amsterdam) 1956, 272.
3. Tareev B, *Physics of dielectric materials* (Mir, Moscow) 1975, 61.
4. Goyal D R, Pnawar O S, Srivastava K K, Lakshminarayan K N, Ashok Kumar & Ravikar D R, *Indian J. pure appl. Phys.*, 15 (1977), 10.
5. Tager A, *Physical chemistry of polymers* (Mir, Moscow) 1972, 303.
6. George Hass, Maurice H, Francombe & Richard W Hoffman, *Physics of thin films*, Vol. 9 (Academic Press, New York), 1977, 10.
7. Gupta C L, *Indian J. pure appl. Phys.*, 15 (1977), 684.
8. Mott N F & Davis E A, *Electronic process in non-crystalline materials* (Clarendon Press, Oxford) 1971, 41.
9. Goswami A & Mandale A B, *Japan J. appl. Phys.*, 17 (1978), 473.

Indian Journal of Pure & Applied Physics
Vol. 18, May 1980, pp. 314-317

Analysis of Crystal Binding Energies of Alkali Halides

JAI SHANKER, V C JAIN* & L P SHARMA
Physics Department, Agra College, Agra 282 002

Received 28 *August* 1978; *accepted* 3 *December* 1979

An analysis of the binding energies of alkali halides is performed using an extended version of the Born model. We consider the long-range electrostatic interactions, short-range attractive forces arising from the van der Waals interactions, and short-range overlap repulsive interactions between nearest neighbours and next nearest neighbours. The binding energies of 20 alkali halides with NaCl and CsCl structures have been obtained considering the various interaction terms. The binding energies thus estimated are found to be in close agreement with the experimental values derived from thermodynamic data.

1. Introduction

Recently, Ladd[1] has derived the experimental values of crystal binding energies for alkali halides using more recent thermodynamic and thermochemical data. These values differ from the earlier values of binding energies quoted by Tosi,[2] being larger by about 10 kcal/mole. This leads to the prediction that the simple Born model becomes less suitable for evaluating the cohesive or binding energies of ionic solids. In the simple Born model, one considers that the point-like ions are held together by long-range electrostatic forces and short-range overlap repulsive forces acting between nearest neighbours only. This model can be improved by including (i) short-range repulsive interactions between next nearest neighbours and (ii) short-range attractive potentials arising from the van der Waals dipole-dipole and dipole-quadrupole interactions. It was shown by Ladd[1] that the agreement with recent data on crystal energies for alkali halides can be achieved if the van der Waals potentials are derived from the static polarizabilities instead of electronic polarizabilities. Since the static polarizabilities correspond to low frequency dielectric constant, these are substantially larger than the electronic polarizabilities derived from the high frequency dielectric constant. As a result, the van der Waals potentials calculated by Ladd turned out to be much larger than those estimated by Mayer.[3] It has been emphasized recently by Catlow *et al.*[4] and Shanker *et al.*[5] that the van der Waals potentials are derived from the electronic polarizabilities of ions and have no concern with static polarizabilities. The analysis performed by Ladd is, therefore, unjustified.

It will be shown in the present study that the agreement between theory and recent experimental values of cohesive energies for alkali halides can be obtained even if we use the van der Waals potentials derived from electronic polarizabilities and hence there is no necessity of using incorrect polarizabilities taken by Ladd. Recently, Narayan[6] has pointed out the utility of the Slater-Kirkwood variational method[7] and its superiority over the London-Margenau perturbation treatment[8,9] for evaluating the van der Waals dipole-dipole and dipole-quadrupole interaction energies. There is, however, a numerical error in the calculations performed by Narayan[6] which has been rectified, and calculations are revised[5] using the new data on electronic polarizabilities of ions.[10] The van der Waals potentials thus obtained are used in the present study to evaluate the cohesive energies of alkali halides. The short-range repulsive interactions operative between next nearest neighbours are also considered. We use the Born-Mayer-Huggins-type exponential law and Pauling's inverse power law for representing the repulsive energy.[11] Values of the repulsive hardness parameter taken are those derived from the overlap integrals computed by Hafemeister and coworkers.[12,13] In earlier studies[2] this parameter was derived empirically by a fit of crystal data on compressibility.

2. Method of Calculation

The crystal lattice energy of an ionic crystal as a function of interionic separation r in a generalized form can be expressed as

$$W = -\frac{\delta e^2}{r} - \frac{C}{r^6} - \frac{D}{r^8} + M\phi_{+-} + \frac{1}{2} M'(\phi_{++} + \phi_{--}) \quad \ldots(1)$$

*Permanent address: P D College, Shikohabad (U P)

where the first term on the right is the Madelung energy (δ is the Madelung constant) arising from the electrostatic interactions between point-like ions. The second and third terms represent, respectively, the van der Waals dipole-dipole and dipole-quadrupole interaction energies. The fourth and fifth terms are the short range overlap repulsive interactions between nearest neighbours and second nearest neighbours.

The van der Waals constants C and D appearing in Eq. (1) are related to the dipole-dipole coefficients (c_{ij}) and dipole-quadrupole coefficients (d_{ij}) through the equations:

$$C = S_{+-}\, c_{+-} + S_{++}\, c_{++} + S_{--}\, c_{--} \qquad ...(2)$$

$$D = T_{+-}\, d_{+-} + T_{++}\, d_{++} + T_{--}\, d_{--} \qquad ...(3)$$

where the constants S and T are the appropriate lattice sums;[2,3] c_{+-}, c_{++} and c_{--} are the dipole-dipole coefficients associated witht he cation-anion, cation-cation and anion-anion interactions. Similarly, d_{+-}, d_{++} and d_{--} are the dipole-quadrupole coefficients. The perturbation treatment of London[8] and Margenau[9] yielded the following formulae for these coefficients

$$c_{ij} = \frac{3}{2}\, \alpha_i\, \alpha_j \frac{E_i\, E_j}{E_i + E_j} \qquad ...(4)$$

and

$$d_{ij} = \frac{9}{4}\, \frac{c_{ij}}{e^2} \left(\frac{\alpha_i\, E_i}{N_i} + \frac{\alpha_j\, E_j}{N_j} \right) \qquad ...(5)$$

where α, E and N are, respectively, the electronic polarizability, the excitation energy parameter and effective number of electrons for the ions i and j. Values of c_{ij} and d_{ij} in alkali halides have been evaluated by several workers.[1,3,14-16] The values estimated by one worker differ largely from those obtained by the other. This is because of the great uncertainties in the values of E_i and E_j. A critical survey of values of E_i and E_j used by various investigators has been presented recently[5] which demonstrates the large variation of these parameters from one investigation to the other. It has been emphasized[6] that the uncertainty in evaluating the van der Waals coefficients c_{ij} and d_{ij} arising from the uncertainty in E_i and E_j can be eliminated if one makes use of the Slater-Kirkwood variational method[7] in place London-Margenau perturbation method.[8,9] The former method yields the following relations[6]

$$c_{ij} = \frac{3}{2}\, \frac{e\hbar}{m^{1/2}}\, \frac{\alpha_i\, \alpha_j}{\left[\left(\frac{\alpha_i}{N_i} \right)^{1/2} + \left(\frac{\alpha_j}{N_j} \right)^{1/2} \right]} \qquad ...(6)$$

$$d_{ij} = \frac{27}{8}\, \frac{\hbar^2}{m}\, \frac{\alpha_i\, \alpha_j \left[\left(\frac{\alpha_i}{N_i} \right)^{1/2} + \left(\frac{\alpha_j}{N_j} \right)^{1/2} \right]^2}{\left[\left(\frac{\alpha_i}{N_i} \right) + \frac{20}{3} \left(\frac{\alpha_i\, \alpha_j}{N_i\, N_j} \right)^{1/2} + \left(\frac{\alpha_i}{N_j} \right) \right]} \qquad (7)$$

where m is electron mass and h is the Planck's constant. It should be noted that Eqs. (6) and (7) do not involve the excitation energy parameters and hence are free from the uncertainties in the values of E_i and E_j. Eqs. (6) and (7) are used by Narayan[6] to evaluate c_{ij} and d_{ij}. However, his calculations suffer from a numerical error which has been rectified.[5] The correct values of c_{ij} and d_{ij} given in Ref. 5 are used in the present study to estimate the magnitudes of van der Waals dipole-dipole and dipole-quadrupole interaction energies.

For representing the repulsive interactions we adopt the inverse power as well as the exponential forms. Following Pauling's inverse power form,[11] we can express the various repulsive interactions given in Eq. (1) as follows

$$\phi_{+-} = b\, \beta_{+-}\, \frac{(r_+ + r_-)^{n-1}}{r^n} \qquad ...(8)$$

$$\phi_{++} = b\, \beta_{++}\, \frac{(2\, r_+)^{n-1}}{r'^n} \qquad ...(9)$$

and

$$\phi_{--} = b\, \beta_{--}\, \frac{(2\, r_-)^{n-1}}{r'^n} \qquad ...(10)$$

If one uses the Born-Mayer-Huggins type exponential form[11] then

$$\phi_{+-} = b' \beta_{+-} \exp\, (r_+ + r_- - r)/\rho \qquad ...(11)$$

$$\phi_{++} = b\, \beta_{++} \exp\, (2\, r_+ - r')/\rho \qquad ...(12)$$

and

$$\phi_{--} = b' \beta_{--} \exp\, (2\, r_- - r')/\rho \qquad ...(13)$$

where b (or b') and n (or ρ) are repulsive parameters; r_+ and r_- are the radii of cation and anion; r and r' are the nearest and next nearest neighbour distances, respectively. β_{ij} are the coefficients introduced by Pauling[17] in order to provide appropriate weightage for various pair interactions.

Values of the repulsive hardness parameter ρ can be derived by making use of the fact that short range repulsive energy arises from the overlap of ions. One can write for the repulsive energy[12,13]

$$W_R = B \exp\, (-r/\rho) = \frac{2\gamma e^2}{r} \sum_{ij} S_{ij}^2 \qquad ...(14)$$

Table 1—Crystal Binding Energies (in kcal/mole) of Alkali Halides

Crystal	Calculated			Experimental (Ref. 1)
	Simple Born model[2]	Present study		
		Inverse power form	Exponential form	
LiF	−242·2	−247·6	−255·0	−246·7
LiCl	−192·9	−198·7	−205·0	−203·2
LiBr	−181·0	−186·7	−194·4	−194·2
LiI	−166·1	−173·0	−181·5	−180·3
NaF	−215·2	−221·0	−226·5	−219·5
NaCl	−178·6	−184·9	−189·8	−187·1
NaBr	−169·2	−175·2	−180·5	−178·5
NaI	−156·6	−163·3	−169·0	−167·0
KF	−189·1	−194·3	−199·8	−194·3
KCl	−161·6	−170·3	−172·4	−170·2
KBr	−154·5	−161·7	−165·7	−163·2
KI	−144·5	−152·3	−156·4	−153·6
RbF	−180·4	−185·0	−190·7	−185·8
RbCl	−155·4	−161·8	−165·7	−163·6
RbBr	−148·3	−155·6	−159·4	−157·2
RbI	−139·6	−145·4	−148·8	−148·5
CsF	−171·2	−175·6	−182·4	−177·0
CsCl	−146·6	−154·2	−158·6	−159·8
CsBr	−141·1	−149·4	−154·0	−154·1
CsI	−132·7	−140·8	−145·2	−146·1

where γ is a dimensionless constant and e the electron charge. $S_{ij} = \int U_i(1)\, U_j(2)\, d\tau_1$ is the overlap integral. The summation of the squares of the orerlap integrals are expressed as

$$\sum_{ij} S_{ij}^2 = 2S^2(ns_{\mathrm{H}}, n's_{\mathrm{M}}) + 2S^2(np_{\mathrm{H}\sigma}, n's_{\mathrm{M}}) + 2S^2(ns_{\mathrm{H}}, n'p_{\mathrm{M}\sigma}) + 2S^2(np_{\mathrm{H}\sigma}, n'p_{\mathrm{M}\sigma}) + 4S^2(np_{\mathrm{H}\pi}, n'p_{\mathrm{M}\pi}) + 2S^2(ns_{\mathrm{H}}, n's_{\mathrm{H}}) + 2S^2(ns_{\mathrm{H}}, n'p_{\mathrm{H}\sigma}) + 2S^2(np_{\mathrm{H}\sigma}, n's_{\mathrm{H}}) + 2S^2(np_{\mathrm{H}\sigma}, n'p_{\mathrm{H}\sigma}) + 4S^2(np_{\mathrm{H}\pi}, n'p_{\mathrm{H}\pi}) + 2S^2(ns_{\mathrm{M}}, n's_{\mathrm{M}}) + 2S^2(ns_{\mathrm{M}}, n'p_{\mathrm{M}\sigma}) + 2S^2(np_{\mathrm{M}\sigma}, n's_{\mathrm{M}}) + 2S^2(np_{\mathrm{M}\sigma}, n'p_{\mathrm{M}\sigma}) + 4S^2(np_{\mathrm{M}\pi}, n'p_{\mathrm{M}\pi}) \quad \ldots(15)$$

where M refers to alkali-metal ion and H refers to the halogen ion. Values of various overlap integrals appearing in Eq. (15) have been obtained by Hafemeister and Flygare.[12] Following Eqs. (14) and (15), Hafemeister and Zahrt[13] have derived the values of ρ for alkali halides. Values of n, the hardness parameter appearing in the inverse power form can be calculated from the relation[2]

$$n = \frac{r}{\rho} - 1 \quad \ldots(16)$$

We have taken r_+ and r_- from Sysio.[18] Since these radii are based on the electron density measurements, they are considered to be model-independent as suggested by Simpson.[19] For evaluating the strength parameter appearing the repulsive potentials, we use the crystal equilibrium condition.

3. Results and Discussion

Values of the crystal binding energies for 20 alkali halides are calculated following the method described above. In Table 1, the calculated binding energies are compared with the experimental values. It is observed that the binding energies obtained from the inverse power form and the exponential form are in close agreement with experimental values. For the sake of comparison we have also included in Table 1 the binding energies calculated from the simple Born model,[2] i.e. without considering the van der Waals and next nearest neighbour interactions. The importance of these interactions is evident from Table 1 from which we see that the binding energies calculated from the simple Born model are substantially lower in magnitude than the experimental values. On the other hand, the binding energies calculated in the present study, by considering the dipole-dipole, dipole-quadrupole and short range next nearest neighbour repulsive interactions, are in good agreement with experiment. It should be emphasized that our calculations of repulsive potentials are based on the values of overlap integrals. The repulsive hardness parameters derived from overlap integrals have been found to present good agreement with compressibility data.[12,13]

References

1. Ladd M F C, *J. chem. Phys.*, 60 (1974), 1954.
2. Tosi M P, *Solid St. Phys.*, 16 (1964), 1.
3. Mayer J E, *J. chem. Phys.*, 1 (1933), 270.
4. Catlow C R A, Diller K M & Norgett M J, *J. Phys.*, C10 (1977), 1395.
5. Shanker J, Agrawal G G & Singh R P, *J. chem. Phys.*, 69 (1978), 670.
6. Narayan R, *J. Phys. Chem. Solids*, 38 (1977), 1097.
7. Slater J C & Kirkwood J G, *Phys. Rev.*, 37 (1931), 682.

8. London F, *Z. phys. Chem.*, **B11** (1930), 222.
9. Margenau H, *Rev. mod. Phys.*, **11** (1939), 1.
10. Jaswal S S & Sharma T P, *J. Phys. Chem. Solids*, **34** (1973), 509.
11. Fumi F G & Tosi M P, *J. Phys. Chem. Solids*, **25** (1964), 31, 45.
12. Hafemeister D W & Flygare W H, *J. chem. Phys.*, **43** (1965), 795.
13. Hafemeister D W & Zahrt J, *J. chem. Phys.*, 47 (1967), 1428.
14. Hajj F, *J. chem. Phys.*, **44** (1966), 4618.
15. Lynch D W, *J. Phys. Chem. Solids*, 28 (1967), 1941.
16. Jain J K, Shanker J & Khandelwal D P, *Phys. Rev.*, **B13** (1976), 2692.
17. Pauling L, *Z. Krist.*, **67** (1928), 377.
18. Sysio P A, *Acta crystallogr.*, **B25** (1969), 2374.
19. Simpson J H, *Can. J. Phys.*, **50** (1972), 729.

Indian Journal of Pure & Applied Physics
Vol. 18, May 1980, pp. 318-323

Electrical Conductivity & Dielectric Constant of Semiconducting Glasses : As-Ge-Te & Se-Ge-Te Alloy Systems

A Kumar, K N Lakshminarayan & K K Srivastava
Department of Physics, Panjab University, Chandigarh 160 014

Received 16 *April* 1979; *revised received* 24 *August* 1979

A critical analysis of the existing theories of ac conduction in chalcogenide glasses has been made. Measurements of conductivity and dielectric constant have been made for various alloys of As-Ge-Te and Se-Ge-Te alloy systems at different temperatures (83 to 383 K) and various frequencies (dc and 0·3 to 5·0 MHz). At low temperatures, the ac conductivity of all the alloys is found to be temperature independent and proportional to ω^s with $s = 0{\cdot}8$. The conductivity and dielectric behaviour of these glasses have been explained on the basis of the 'dangling bond' theory of NF Mott *et al.* [*Phil. Mag.*, 32 (1975), 961]. The measurements also suggest that, near Fermi level, the density of states is higher in the case of Se-Ge-Te alloys.

1. Introduction

The conductivity of semiconducting glasses is known to be frequency dependent which, as expected, is due to conduction in localized states. Measurement of ac conductivity, therefore, is a powerful experimental method to obtain information about the existence and location of these states. Such measurements on chalcogenide glasses have been reported by many workers.[1-7] ω^s dependence of ac conductivity $\sigma(\omega)$ with $s \leqslant 1$ is found to be a general characteristic for these glasses up to the frequencies $\sim 10^6$ Hz. However, there is an apparent controversy over the nature of the temperature dependence of $\sigma(\omega)$. Some workers[1-4] have reported a temperature-dependent ac conductivity, whereas others[5-7] have observed temperature-independent behaviour of $\sigma(\omega)$ even at frequencies as low as 1 kHz. Various theories have been put forward to explain the observed behaviour of $\sigma(\omega)$ in these materials. This paper offers a critical analysis of these theories on the basis of experimental results, obtained for two different kinds of glassy alloy-systems; one having memory switching (As-Ge-Te alloys) and the other threshold switching (Se-Ge-Te alloys). Four alloys of As-Ge-Te ($As_5Ge_{10}Te_{85}$, $As_{15}Ge_{10}Te_{75}$, $As_{25}Ge_{10}Te_{65}$, $As_5Ge_{15}Te_{80}$) and two alloys of Se-Ge-Te ($Se_{20}Ge_{20}T_{60}$, $Se_{25}Ge_{20}Te_{55}$) have been prepared and their conductivities (ac and dc) and dielectric constants have been measured in the temperature range 83-383 K. Field dependence of dc conductivity has also been studied for these glasses. The results have been interpreted in terms of Mott's theory of dangling bonds which seems to explain the experimental results better than the other existing theories.

2. Experimental Details

Preparation of alloys—All the alloys of As-Ge-Te and Se-Ge-Te were prepared by rapid cooling of the melt in liquid nitrogen. The glassy state was verified by X-ray photographs. DTA results, obtained for these alloys, were consistent with those reported in the literature. All the four alloys of As-Ge-Te displayed memory switching in contrast to Se-Ge-Te alloys which showed threshold switching at room temperature for the bulk samples.

Preparation of samples—Bulk samples, in the form of strong pellets (diam. = 0·712 cm, thickness ~ 0·05 cm), were obtained by finely grinding the alloy and compressing the powder in a die under a pressure of $1{\cdot}4 \times 10^6$ kg/m^2. Both the faces of these pellets were coated with aluminium film by vacuum evaporation. Thin-film samples were prepared in a vacuum level $\sim 10^{-5}$ torr. They were made in planar geometry on microslide glass-substrate with predeposited indium electrodes (0·6 cm wide, 1-5 μm thick and a gap of 0·2 mm) held at room temperature.

In case of thin films, where the measurements were made at high electric fields, the authors used indium as an electrode material because it did not show any migration in contrast to aluminium which has been found to migrate[8] into amorphous films of As-Ge-Te. However, in case of thick pellets, where low field existed, no differences were observed when coated with aluminium or indium. The authors preferred aluminium because of its relatively better adhesive capability.

Measurement of conductivity—Bulk samples were used for the measurements of ac and dc conductivity. These measurements were made between a tempera-

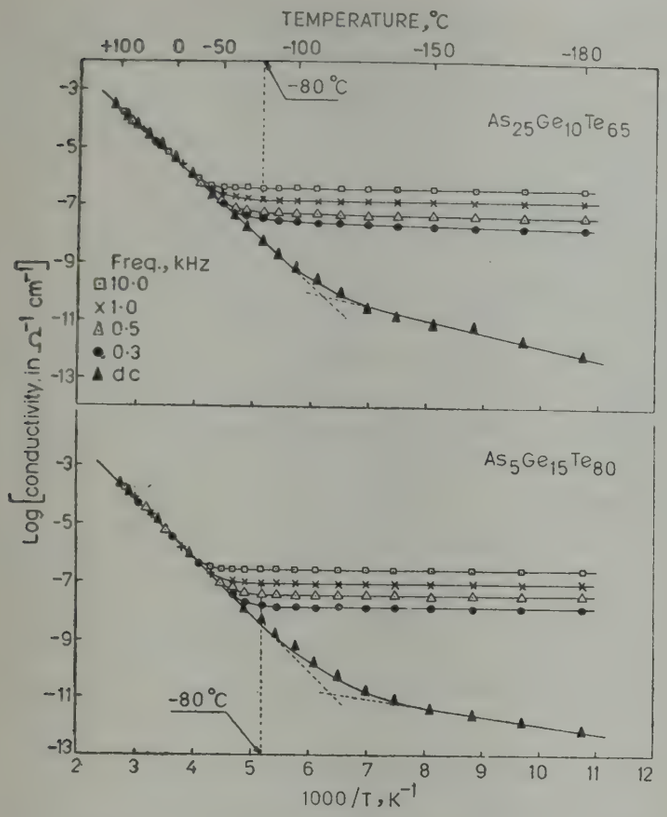

Fig. 1—Variation of conductivity with temperature at different frequencies for $As_{25}Ge_{10}Te_{65}$ and $As_5Ge_{15}Te_{80}$

ture-range: 83 to 383 K. Total conductivity $\sigma_T(\omega)$ was measured on Philips bridge, type GM-4144, and ac conductivity $\sigma(\omega)$ was calculated by using the relation.

$$\sigma_T(\omega) = \sigma(\omega) + \sigma_{dc}$$

where σ_{dc} (dc conductivity) was measured on a BPL megohmmeter, type RM 160/3. The ac conductivity was measured at frequencies of 0·3, 0·5, 1·0 and 10·0 kHz.

In order to make measurements at a given frequency, separate pellets were used for each temperature cycle. The reproducibility of the results was checked by making many runs at different times over the entire temperature and frequency ranges. It was observed that (i) the conductivity-behaviour was always same and (ii) the values of conductivity were within ± 2% error in different runs. However, only the results of one single run for each frequency are reported here. No annealing effect on conductivity was observed for any glass below the glass transition temperature.

Measurement of dielectric constant—Dielectric constant was measured over the temperature range: 83-373 K at different frequencies, i.e. 0·2, 0·5, 1·0, 2·6 and 5·0 MHz. Pellet-samples were used for these measurements under a dry atmosphere by locking the pellet tight between the steel electrodes of a cell assembly.[9] A high precision instrument, described earlier,[10] has been used for capacitance measurements. The capacitance measuring ability of the instrument was ± 0·0005 pF and it remained stable within ± 0·001pF for several hours. Separate pellets were cycled through the desired temperature range for each frequency of operation. To start with, the dielectric constant of the material was determined at room temperature by using pellet method.[11] Thereafter, the values of dielectric constant at other temperatures were determined by measuring the relative change in capacitance with temperature. Different runs, taken at different temperatures and frequencies, showed a similar behaviour and the values of dielectric constant showed variations within ± 2%.

3. Results and Discussion

Figs. 1 and 2 show the temperature and frequency dependence of conductivity for various alloys of As-Ge-Te and Se-Ge-Te. The other two compositions, i.e. $As_5Ge_{10}Te_{85}$ and $As_{15}Ge_{10}Te_{75}$, also showed a behaviour similar to that seen in Fig. 1.

These figures reveal the following:

(i) In both the alloy systems, frequency is found to have a pronounced effect on conductivity only at low temperatures, and $\sigma_T(\omega)$ approaches σ_{dc} at higher temperatures. In the low temperature region, the ac conductivity can be expressed as $\sigma(\omega) = A\,\omega^s$. It has been observed that the value of s does not

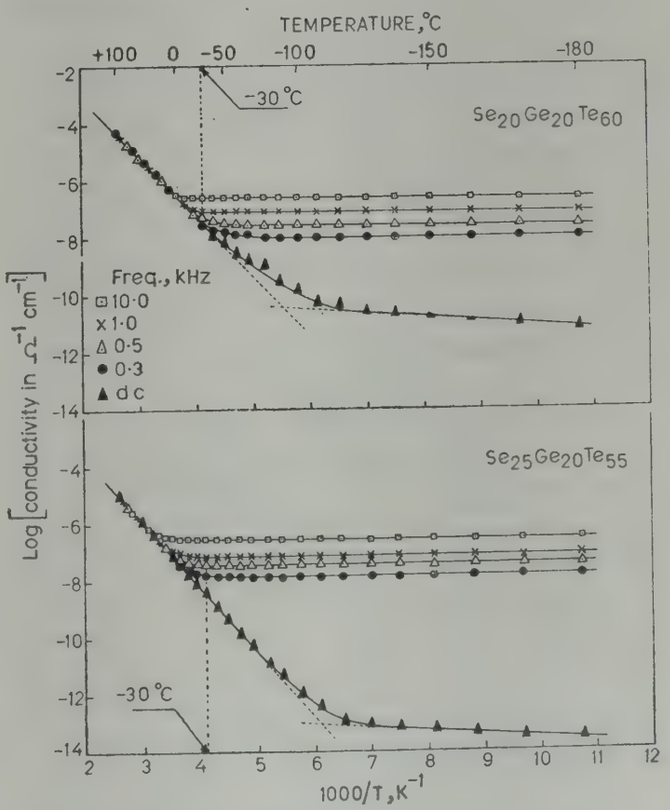

Fig. 2—Variation of conductivity with temperature at different frequencies for $Se_{20}Ge_{20}Te_{60}$ and $Se_{25}Ge_{20}Te_{55}$

change and remains around 0·8 for all the six glasses over the temperature range: 83-203K.

(ii) At low temperatures ($T < T_c$; Figs. 1 and 2) σ_T (ω) is much higher than σ_{dc} and is temperature independent even at frequencies as low as 0·3 kHz. It was also observed that the ac conductivity, at a given temperature and frequency, remains almost constant for all the six glasses (see Table 1).

(iii) Temperature T_c, below which the conductivity becomes temperature independent, is same for all the reported compositions of As-Ge-Te but T_c changes markedly when one goes to Se-Ge-Te alloys, e.g. T_c at 1 kHz for As-Ge-Te alloys is around −80°C (Fig. 1), while it is −30°C for both the compositions of Se-Ge-Te (Fig. 2).

Three types of conduction mechanisms have been suggested in the literature for amorphous semiconductors: (a) band conduction which is similar to that for crystalline semiconductors; (b) conduction in localized states at the edges of the valence and/or the conduction band; and (c) conduction in localized states near Fermi level.

For band conduction, the conductivity is expected to be frequency independent up to UHF region, and thereafter should decrease as ω^{-2} when frequency exceeds the inverse of carrier relaxation time.[12] No contribution to ac conductivity due to extended states is expected[12] in the amorphous semiconductors up to frequencies $\sim 10^7$ Hz.

An $\omega^{0.8}$ dependence of σ (ω) can be expected due to hopping conduction in localized states near band edges. But conduction of this type demands[12] that σ (ω) must be temperature dependent similar to that of dc conductivity. Rockstad[1] has reported strong temperature dependence in As_2Te_3, Te_2AsSi and Te-As-Si-Ge. He has suggested a contribution to ac conductivity due to hopping in these states. But in the case of six glasses, reported here, we have observed that σ (ω) remains temperature independent over the range 83-203 K and, therefore, one would not expect any contribution of ac conductivity due to these states.

Table 1—Values of ΔE, W_M, σ (ω), β and s for the various Glassy Alloys

Alloy	Activation energy* ΔE (eV)	$W_M \sim$ Band gap $= 2\times\Delta E$ (eV)	σ (ω) at 10^4 Hz and 203 K (Ω^{-1} cm^{-1})	β calc. from Eq. (3)	s Calc. from Eq. (4)
$As_5Ge_{10}Te_{85}$	0·27	0·54	$2·7\times10^{-7}$	0·20	0·80
$As_{15}Ge_{10}Te_{75}$	0·31	0·62	$2·6\times10^{-7}$	0·17	0·83
$As_{25}Ge_{10}Te_{65}$	0·37	0·74	$3·4\times10^{-7}$	0·14	0·86
$As_5Ge_{15}Te_{80}$	0·39	0·78	$2·4\times10^{-7}$	0·13	0·87
$Se_{20}Ge_{20}Te_{60}$	0·42	0·84	$2·5\times10^{-7}$	0·12	0·88
$Se_{25}Ge_{20}Te_{55}$	0·46	0·92	$2·9\times10^{-7}$	0·11	0·89

* The values of ΔE were calculated from the slopes of log σ_{dc} versus $1000/T$ curves in the high temperature region.

The most widely used concept is based on pair-model[13] according to which thermally assisted tunneling is responsible for conduction between localized states lying deep within the energy gap. On the basis of this model, the ac conductivity can be expressed[14,15] as:

$$\sigma(\omega) = \pi/3\,[N(E_F)]^2\; k\,T\,e^2\,\alpha^{-5}\,\omega\,[\ln(\nu_{ph}/\omega)]^4 \qquad \ldots(1)$$

where α is the radial decay of the localized wave function and ν_{ph} is the phonon frequency.

This formula predicts that σ(ω) is proportional to temperature (T) and has $\omega^{0.8}$ dependence. The present authors did experimentally observe $\omega^{0.8}$ frequency dependence, but the ac conductivity has been found to be almost temperature independent in the range 83-203 K. It is, therefore, obvious that Eq. (1) is not valid for all the six materials. Polanco and Roberts[5] and Le Cleac'h and Palmier[7] also observed a temperature-independent behaviour of σ(ω) in the case of As_2S_3 and $(As_2Te_3)_{95}Ge_5$ respectively.

Elliott[16] has recently given a different theory of ac conduction for chalcogenide glasses, Based on Pike's model.[17] He rules out the possibility of tunneling and considers hopping of carriers between two sites over a barrier separating them. Elliott considered the hopping species to be doubly-occupied, bipolaron state as envisaged in the work of Mott *et al.*[18] and Kastner *et al.*[19] According to this theory, the ac conductivity is

$$\sigma(\omega) = \frac{\pi^2 N^2 \epsilon}{24}\left[\frac{8\,e^2}{\epsilon\,W_M}\right]^6 \frac{\omega^s}{\tau_0^\beta} \qquad \ldots(2)$$

where

$$\beta = \frac{6\,k\,T}{W_M} \qquad \ldots(3)$$

and

$$s = 1 - \beta \qquad \ldots(4)$$

W_M, the binding energy of the carrier in its localized site, has been assumed to be equal to band gap; ε is

the effective dielectric constant and N is the spatial density of states at Fermi level.

According to the present authors Eq. (2) also deserves a critical examination. One can see that this equation does not directly incorporate T. But, s is temperature dependent and according to Eqs. (3 and 4), its value decreases with increase in temperature. Also, the value of s should change for materials having different values of W_M. We estimated the values of s at a given temperature (say 203 K) for all the six alloys by using Eqs. (3) and (4) and found that s varied from 0·80 to 0·89 (see Table 1). This is in contradiction to what we observed experimentally, i.e. s is almost independent of the material; its value being $0{\cdot}80 \pm 0{\cdot}01$ at 203 K. Another noteworthy feature is that the value of s remains almost constant in the temperature range 83-203 K for all the glasses, whereas according to Eqs. (3) and (4), s should decrease with increasing temperature. Further, Eq. (2) emphasizes that $\sigma(\omega)$ is proportional to $(W_M)^{-6}$, i.e. a small change in the size of the band gap should show a marked effect on the magnitude of $\sigma(\omega)$. This again is in direct conflict with our experimental observations. Table 1 reveals that the values of $\sigma(\omega)$ remain nearly the same for all the glasses at a given temperature and frequency, but the band gap varied from 0·54 eV to 0·92 eV. It therefore, seems obvious that Elliott's theory cannot be said to be applicable in general to chalcogenides.

Other theories based on (i) ionic conduction,[20] (ii) distribution of dipoles[21] and (iii) hopping between the short range order clusters of crystalline state[4] also lead to a temperature-dependent $\sigma(\omega)$. It has been pointed out[7] that polaron theory may also lead to a temperature-dependent ac conductivity.

Recently, Mott and his collaborators[18] have proposed an interesting model for chalcogenide glasses. They suggest that (i) the states in the gap, near Fermi level, are due to dangling bonds and (ii) if the reaction $2D^0 \rightarrow D^+ + D^-$ is exothermic, then only paired defect states are found in the gap. It is this model which can successfully explain the results obtained for materials reported here.

Since these defect states are paired in which half of the charge carriers (dangling bonds) are positively charged and the remaining half are negatively charged, the present authors assume that the paired states are analogous to electric dipoles and hence the entire system may be considered to be virtually a dipolar system.

At low temperature, one would expect a large distribution of relaxation times because of hindered rotation of these dipoles. Therefore a Debye-type relaxation may lose its significance at such low temperatures. A very large distribution of relaxation time should give a dielectric loss (and hence the ac conductivity) which would be almost independent of temperature. As the temperature increases, the dipoles slowly attain freedom of rotation and, therefore, a Debye-type relaxation should be observable. Under such circumstances, the dielectric loss [or $\sigma(\omega)$] is expected to become temperature and frequency dependent.

If the above assumption is true then the measured values of dielectric constant should be independent of temperature and frequency at lower temperatures, whereas at higher temperatures, when the dipoles are attaining rotational freedom, the dielectric constant should decrease with the increasing frequency and increase with increasing temperature, as expected in a dipolar system. We did observe this behaviour experimentally for all the reported glasses and our results for As-Ge-Te and Se-Ge-Te alloys are shown in Figs. 3 and 4 respectively. Other alloys of As-Ge-Te also displayed a behaviour similar to that shown in Fig. 3. In our earlier communications[22-24] we had conclusively discussed that the dielectric behaviour of chalcogenides can be successfully explained on the basis of molecular theory of dielectric relaxation. It, therefore, seems correct that Mott's concept of dangling bonds, along with our assumption of a dipolar behaviour, can explain the conductivity behaviour of all the chalcogenides reported here.*

Figs. 1 and 2 reveal that T_c, the temperature below which $\sigma(\omega)$ becomes temperature independent, is different for the two alloy-systems, i.e. T_c (at 1 kHz) is $-30°C$ for Se-Ge-Te alloys and $-80°C$ for As-Ge-Te alloys. This shift in T_c can also be explained by using Mott's concept of dangling bonds. Our dielectric measurements clearly indicate (see Figs. 3 and 4) that T_c is the temperature at which rotational freedom of dipoles begins, and this temperature is higher for Se-Ge-Te as compared to As-Ge-Te alloys; the difference being 50°C. Incidentally, the same difference in T_c has also been observed in conductivity measurements. One would indeed expect a similarity even in the actual values of T_c if the conductivity measurements could be carried out at the same frequencies as the dielectric measurements. Our study of field-dependent activation

* It is true that the conductivity and dielectric measurements could not be made at the same frequencies, but the present authors feel justified to compare the behaviour of these two parameters because the literature[4-7] provides sufficient evidence that the behaviour of ac conductivity ($\omega^{0.8}$ dependence) is maintained even up to 10^6 Hz, i.e. the operating range of dielectric measurement.

energy (as discussed later) indicates that the density of states is higher in case of Se-Ge-Te as compared to As-Ge-Te alloys. This implies a higher density of $D^+ - D^-$ states (or a higher dipolar concentration) in case of Se-Ge-Te alloys. Obviously, therefore, the inter-dipolar interaction will be more for Se-Ge-Te alloys. This would mean that more thermal energy is to be provided to the system to disengage the dipoles for their rotational freedom. Figs. 1-4 clearly reveal that a temperature-independent behaviour of $\sigma(\omega)$ begins as and when dipoles start losing their rotational freedom. It is, therefore, evident that T_c should be higher for Se-Ge-Te alloys which is in agreement with our experimental observations.

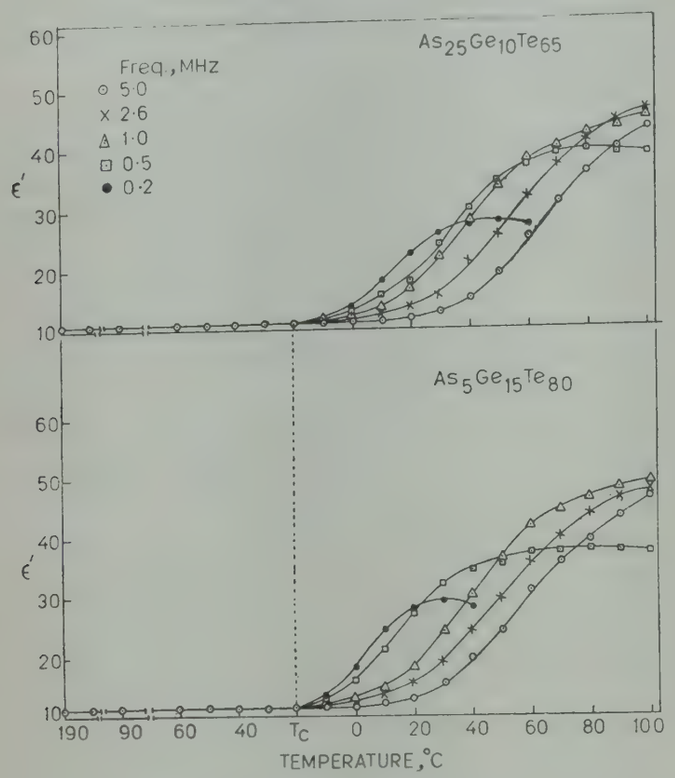

Fig. 3 – Variation of dielectric constant (ϵ') with temperature at different frequencies for $As_{25}Ge_{10}Te_{65}$ and $As_5Ge_{15}Te_{80}$

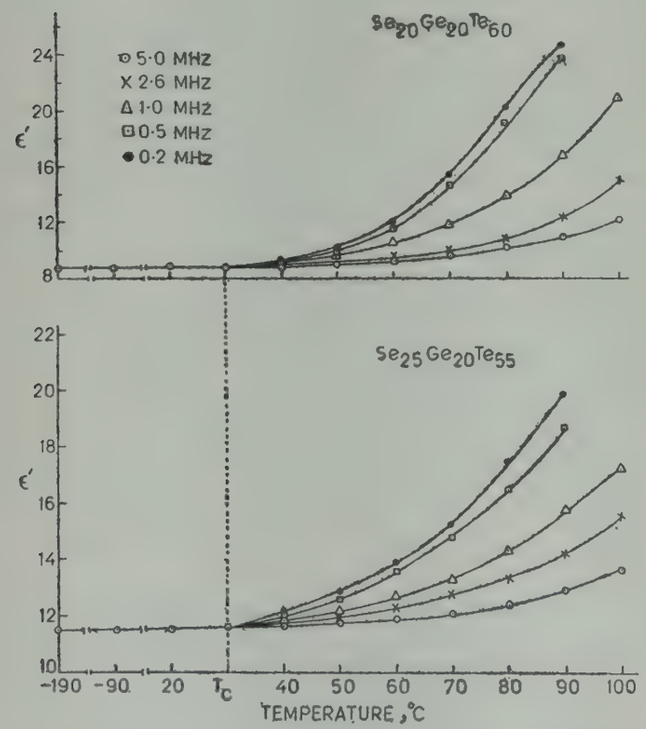

Fig. 4—Variation of dielectric constant (ϵ') with temperature at different frequencies for $Se_{20}Ge_{20}Te_{60}$ and $Se_{25}Ge_{20}Te_{55}$

The results of field-dependent activation energy, obtained for $As_{25}Ge_{10}Te_{65}$ and $Se_{25}Ge_{20}Te_{55}$, are shown in Fig. 5. Other compositions also showed a similar behaviour. Measurements of dc conductivity at different fields were made on thin-film samples of these alloys and the activation energies were calculated by obtaining the slopes of log σ_{dc} versus $1000/T$ curves at different electric fields. We found that the activation energy (ΔE) decreases with the increase of field (F) and follows the relation :

$$\Delta E = \Delta E_0 - m \log F \qquad \ldots(5)$$

where m is the slope of the curve shown in Fig. 5.

Mott[25] has recently pointed out that if an amorphous film carries a negative surface charge due to the application of an electric field, then, within a distance from the surface called screening length, the Fermi level must be raised or lowered owing to the additional density of electrons there. Therefore, an additional term in the conductivity, with lower activation energy, is observed. Obviously, this 'field-effect current' must be dependent on the density of states near Fermi level.[25] The higher the density of states, the higher would be the surface charge and hence more would be the effect on conductivity and activation energy. It is therefore, obvious that, the larger the value of m, the higher should be the density of states at Fermi level. Fig. 5

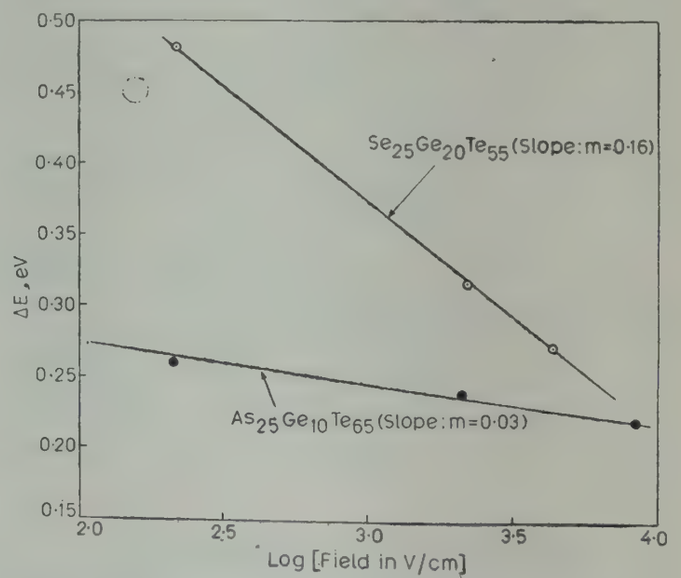

Fig. 5—Field dependence of activation energy (ΔE) for $As_{25}Ge_{10}Te_{65}$ and $Se_{25}Ge_{20}Te_{55}$

shows that m is much higher in $Se_{25}Ge_{20}Te_{55}$ as compared to $As_{25}Ge_{10}Te_{65}$. It may be mentioned that the values of m were found to be almost the same for all the compositions of a given alloy-system. Higher value of m for Se-Ge-Te alloys, provides a positive evidence of the existence of higher density of states in case of Se-Ge-Te glasses as compared to As-Ge-Te ones.

4. Conclusions

Conductivity and dielectric constant measurements for various alloys of As-Ge-Te and Se-Ge-Te have been made at various temperatures and frequencies. Existing theories of ac conduction have been analyzed for interpretation of the present results and it is found that Mott's concept of 'dangling bonds', along with our assumption of a dipolar behaviour, can explain these results better than any of the existing theories. Dielectric behaviour of these glasses is also consistent with the concept of a dangling bond theory.

Acknowledgements

The authors are grateful to Mr S R Ovshinsky, President, Energy Conversion Devices Inc., Michigan, USA, for gifting the alloys of As-Ge-Te. We are also indebted to (Late) Prof. G F Wright of the University of Toronto for gifting the dielectric equipment referred to in this paper. One of us (A K) is grateful to CSIR, New Delhi for providing funds (through awarding a fellowship) during the course of this work.

References

1. Rockstad H K, *Solid St. Commun.*, 7 (1969), 1507; 9 (1971), 2233; *J. Non-Cryst. Solids*, **2** (1970), 224.
2. Owen A E & Robertson J M, *J. Non-Cryst. Solids*, **2** (1970), 40.
3. Ivkin E B & Kolomiets B T, *J. Non-Cryst. Solids*, 3 (1970), 40.
4. Segawa H, *J. phys. Soc. Japan*, 36 (1974), 1087.
5. Polanco J I & Roberts G G, *Phil. Mag.*, 25 (1972), 117.
6. Kitao M, *Japan J. appl. Phys.*, 11 (1972), 1472.
7. Lecleac'h X & Palmier J F, *J. Non-Cryst. Solids*, 18 (1975), 265.
8. Panwar O S, Goyal D R, Kumar A, Ravikar D R, Srivastava K K & Lakshminarayan K N, *Nat. Acad. Sci. Lett.*, **1** (1978), 227.
9. Lal K & Pahwa D R, *Rev. scient Instrum.*, 42 (1971), 534.
10. Meredith C C & Wright G F, *Can. J. Technol.*, 33 (1955), 182.
11. Bedard M, Huber H, Myers J L & Wright G F, *Can. J. Chem.*, 40 (1962), 2278.
12. Mott N F & Davis E A, *Electronic process in non-crystalline semiconductors* (Clarendon Press, London), 1971, p. 211.
13. Pollak M, Geballe T H, *Phys. Rev.*, **122** (1961), 1742.
14. Austin I G & Mott N F, *Adv. Phys.*, **18** (1969), 41.
15. Mott N F & Davis E A, *Phil. Mag.*, **22** (1970), 903.
16. Elliott S R, *Phil. Mag.*, **35** (1977), 1291.
17. Pike G E, *Phys. Rev.*, **B6** (1972), 1572.
18. Mott N F, Davis E A & Street R A, *Phil. Mag.*, **32** (1975), 961.
19. Kastner M, Adler D & Fritzsche H, *Phys. Rev. Lett.*, **37** (1976), 1504.
20. Pollak M & Pike G E, *Phys. Rev. Lett.*, 28 (1972), 1449.
21. Street R A & Yoffe A D, *J. Non-Cryst. Solids*, **8-10** (1972), 745.
22. Srivastava K K, Goyal D R, Kumar A, Lakshminarayan K N, Panwar O S & Krishan I, *Phys. Status. Solidi*, **(a), 41** (1977), 323.
23. Panwar O S, Kumar A, Goyal D R, Srivastava K K, & Lakshminarayan K N, *J. Non-Cryst. Solids*, 30 (1978), 37.
24. Srivastava K K, Kumar A, Panwar O S & Lakshminarayan K N, *J. Non-Cryst. Solids*, 33 (1979), 205.
25. Mott N F, *Contemp. Phys.*, **18** (1977), 225.

Indian Journal of Pure & Applied Physics
Vol. 18, May 1980, pp. 324-326

Calculation of Multiplet Splittings of $A^2\Pi$ States of Some Diatomic Alkaline-earth Halides by Extended Hückel Approach

D P Nanda & B S Mohanty

Department of Physics, B J B College, Bhubaneswar, Orissa

Received 23 *August* 1979

Spin-orbit interaction is introduced into the semi-empirical extended Hückel molecular orbital scheme by adding the phenomenological spin-orbit interaction operator to the effective Hamiltonian. Assuming that the spin-orbit interaction in a molecule can be expressed in terms of the spin-orbit interaction operators of the atomic constituents, splittings of the $A^2\Pi$ states of the alkaline-earth halides have been calculated. Good agreement with the observed spin-splittings is obtained.

1. Introduction

Semi-empirical molecular orbital methods have been developed for the study of large molecules where the use of *ab initio* techniques in one-electron approximation is precluded on computational cost grounds. Out of the many forms of the semi-empirical methods, the most widely used are the extended Hückel theory[1] (EHT) and the method of complete neglect of differential overlap[2,3] (CNDO). The application of EHT to diatomic molecules however, has been limited.[4,5] The present work in determining multiplet splittings of $A^2\Pi$ states of a class of di-atomic molecules supplements the studies made so far by EHT methods.

It is well known that the $A^2\Pi$-states of the fluorides, chlorides and bromides of alkaline-earth metals exhibit spin-orbit coupling. The separations between the $2\Pi_{1/2}$ and $2\Pi_{3/2}$ states for these molecules are also known.[6] In an earlier paper,[7] the ionization potentials, orbital energies and the first excitation potentials of diatomic calcium halides were computed employing EHT without considering the spin-orbit interactions. Consequently, the doublet splittings in the first excited states $A^2\Pi$ of this class of molecules have not been computed so far. Manne *et al.*[8] have employed a semi-empirical method for calculating the ionization potentials of molecules containing heavy atoms by amending the extended Hückel hamiltonian with a phenomenological one-electron spin-orbit interaction operator. They have obtained satisfactory results for the hydrogen halides, diatomic halogens and the interhalogens. In the present work, we report the results of treating spin-orbit interaction in a molecule in terms of those of the constituent atoms of the alkaline-earth halides.

2. Theory

In the extended Hückel approach, the diagonal elements of the Hamiltonian H_{ii} are replaced by the appropriate multiplicity weighted average ionization potentials of all states arising out of the electronic configuration of the ith atom. The off-diagonal elements H_{ij} are then written as :

$$H_{ij} = K\,\Delta_{ij}\,(H_{ii} + H_{jj})/2 \qquad \ldots(1)$$

where Δ_{ij} is the overlap integral and K is the Wolfsberg-Helmholz constant. The value of this constant was empirically fixed for a given class of molecules to give the best experimental fit. In the present case, $K = 1{\cdot}75$ has been used.

The *l-s* interaction operator can be written as A l.s., where A is the spin-orbit interaction parameter to be fixed from atomic fine structure splitting. At this stage, we assume that the spin-orbit interaction in a molecule can be expressed in terms of the atomic spin-orbit interaction operators estimated from the atomic splittings of the constituent atoms. If we label each basis atomic orbital by A (atomic label), l_i, m_i, ζ_i, the one-electron operator may then be written as :

$$(\mathbf{l.s})_{\text{mol}} = \sum \Big| A, l_i, m_i, \zeta_i \Big\rangle \xi_{A,l}\, \mathbf{l}_A \cdot \mathbf{s}_A \Big| A, l_j, m_j, \zeta_j \Big\rangle \Big\langle A, l_j, m_j \zeta_j \Big| \qquad \ldots(2)$$

with summation over A, l_i, m_j, ζ_i, l_j, m_j and ζ_j. The constant $\zeta_{A,l}$ is empirically chosen to reproduce atomic spin-orbit interaction. This operator leads to relatively complicated two centre integrals. However, in the present programme, the contribution due to the two centre terms are neglected. This approximation seems to be well justified by Moores *et al.*[9]

The spin-orbit interaction matrix $\langle A, l_i, m_i, \zeta_i \left| \xi_{A,l} (l_A \cdot s_A) \right| A, l_j, m_j, \xi_j \rangle$ calculated for p and d orbitals is then added to the matrix elements H_{ij} of the Hückel Hamiltonian and the new matrix is diagonalized to yield the energy eigen values.

3. Computational Aspects

With real atomic orbitals (Slater type) as used in the present calculations, the matrix elements of the spin-orbit interaction operator are in general complex and, therefore, the overlap integrals would be complex. However, for linear molecules, the problem of complex arithmetic can be minimized. The full matrix eigen value problem can now be written as:

$$(\tilde{H}_{n\cdot r} + \tilde{H}_{s\cdot o})\, \tilde{V} = \tilde{\Delta}\, \tilde{V}\, \tilde{E} \qquad \ldots(3)$$

where $\tilde{H}_{n\cdot r}$ is the non-relativistic part and $\tilde{H}_{s\cdot o}$ is the spin-orbit interaction part of the effective Hamiltonian. $\tilde{\Delta}$ is the overlap matrix, $\tilde{V}$ is the eigen-vector matrix satisfying the orthonormality condition $\tilde{V}^{\dagger}\, \tilde{\Delta}\, \tilde{V} = 1$ and $\tilde{E}$ the diagonal eigen value matrix. The matrices are of order $2N$ including both spin directions. Separation of spin directions yield:

$$\tilde{H}_{n\cdot r} = \begin{pmatrix} H_{n\cdot r} & 0 \\ 0 & H_{n\cdot r} \end{pmatrix}; \quad \tilde{\Delta} = \begin{pmatrix} \Delta & 0 \\ 0 & \Delta \end{pmatrix}$$

and the non-relativistic (real) eigen value problem of order N as:

$$H_{n\cdot r}\, C = \Delta\, C\, E_{n\cdot r} \qquad \ldots(4)$$

with the orthonormality condition $C^{\dagger}\, \Delta = 1$.

After obtaining $E_{n\cdot r} = C^{\dagger}\, H_{n\cdot r}\, C$ from Eq. (4) the spin-orbit interaction matrix $\tilde{H}_{s\cdot o}$ is transformed by

$$\tilde{C} = \begin{pmatrix} C & 0 \\ 0 & C \end{pmatrix}$$

to an MO basis as $\tilde{C}^{\dagger} \tilde{H}_{s\cdot o}\, \tilde{C}$. The non-relativistic part of the Hamiltonian in this basis is diagonal and may be written as:

$$\tilde{E}_{n\cdot r} = \tilde{C}\, \tilde{H}_{n\cdot r}\, \tilde{C} = \begin{pmatrix} E_{n\cdot r} & 0 \\ 0 & E_{n\cdot r} \end{pmatrix}$$

and the eigen value problem reduces to

$$(\tilde{E}_{n\cdot r} + \tilde{C}\, \tilde{H}_{s\cdot o}\, \tilde{C})\, \tilde{U} = \tilde{U}\, \tilde{E} \qquad \ldots(5)$$

Table 1—Parameters Used for Different Halide Constituents

Atom	Valency orbital	Valence state ionization energy (H_{ii}), eV	Slater exponent	Spin-orbit interaction parameter (eV)
Mg	3*s*	−7·6433	1·1025	0
	3*p*	−3·2992	1·1025	0.015
	3*d*	−1·6995	0·3333	0·005
Ca	4*s*	−6·111	1·0995	0
	4*p*	−4·223	1·0995	0·03
	3*d*	−3·4029	0·6667	0·009
Sr	5*s*	−5·692	1·2141	0
	5*p*	−3·0028	1·2141	0·096
	4*d*	−3·1947	0·5405	0·016
Ba	6*s*	−5·210	1·2625	0
	6*p*	−2·971	1·2625	0·20
	5*d*	−3·797	0·5000	0·04
F	2*s*	−38·01	2·5638	0
	2*p*	−17·57	2·5500	0·033
Cl	3*s*	−25·30	2·3561	0
	3*p*	−13·70	2·0387	0·073
Br	4*s*	−24·00	2·6382	0
	4*p*	−12·30	2·2570	0·304

The following internuclear separations (in Å) have been used:

r (MgF) = 1·75, r (MgCl) = 2·20, r (MgBr) = 2·33

r (CaF) = 1·927, r (CaCl) = 2·203, r (CaBr) = 2·351

r (SrF) = 2·0757, r (SrCl) = 2·3522, r (SrBr) = 2·4997

r (BaF) = 2·163, r (BaCl) = 2·44.

Table 2—Spin-orbit Splittings of $A^2\,\Pi$ States

Molecule	Observed Splitting, cm^{-1}	Calculated splitting cm^{-1}
MgF	34·3	35·01
CaF	75·1	74·89
SrF	279·3	279·8
BaF	633·8	635·50
MgCl	55·0	55·4
CaCl	69·5	69·43
SrCl	294·2	293·61
BaCl	884·7	886·2
MgBr	110·1	110·47
CaBr	63·3	62·9
SrBr	301·3	301·00

where $\tilde{U}$ gives the eigen vectors in terms of the non-relativistic MO's. In terms of the original AO's they are obtained as $\tilde{V} = \tilde{C}\,\tilde{U}$. Due to Kramers degeneracy all eigen values in $\tilde{E}$ are at least doubly degenerate.

4. Calculations

The actual calculation is done in two steps. First the non-relativistic (real) part of the Hamiltonian matrix is diagonalized and then the spin-orbit matrix is transformed to the basis of these non-relativistic MO's before the diagonalization of the complex Hamiltonian. Thus the use of complex arithmetic is minimized.

The atomic parameters used in the present calculations are given in Table 1. For halogen atoms, the basis functions are *s* and *p* AO's, whereas for the metal atoms the basis also includes *d* orbitals, all AO's being of Slater-type. Exponents of Slater orbitals are taken from Clementi and Raimondi.[10] Otherwise, they are calculated using Slater's rules.[11] Inter-nuclear separations (r) were taken as the experimental or estimated equilibrium distances.[12] Computations are made on an IBM 370/155-II computer. The results of the calculations together with the experimentally observed values for the diatomic alkaline-earth halides are presented in Table 2.

5. Discussion

The $^2\Pi$ splittings of the A-states in the alkaline-earth halides are well reproduced indicating an interesting feature that the two centre integrals contribute negligibly to the splitting of the energy levels. The good agreement between the experimental and calculated values further points to the fact that large molecules can be quantitatively discussed in terms of their smaller component parts.

Acknowledgement

The authors are thankful to Dr N Barik, Department of Physics, Utkal University, Bhubaneswar, for discussions relating to computation. One of the authors (DPN) is grateful to the University Grants Commission, New Delhi, for financial support for computation.

References

1. Hoffmann R, *J. chem. Phys.*, 39 (1963), 1397.
2. Pople J A, Santry D P & Segal G A, *J. chem. Phys.*, 43 (1965), 5129.
3. Pople J A & Segal G A, *J. chem. Phys.*, 44 (1966), 3289.
4. Cooper W F, Clarke G A & Hare C R, *J. phys. Chem.*, 76 (1972), 2268.
5. Politzer P, Smith R K & Kasten S D, *Chem. Phys. Lett.*, 15 (1972), 226.
6. Herzberg G, *Molecular spectra and molecular structure*: I *Spectra of diatomic molecules* (Van Nostrand, New York), 1950.
7. Nanda D P & Mohanty B S, *Indian J. pure appl. Phys.*, 12 (1974) 704.
8. Manne R, Wittel K & Mohanty B S, *Molec. Phys.*, 29 (1975), 485.
9. Moores W H & Mc Weeny R, *Proc. R. Soc.*, A 332 (1973), 365.
10. Clementi E & Raimondi D L, *J. chem. Phys.*, 38 (1963), 2686.
11. Slater J C, *Quantum theory of atomic structure*, Vol. I, (Mc Graw-Hill, New York), 1960.
12. *Interatomic distances and supplement*, Special Publication: No. 11 and 18, edited by L E Sutton (The Chemical Society, London), 1958, 1965.

Indian Journal of Pure & Applied Physics
Vol. 18, May 1980, pp. 327-331

Semi-Empirical π-Electron Calculations on Some Mono Substituted Acetophenones

DAVINDER GUPTA*
Department of Physics, Jammu University, Jammu 180 001
and
R M P JAISWAL
Department of Physics, Kurukshetra University, Kurukshetra 132 119

Received 16 *April* 1979; *revised received* 15 *November* 1979

Semi-empirical SCF-MO calculations using the PPP-CI method have been conducted on *o*-, *m*- and *p*-hydroxy and methoxy acetophenones. The core resonance integrals are obtained from Linderberg relationship based upon the overlap gradients calculated from overlap integrals tabulated by Mulliken *et al.* A consistent set of parameters is used to compute various properties such as electronic spectra, polarization of observed transitions, ionization potential, dipole moment and reactivity of each molecule. The calculated values of various molecular parameters have been compared with their observed values.

1. Introduction

The observed electronic absorptions spectra of benzaldehyde and its mono derivatives have been rationalized by several workers[1-6] using the semi-empirical SCF-MO Pariser-Parr-Pople configuration interaction (PPP-CI) method.[7,8] In their approaches, while many of the workers[1-5] have used various empirical relationships to evaluate core resonance integrals ($\beta_{\mu\nu}$'s) for various bonds, others[6] have applied a Linderberg relationship[9] for the same in case of benzaldehyde and acetophenone molecules. It has been found that the agreement of calculated results with the observed spectrum of benzaldehyde molecule in the latter case is better than any of the former. The observed spectrum of acetophenone could also be explained satisfactorily by the latter approach. Hence, it was considered worthwhile to use this method for further study of mono-hydroxy and methoxy derivatives of acetophenone. Although electronic absorption spectra in case of some of these molecules have been studied experimentally by previous workers,[10-12] no theoretical work concerning these studies is available in literature.

2. Theoretical Method

All the molecules are assumed to be planar. The methyl group attached to the carbonyl group in acetophenone is assumed to be a pseudo heteroatom (X) contributing a pair of electrons to the system. In Π-electron approximation, methoxy group, similar to a hydroxy group, is treated as a simple oxygen atom contributing a pair of electrons to the system. However, the inductive effect of methyl group on the oxygen atom is suitably accounted for. All the ring distances are taken as 1·397 Å and the C=O, C—C, C—X and C—O bond distances as 1·21, 1·47, 1·51 and 1·36 Å respectively.[13] All the ring angles and C—C=O, X—C=O and C—C—O angles, however, are taken to be 120° for simplicity. The one-centre electron repulsion integrals ($\mu\mu/\mu\mu$) are calculated by the Pariser approximation.[14] The two-centre electron repulsion integrals ($\mu\mu/\nu\nu$) are evaluated by the formula of Mataga and Nishimoto.[15] All resonance integrals ($\beta_{\mu\nu}$'s) are estimated by using the Linderberg relationship,[9]

$$\beta_{\mu\nu} = \frac{1}{r_{\mu\nu}} \left[\frac{d\, S_{\mu\nu}}{d\, r_{\mu\nu}} \right] \qquad \ldots(1)$$

where $S_{\mu\nu}$ is the overlap integral between the orbitals μ and ν. The overlap integrals are obtained using Slater basis functions. The orbital exponents (Z) needed for the evaluation of overlap gradients are taken from the work of Mulliken *et al.*[16] A limited configuration interaction treatment involving configurations obtained from single electron excitation from three highest occupied MO's to three lowest unoccupied MO's is considered as justified by several previous workers.[17-19]

Various parameters used in the present calculations for hydroxy acetophenones have been taken from literature.[6,20,21] These values have been further parametrized for methoxy acetophenones by varying

* Present address : Infrared section, National Physical Laboratory, New Delhi-12

the Coulomb integral or valence state ionization potential[22] of the oxygen atom belonging to the substituent group (inductive effect of methyl group). The values of core resonance integrals ($\beta_{\mu\nu}$'s) for various bonds obtained in the present calculations by using the Linderberg relationship have been compared (Table 1) with those obtained by previous workers.[1-5]

3. Experimental Details

The electronic absorption spectra of the molecules under study have been recorded on a Carl-Zeiss VSU-2P spectrophotometer in the 200-380 mμ region in spectroscopically pure polar (methanol) as well as non-polar (hexane) solvents. The thickness of quartz cell containing the sample was kept at 0·5 cm. Because of the non-availability of *meta* substituted acetophenones, their spectra could not be recorded afresh and results of previous workers[25] have been used. The oscillator strengths have been determined[26] only for the absorption bands appearing in a polar solvent.

4. Results and Discussion

The results of the present studies are presented in Tables 2, 3 and 4. The results obtained here are satisfactory as only approximate geometries have been used and a consistent set of parameters employed to explain all the molecular properties. The positions and intensities of observed absorption bands are explained by calculated singlet transition energies and oscillator strengths. However, the triplet state energies could not be verified due to lack of experimental data. The experimentally observed spectra of molecules under study have also been reported earlier[25] but these were measured usually in the region 220-350 mμ. The present spectra have been recorded in the region of 200-380 mμ and also agree closely with the ones reported earlier.

Fig. 1 shows the spectral change due to substitution of a hydroxy and a methoxy group in acetophenone molecule at *ortho*, *meta* and *para* positions. It is observed experimentally that substitution of a hydroxy group in *ortho* position (2-position) in acetophenone causes a decrease in energy by 0·63 eV of the the lowest energy band appearing at about 4·4 eV. However, the corresponding calculated value is 0·28 eV only. The difference of 0·35 eV in the experimental and calculated values could be attributed to the presence of strong intramolecular hydrogen bond formation (chelation) in the molecule.[26,27] Theoretically predicted values of oscillator strengths for the lowest energy bands in *para* hydroxy and methoxy acetophenones (IV, VII) are 0·002 and 0·003 respectively. These extremely low values of oscillator strengths explain the non-appearance of the corresponding bands. A close agreement between the calculated and observed energies (Fig. 1) of second to the lowest energy band in case of all the isomers (including the *ortho*) suggests that hydrogen bonding has little effect on the location of this band, although it does effect the oscillator strength (Table 3). A similar view has been expressed by Forbes and Mueller[28] purely on the basis of experimental observations.

There is another band appearing at about 6·0 eV. An ambiguity exists in literature about the origin of this band. Morton and Stubbs[10] have assigned this

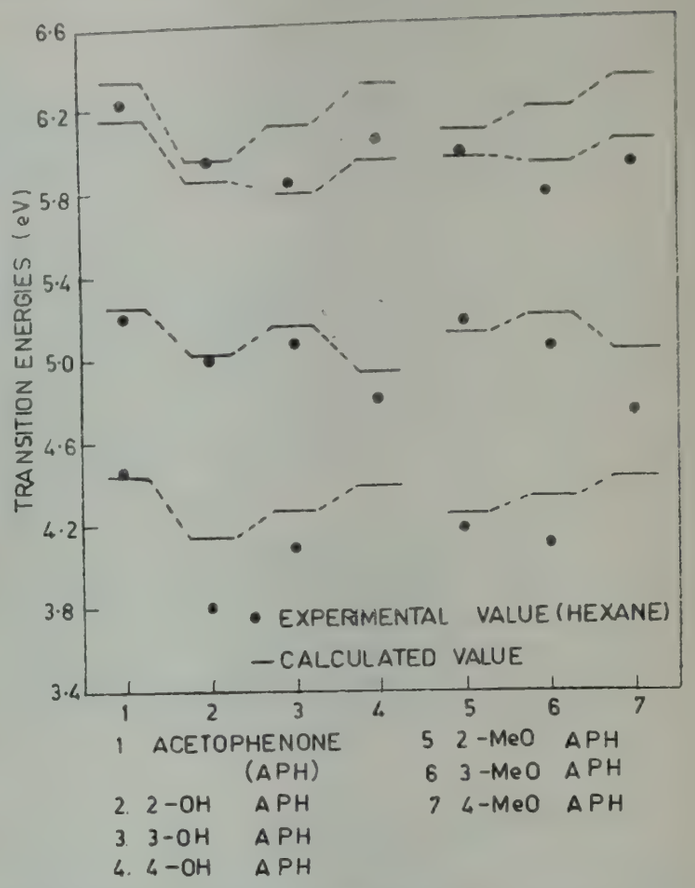

Fig. 1—Effect of hydroxy and methoxy groups on spectra of acetophenone

Table 1—Core Resonance Integrals ($\beta^{\mu}{}_{\nu}$'s) Used

Bond	$\beta^{\mu}{}_{\nu}$ (eV) Present values	From literature
C—C (ring)	−2·226 (1·397)	−2·330[a] (1·39)[d]
C—C	−1·909 (1·47)	−1·620[b] (1·46)[d]
C—X (CH_3)	−1·781 (1·51)	—
C=O	−2·704 (1·21)	−3·032[c] (1·22)[d]
C—O	−1·665 (1·36)	—

[a], Ref. 23; [b], Ref. 11; [c], Ref. 24; and [d], Ref 4

* Quantities within parenthesis indicate bond distances in Å.

as arising due to the carbonyl chromophoric group while Doub and Vandenbelt[11,12] have explained it as a result of $^1E_{2u} \leftarrow {}^1A_{1g}$ transition of benzene and have termed it as the second primary band. Both these assignments are based upon experimental studies only. Our experimental and theoretical studies unambiguously suggest that this band should be benzenoid in origin. Since a substitution in the aromatic ring removes degeneracy of the $^1E_{2u}$ state due to reduction in symmetry, the second primary band of benzene splits into two components. A similar conclusion has been drawn by Kimura and Nagakura[29] for mono-substituted benzenes. Theoretical calculations done here explain quantitatively the appearance of lower energy component of the second primary band. The observed spectra of 2-OH and 2-MeO acetophenones (II, V) however, show a single broad band at 5·93 eV and 5·97 eV respectively. This is explained by the fact that the magnitude of splitting in these molecules is small (~ 0·10 eV). Only lower energy component is observed in *meta* and *para* isomers (III, IV, VI, VII) because the higher component expected to appear around 6·20 eV could not be measured as the prism of the spectrophotometer starts showing complete absorption below 200mμ (6·16 eV). The *x*- and *y*- components of singlet transition moments (STM) as given in Table 2 indicate the direction of polarization of the singlet Π*—Π transitions. The experimental results[30] which are available for acetophenone molecule only are in complete agreement with the present calculated values.

Table 3 presents Π-electron dipole moment, ionization potential, electron affinity values, for each molecule. It can be seen that the calculated dipole moments for *meta* and *para* substituted acetophenones (III, IV, VI, VII) are in agreement with their experimental values. The present results show better agreement than those of Granzhan and coworkers.[36]

Table 2—Transition Energies (eV) and Oscillator Strength/log ε†

Exptl values		Calc. values	
MeOH	Hexane	Singlet	Triplet
Acetophenone (Aph)			
4·43 (0·0197)	4·45	4·43 (0·0124)	2·59
	4·31		
5·14 (0·2378)	5·20	5·24 (0·389)	3·50
6·23*	—	6·14 (0·391)	3·56
—	—	6·33 (0·696)	3·89
2-OH Aph			
3·81 (0·090)	3·82	4·15 (0·075)	2·61
4·96 (0·206)	4·99	5·02 (0·180)	3·28
	4·85		
5·95 (0·4920)	5·93	5·84 (0·218)	3·54
		5·94 (0·905)	4·47
3-OH Aph			
3·98 (3·70)**	4·08**	4·26 (0·034)	2·60
4·91 (4·00)**	5·06**	5·14 (0·295)	3·34
5·68 (4·40)**	5·83**	5·78 (0·649)	3·54
—	—	6·10 (0·385)	4·35
4-OH Aph			
—	—	4·38 (0·002)	2·58
4·52 (0·587)	4·79	4·92 (0·492)	3·53
5·75 (0·481)	6·04	6·93 (0·454)	3·59
—	—	6·29 (0·553)	4·22
2-MeO Aph			
4·07 (0·041)	4·17	4·24 (0·055)	2·59
5·06 (0·095)	5·16	5·10 (0·253)	3·34
6·01 (0·235)	5·97	5·94 (0·300)	3·56
		6·07 (0·832)	4·04
3-MeO Aph			
4·05 (3·39)**	4·10**	4·32 (0·0263)	2·58
4·98 (3·94)**	5·04**	5·18 (0·331)	3·39
5·71 (4·35)**	5·77**	5·90 (0·538)	3·54
—	—	6·17 (0·512)	4·03
4-MeO Aph			
—	—	4·40 (0·003)	2·56
4·57 (0·525)	4·72	5·02 (0·463)	3·53
5·82 (0·421)	5·90	6·00 (0·445)	3·59
—	—	6·31 (0·612)	3·99

* Ref. 10; ** Ref. 23 and † values within parentheses belong to the present study

Table 3—Π-Electron Dipole Moment (μ_π in debye), Ionization Potential (in eV), Electron Affinity (in eV)

S. No.	Molecule	μ_π		IP		EA
		Calc.	Obs.	Calc.	Obs.	
I	Aph	3·08	2·97[a]	10·38	9·32[d]	2·029
				9·43[e]	9·43[e]	
II	2—OH Aph	2·17	2·81[b]	9·78	—	1·947
III	3—OH Aph	2·69	2·96[b]	9·83	—	1·946
IV	4—OH Aph	3·56	3·61	9·84	8·70[d]	1·878
			±0·10[c]	9·30[e]		
V	2—MeO Aph	2·31	4·02[b]	9·94	—	1·961
VI	3—MeO Aph	2·76	2·88[b]	9·97	—	1·961
VII	4—MeO Aph	3·61	3·51	9·98	8·60[d]	1·902
			±0·10[c]	8·70[e]		

[a], Ref. 31; [b], Ref. 32; [c], Ref. 33; [d], Ref. 34; and [e], Ref. 35.

Table 4—Electron Densities, Free Valence Indices and Bond Orders

Substitution Y	π-Electron densities and free valences idices at position 1	2	3	4	5	6	7	8	9	Y
2-OH	1·0569	0·9469	1·0303	0·9772	1·0195	0·9825	0·6924	1·4343	1·9358	1·9292
	0·1885	0·1963	0·4171	0·4031	0·4007	0·4128	0·3071	0·8867	1·4445	1·4527
2-OH	1·0220	0·9896	0·9845	1·0128	0·9987	1·0036	0·6920	1·4233	1·9358	1·9377
	0·1750	0·4397	0·1900	0·4222	0·3950	0·4245	0·3149	0·8792	0·4440	1·4821
4-OH	1·0410	0·9549	1·0288	0·9685	1·0330	0·9828	0·6937	1·4259	1·9364	1·9350
	0·1784	0·4201	0·4135	0·1940	0·4136	0·4183	0·3119	0·8812	1·4460	1·4753
2-MeO	1·0519	0·9444	1·0253	0·9777	1·0165	0·9831	0·6923	1·4318	1·9358	1·9411
	0·1861	0·2175	0·4130	0·4035	0·3996	0·4198	0·3084	0·8849	1·4444	1·4852
3-MeO	1·0223	0·9851	0·9828	1·0081	0·9991	1·0070	0·6922	1·4229	1·9358	1·9511
	0·1754	0·4361	0·2090	0·4187	0·3953	0·4234	0·3149	0·8790	1·4444	1·5101
4-MeO	1·0383	0·9554	1·0240	0·9666	1·0283	0·9833	0·6935	1·4251	1·9363	1·9491
	0·1779	0·4205	0·4102	0·2135	0·4101	0·4184	0·3124	0·8807	1·445	1·5043

	Ground state bond orders between atoms 1-2	2-3	3-4	4-5	5-6	1-6	1-7	7-8	7-9	Ar-Y
2-OH	0·6161	0·6403	0·6747	0·6543	0·6770	0·6352	0·2922	0·8453	0·2875	0·2793
3-OH	0·6446	0·6476	0·6446	0·6652	0·6718	0·6357	0·2767	0·8528	0 2876	0·2499
4-OH	0·6359	0·6759	0·6425	0·6388	0.6796	0·6344	0·2883	0·8508	0·2860	0·2567
2-MeO	0·6213	0·6463	0·6727	0·6559	0·6755	0·6357	0·2889	0·8471	0·2876	0·2468
3-MeO	0·6438	0·6521	0·6490	0·6644	0·6724	0·6363	0·2766	0·8530	0·2876	0·2219
4-MeO	0·6369	0·6746	0·6473	0 6435	0·6784	0·6352	0·2820	0·8513	0·2863	0·2277

* see Fig. 2 for the numbering scheme.

However, for 2-OH acetophenone (II), calculated values of the dipole moment is slightly lower than the experimental value. This difference is considerably high in case of 2-MeO acetophenone. Similar disagreements have been reported by Granzhan *et al.*[36] who have explained them on the basis of hydrogen bonding in the former and steric repulsion in the latter. Ionization potentials and electron affinities have been obtained by Koopmaans' theorem.[37,38] The calculated ionization potentials are in agreement with the available experimental values. The results of ω-technique calculations conducted by Cantone and coworkers[35] however, show a better agreement with the experimental values. This may be accounted for by the fact that they have adjusted the parameters empirically so as to obtain best results for a single property of the molecule while in the present work different properties of the molecules are explained by a consistent set of parameters.

The Π-electron densities, free valence indices and bond orders for various molecules are presented in Table 4. As it is evident from Table 4, the electron density at carbonyl oxygen atom in case of various substituted acetophenones is in the order *ortho* > *para* > *meta*.

It is also clear from electron densities and free valence indices of *o*-, *m*- and *p*- derivatives of acetophenone that while a electrophilic substitution would

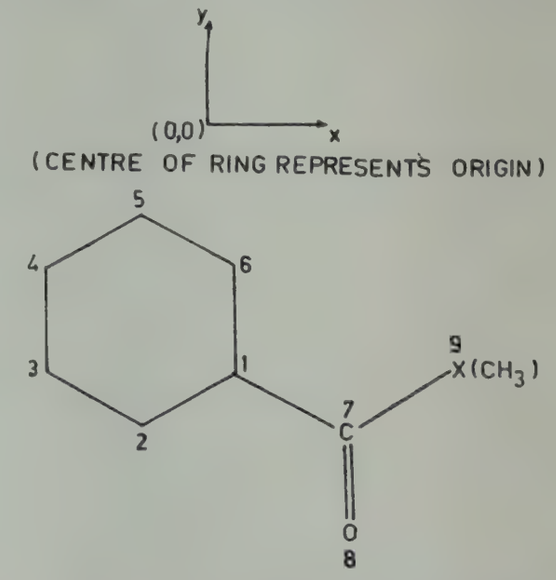

Fig. 2—Scheme of numbering of atoms in acetophenone

take place in them at 3rd and 5th, 6th and 4th and 3rd and 5th positions respectively, the corresponding positions for a nucleophilic substitution would be 6th and 4th, 2nd and 5th and 2nd and 6th [Fig. 2].

This is in complete agreement with the experimental observations.[39] The orders of various bonds depend upon the position and nature of the substituent in the aromatic ring. A higher value of the order of C—C bond than C—CH_3 bond is in agreement with the experimental observations.[13]

Acknowledgement

The authors wish to thank Prof. N Nath, Head of the Physics Department, Kurukshetra University, Kurukshetra, for providing necessary facilities. One of the authors (D G) is thankful to Prof. Y Prakash, Head of the Physics Department, Jammu University, Jammu, for his keen interest in the present work. He also acknowledges the financial assistance given to him by University Grants Commission, New Delhi through Jammu University, Jammu.

References

1. Bloor J E & Peradejordi F, *Theoret. Chim. Acta*, 1 (1962), 83.
2. Inuzuka K & Yokota T, *Bull. Chem. Soc. Japan*, 37 (1964), 122.
3. Inuzuka K & Yokota T, *Bull. Chem. Soc. Japan*, 38 (1965), 1055.
4. Bhaumik D, *Indian J. Phys.*, 48 (1974), 895.
5. Kiss A I & Szoke J, *KFKI Rep*, 74-91 (1975), 9PP.
6. Gupta D & Gupta V P, *Indian J. pure appl. Phys.*, 16 (1978), 968.
7. Pariser R & Parr R G, *J. chem. Phys.*, 21 (1953), 466, 767.
8. Pople J A, *Trans. Faraday Soc.*, 49 (1953), 1375.
9. Linderberg J, *Chem. Phys. Lett.*, 1 (1967), 39.
10. Morton R A & Stubbs A L, *J. chem. Soc.*, (1940), 1347.
11. Doub L & Vandenbelt J M, *J. Am. chem. Soc.*, 69 (1947), 2714.
12. Doub L & Vandenbelt J M, *J. Am. chem. Soc.*, 71 (1949), 2414.
13. Sutton L E, *Interatomic distances and configuration in molecules and ions*, Chemical Society Special Publication, London, No. 18, (1965).
14. Pariser R, *J. chem. Phys.*, 21 (1953), 568.
15. Mataga N & Nishimoto K, *Z. phys. Chem.*, 13 (1957), 140.
16. Mulliken R S, Rieke C A, Orloff O & Orloff H, *J. chem. Phys.*, 17 (1949), 1248.
17. Weltin E, Weber J P & Heilbronner E, *Theoret. chem. Acta*, 2 (1964), 114.
18. Pukanic G W, Forshey D R, Br. Jerome, Wegener D & Greenshields J B, *Theoret. Chim. Acta*, 9 (1967), 38.
19. Ahuja V K, Kapoor K L & Ray N K, *Indian J. Chem.*, 11 (1973), 143.
20. Nishimoto K & Forster L S, *Theoret. Chim. Acta (Berl.)*, 4 (1966), 155.
21. Ray N K & Narasimham P T, *Chem. Phys., Lett.*, 2 (1968), 101, 634.
22. Flurry (Jr) R L, *Theoret. Chim. Acta (Berl.)*, 9 (1967), 96.
23. Knowlton P & Carper W R, *Molec. Phys.*, 11 (1966), 213.
24. Kon H, *Bull. Chem. Soc. Japan*, 28 (1955), 275.
25. Kamlet (Jr) M, *Organic electronic spectral data*, Vol. 1, (Interscience, New York), 1960.
26. West W, *Chemical application of spectroscopy* (John Wiley, New York), 1968.
27. Stevenson P E, *J. Molec. Spectrosc.*, 13 (1965), 220.
28. Forbes W F & Mueller W A, *Can. J. Chem.*, 35 (1957), 488.
29. Kimura K & Nagakura S, *Molec. Phys.*, 9 (1965), 117.
30. Shimada R & Goodman L, *J. chem. Phys.*, 43 (1965), 2027.
31. Pilpel N, *J. Am. chem. Soc.*, 77 (1955), 2949.
32. Lutskii A E, *Zhur. Fiz. Chim.*, 23 (1949), 361.
33. Rogers M T, Barrow G M & Bordwell F G, *J. Am. chem. Soc.*, 78 (1956), 1790.
34. Foffani A, Pignataro S, Cantone B & Grasso F, *Z. Phys. Chem.*, 42 (1964), 221.
35. Cantone B, Grasso F & Pignataro S, *Molec. Phys.*, 11 (1966), 221.
36. Granzhan V A, Manole, Laktionova S K & Fillippov M P, *Zh. Struct. Chem.*, 12 (1971), 430.
37. Pople J A, *Proc. phys. Soc.*, 68A (1955), 81.
38. Hush M S & Pople J A, *Trans. Faraday Soc.*, 51 (1955), 600.
39. Morrison R T & Boyd R N, *Organic chemistry* (Prentice, New Delhi), 1975, p. 340.

Indian Journal of Pure & Applied Physics
Vol. 18, May 1980, pp. 332-336

Π^*--Π Systems in the Quartz Ultraviolet Electronic Absorption Spectra of Some Di- & Trisubstituted Acetophenones

DEVINDER GUPTA*
Department of Physics, Jammu University, Jammu 180 001
&
R M P JAISWAL
Department of Physics, Kurukshetra University, Kurukshetra 132 119

Received 16 *April* 1979; *revised received* 15 *November* 1979

Electronic absorption spectra of seventeen derivatives of acetophenone, viz. 2-hydroxy-, 2-methoxy-, 2,4-, 2,5-, 2, 6-dihydroxy-, 2-hydroxy, 4-methoxy-, 2-hydroxy 6-methoxy-, 2, 4-, 2, 6-dimethoxy-, 2, 4, 6-, 2,3,4-, 2, 4, 5-, 2, 3, 6-trihydroxy-, 2, 4-dihydroxy, 6-methoxy-, 2, 6-dihydroxy, 4-methoxy-, 2-hydroxy, 4, 6-dimethoxy-, 2,4,6-trimethoxy- acetophenones, have been recorded in a polar (methanol) and a non-polar (hexane) solvent in the wavelength region 200-380 mμ. Theoretical calculations using the semi-empirical Pariser-Parr-Pople configuration interaction (PPP-CI) method have also been performed so as to rationalize the experimental data.

1. Introduction

Some experimental studies relating to the electronic absorption spectra of a few mono- and di-substituted hydroxy- and methoxy-acetophenones are available in literature.[1-7] However, in most of these studies only those absorption bands which appear on higher wavelength side of 240 mμ have been discussed. Only recently, the present authors[8] have recorded absorption spectra of mono-hydroxy- and methoxy-acetophenones in the region 200-380 mμ and explained them theoretically on the basis of calculations using the semi-empirical SCF MO PPP-CI method. The Linderberg relationship[9] for the evaluation of all the resonance integrals was adopted successfully in case of acetophenone[10] and its mono-hydroxy- and methoxy-derivatives.[8] Hence, it was considered worthwhile to extend this method further to di- and tri-substituted acetophenones so as to test the validity of the above approach for these type of molecules.

The present work comprises a systematic study of electronic absorption spectra of a series of di- and tri-substituted hydroxy- and methoxy-acetophenones (most of which possess a —OH group at *ortho* position with respect to the acetyl group) experimentally as well as theoretically. The electronic absorption spectra of these molecules have been obtained in a polar (methanol) and a non-polar (hexane) solvent in the region 200-380 mμ. Interpretations have been provided for all the observed absorption bands on the basis of theoretical results obtained from semi-empirical SCF MO PPP-CI calculations and the solvent effect studies. The experimentally observed substituent effects regarding positions and intensities of various absorption bands have been discussed in the light of their theoretically estimated values.

2. Theoretical Method

Semi-empirical self consistent field molecular orbital (SCF-MO) method as proposed by Pariser and Parr[15] and Pople[16] has been employed to predict theoretically the electronic spectra of the molecules under study. The detailed procedure adopted in this work has already been reported earlier.[8,10] One-centre and two-centre electron repulsion integrals were evaluated from the Pariser[17] and Mataga and Nishimoto[18] formulae respectively. The core resonance integrals were estimated by the use of Linderberg relationship[9] and the overlap gradients were obtained from the work of Mulliken *et al.*[19]

The methoxy group, in the Π-electron approximation was treated as a simple oxygen atom donating a pair of electrons to the Π-system (similar to the case of a hydroxy group). However, the inductive effect of methyl group on the oxygen atom was suitably accounted for by varying its valence state ionization potential as described earlier.[8] All the molecules were assumed to be planar and their approximate geometries have been used. Thus the ring C—C distances have been taken as 1·397 Å and the C=O,

* Present address : Infrared Section, National Physical Laboratory, New Delhi-12.

C—C, C—X (CH_3) and C—O bond distances as 1·21, 1·47, 1·51, and 1·36 Å respectively.[20] All the angles and C—C=O, X—C=O and C—C=O angles were taken as 120°, for simplicity. Various parameters used in the recent calculations have been taken from literature.[8,9,21,22] A limited configuration interaction treatment involving configurations obtained from single electron excitations from three highest occupied MO's to three lowest unoccupied MO's has been considered as done by several other workers.[23-25] Out of the nine resulting states, only four are needed to explain the observed data.

3. Experimental Procedure

The spectra were recorded on a Carl-Zeiss VSU-2P spectro-photometer in solvents of spectroscopic purity. A 0·5 cm thick quartz cell was used to contain the samples. Spectra of almost all the compounds were recorded with their known concentrations of $\sim 10^{-4}$ mole dm^{-3} in the polar solvent. However, because of the poor solubility of the compounds in the non-polar solvent, their concentrations could not be estimated. As such, oscillator strengths of bands observed in polar solvents only are determined. The present spectral data in case of those molecules which have been studied by previous workers[1-7] agree closely with the reported one; generally within $\pm$ 1 mμ. Two additional absorption bands appearing in the region 200-240 mμ which were not measured by the previous workers have also been analyzed. In case of 2,4-, 2,6-dimethoxy- and 2,4,6-trimethoxy-acetophenones, experimental data reported by previous workers [11-14] have been used to compare them with the theoretically calculated results of the present work.

4. Results and Discussion

The results of the present studies are presented in Table 1. The positions and intensities at peak absorption of bands appearing in the spectra of the molecules are explained in terms of benzenoid singlet $\Pi^*-\Pi$ transitions, the energies and oscillator strengths of which have been calculated. In view of the fact that only approximate geometries have been used in the present calculations, the calculated results agree satisfactorily with the observed spectra. Triplet state energies could not be verified due to lack of experimental data.

The molecules under study are expected to give two distinct types of bands corresponding to Π^*-n and $\Pi^*-\Pi$ transitions. In most of them, the weak Π^*-n transition expected to appear around 320 mμ (3·87 ev) is completely masked with a highly intense $\Pi^*-\Pi$ band[2,26] due to pronounced resonance effect between the electron acceptor (acetyl) and electron donor (hydroxy or methoxy) groups through the benzene ring,[27] which causes shift towards the longer wavelength side and enhancement in the intensity of the $\Pi^*-\Pi$ band. Further, since all the bands observed show a shift towards the longer wavelength side when spectra are recorded first in a non-polar and then in a polar solvent, they have been taken to correspond to $\Pi^*-\Pi$ transitions.[26,27] Doub and Vandenbelt[3,4] have also interpreted similar bands observed in case of some of the substituted benzenes including a few acetophenone derivatives in terms of benzenoid $\Pi^*-\Pi$ transitions. Some of the authors[27,28] have, however, called the first two lowest energy bands as charge transfer bands.

In Fig. 1, the spectral changes due to substitution of hydroxy and methoxy groups in 2-OH acetophenone (APH) molecule at various positions of the ring have been shown. For the lowest energy band, a difference of 0·2 to 0·35 eV between its calculated and observed values (Fig. 1) has been noticed only in case of all those molecules which possess a —OH group in the *ortho* position with respect to the acetyl group. This can be understood in terms of intramolecular hydrogen bonding.[26,27] Substitution of a —OH group at the 4th position in the aromatic ring gives rise to either no shift or a hypsochromic shift of first lowest energy band (in a non-polar solvent) while substitution of this group at all other positions causes a bathochromic shift of this band as is evident from the experimental values in Table 2. Thus, the order of shifts of the above band for substitution at various positions can be put as

$$5\text{-OH} > 3\text{-OH} > 6\text{-OH} > 4\text{-OH}$$

The calculated results also predict the same order of shifts but their magnitudes are usually somewhat

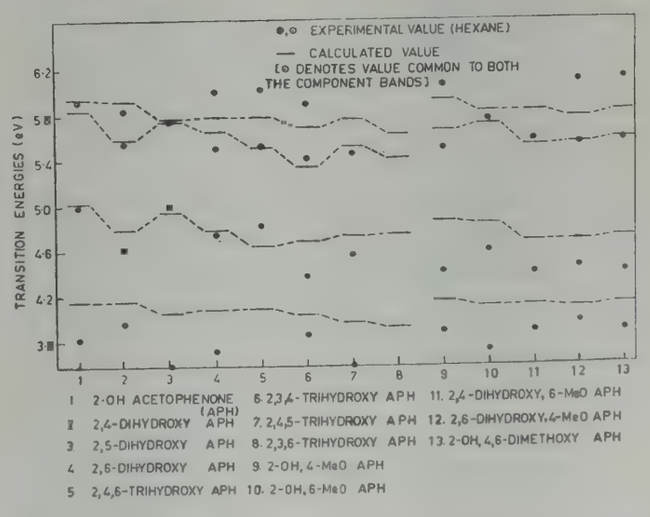

Fig. 1—Effect of hydroxy and methoxy groups on spectra of 2-OH acetophenone

Table 1—Transition Energies (in eV) and Oscillator Strengths/log ϵ Values (within parentheses)

Molecule	Observed values		Calculated values	
	MeOH	Hexane	Singlet	Triplet
2-OH Acetophenone				
	3·81 (0·090)	3·82	4·15 (0·075)	2·61
	4·96 (0·206)	4·99	5·02 (0·180)	3·28
		4·85		
	5·95 (0·492)	5·93	5·84 (0·218)	3·54
			5·94 (0·905)	4·47
2-MeO APH				
	4·07 (0·041)	4·17	4·24 (0·055)	2·59
	5·06 (0·095)	5·16	5·10 (0·253)	3·34
	6·01 (0·235)	5.97	5·94 (0·300)	3·56
			6·07 (0·832)	4·04
2, 4-Dihydroxy APH				
	3·94 (0·098)	3·96	4·15 (0·069)	2·62
	4·50 (0·147)	4·61	4·79 (0·300)	3·36
	5·41 (0·089)	5·55	5·58 (0·300)	3·48
	5·89 (0·244)	5.84	5·92 (0·795)	4·26
2-OH, 4-MeO APH				
	3·79 Sh	3·88 Sh	4·15 (0·068)	2·62
	4·33 (0·272)	4·41	4·86 (0·264)	3·36
	5·49 Sh	5·51	5·66 (0·298)	3·50
	6·03 (0·356)	6·07	5·93 (0·816)	4·31
2, 4-Dimethoxy APH				
	(12)	(12)		
	4·11 (3·98)	4·20	4·24 (0·048)	2·59
	4·64 (4·08)	4·80	4·91 (0·340)	3·42
	5·43 (4·15)	5·60	5·77 (0·335)	3·53
	—	—	6·06 (0·777)	4·30
2, 5-Dihydroxy APH				
	3·43 (0·065)	3·58	3·96 (0·107)	2·62
	4·88 (0·118)	4·99	4·94 (0·101)	3·06
	5·58 (0·553)	5·75	5·74 (0·083)	3·51
			5·76 (1·067)	4·64
2, 6-Dihydroxy APH				
	3·64 (3·45)*	3·72	4·08 (0·064)	2·63
	4·63 (4·05)*	4·76	4·78 (0·231)	3·20
	5·41 (4·18)*	5·51	5·65 (0·276)	3·51
	5·72	6·01	5·78 (0·661)	4·52
2-OH, 6-MeO APH				
	3·67 (0·048)	3·72	4·10 (0·063)	2·63
	4·55 (0·166)	4·60	4·84 (0·229)	3·23
	5·83 (0·281)	5·77	5·71 (0·248)	3·52
	6·16 (0·330)	—	5·83 (0·741)	4·52
2, 6-Dimethoxy APH				
	(13)	(5)		
	4·41 (3·60)	4·44	4·18 (0·047)	2·59
	4·85 (3·60)	5·16	4·94 (0·299)	3·29
	—	—	5·79 (0·289)	3·54
	—	—	5·94 (0·733)	4·48
2, 4, 6-Trihydroxy APH				
	3·75 Sh	—	4·09 (0·038)	2·63
	4·35 (0·195)	4·83	4·64 (0·337)	3·32
	5·51 (0·222)	5·83	5·51 (0·348)	3·46
	6·10 (0·274)	6·13	5·78 (0·583)	4·28
2, 4-Dihydroxy, 6-MeO APH				
	—	3·88 Sh	4·11 (0·041)	2·63
	4·31 (0·477)	4·44	4·68 (0·339)	3·34
	5·53 (0·297)	5·58	5·53 (0·327)	3·46
	6·04 (0·375)	—	5·83 (0·671)	4·28
2, 6-Dihydroxy, 4-MeO APH				
	3·75 Sh	3·96	4·09 (0·042)	2·63
	4·35 (0·199)	4·45	4·68 (0·305)	3·30
	5·53 (0·193)	5·56	5·55 (0·340)	3·48
	6·04 (0·420)	6·10	5·78 (0·618)	4·33
2-OH, 4, 6-Dimethoxy APH				
	3·80 Sh	3·88 Sh	4·12 (0·044)	2·63
	4·32 (0·356)	4·40	4·73 (0·306)	3·33
	5·58 Sh	25·58	5·59 (0·321)	3·48
	6·01 (0·731)	6·13	5·83 (0·692)	4·33
2, 4, 6-Trimethoxy APH				
	(14)	(15)		
	—	—	4·19 (0·294)	2·62
	4·52 (3·76)	4·92	4·79 (0·374)	3·39
	5·51 Sh (4·1)	—	5·68 (0·359)	3·50
	—	—	5·93 (0·661)	4·34
2, 3, 4-Trihydroxy APH				
	—	3·75	4·03 (0 036)	2·57
	4·24 (0·094)	4·38	4·68 (0·315)	3·20
	5·26 (0·055)	5·41	5·34 (0·286)	3·38
	5·87 (0·145)	5·90	5·67 (0·724)	4·11
2, 4, 5-Trihydroxy APH				
	3·56 (0·113)	3·58	3·96 (0·110)	2·58
	4·42 (0·152)	4·57	4·73 (0·190)	3·14
	5 16 (0·197)	5·46	5·52 (0·329)	3·43
	5·98 (0·329)	—	5·76 (0·832)	4·35
2, 3, 6-Trihydroxy APH				
	4·17 (0·191)	—	3·92 (0·080)	2·59
	—	—	4·74 (0·215)	2·99
	5·60	—	5·41 (0·412)	3·44
	—	—	5·62 (0·423)	4·49

* Ref. 5; and Sh denotes shoulder

less than the observed ones. However, unlike for transition energy, no definite sequence in the variation of oscillator strength of first lowest energy band was identified with the change in the position of the substituent.

It is interesting to note that the order of shifts is completely reversed in the case of second lowest energy band. The observed shifts can be put as

4-OH > 6-OH ≳ 3-OH > 5-OH

However, the calculated results suggest this order as

4-OH ≅ 6-OH > 3-OH > 5-OH

There are two more absorption bands in the spectra of substituted acetophenones which appear close to each other in a higher energy region of 6·0 eV as also expected theoretically. These bands can be interpreted as the two components of $^1E_{2u} \leftarrow {}^1A_{1g}$ transition of benzene[4,8] in the reduced symmetry of acetophenones as done by previous workers.[29] Calculations for 2,5-dihydroxy-acetophenone show two very close bands with energies of 5·74 eV and 5·76 eV. In agreement with this result a single broad band is observed at a mean energy of 5·75 eV. A similar justification has been given in case of 2-OH acetophenone and 2-MeO acetophenone.[8] It is seen that the agreement between the calculated and observed energy values is fairly good for the component band with lower energy. However, in case of higher energy band, the agreement is not as good. This may be due to dissociation of intramolecular hydrogen bonds.[30] The intensity of higher energy component band is usually more than that of lower energy component band. This trend is in agreement with the calculated results.

Methylation of phenolic groups in substituted acetophenones is found to cause small inconsistent spectral changes as also reported by Buraway and Chamberlain[31] in case of substituted phenols. This may probably be due to small steric effects. Steric effects are usually weak and are found to cause certain decrease in the intensities of absorption bands.[32] However, when both *ortho* positions with respect to the acetyl group are occupied by MeO groups as in case of 2,6-dimethoxy- and 2, 4, 6-trimethoxy-acetophenones, steric interaction between methyl groups belonging to one of the MeO group and the acetyl group reduces the conjugation within the molecule and thus results in hypsochromic shifts (increase in energies) accompanied by considerable decrease in the intensities of the absorption bands.[31] A comparison between calculated and observed energies for 2, 6-dimethoxy-acetophenone shows a difference of 0·26 eV for the first and 0·22 eV for the second lowest energy band, while for 2,4,6-trimethoxy-acetophenone shows a difference of 0·12 eV for the second lowest energy band (Fig. 2). These differences may be attributed to steric inhibition in these molecules.

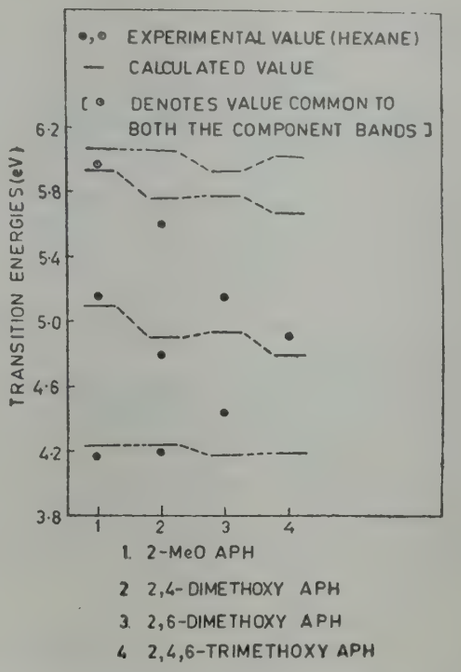

Fig. 2—Effect of methoxy groups on spectra of 2-MeO acetophenone

Acknowledgement

The authors wish to thank Prof. N Nath, Head of the Physics Department, Kurukshetra University, Kurukshetra, for providing necessary facilities. One of the authors (DG) is thankful to Prof. Y Prakash, Head of the Physics Department, Jammu University, Jammu, for his keen interest in the present work. He also acknowledges the financial assistance given to him by the University Grants Commission, New Delhi, through, the Jammu University, Jammu.

References

1. Morton R A & Sawires Z, *J. chem. Soc.*, (1940), 7052.
2. Morton R A & Stubbs A L, *J. chem. Soc.*, (1940), 1347.
3. Doub L & Vandenbelt J M, *J. Am. chem. Soc.*, **69** (1947), 2714.
4. Doub L & Vandenbelt J M, *J. Am. chem. Soc.*, **71** (1949), 2414.
5. Cram D O & Cranz F W, *J. Am. chem. Soc.*, **72** (1950), 595.
6. Forbes W F, Mueller W A, Ralph A S & Templetion J F, *Can. J. chem.*, **35** (1957), 1049.
7. Forbes W F & Templetion J F, *Can. J. chem.*, **36** (1958), 180.
8. Gupta D & Jaiswal R M P, *Indian J. pure appl. Phys.*, **18** (1980), 327
9. Linderberg J, *Chem. Phys. Lett.*, **1** (1967), 39.
10. Gupta D & Gupta V P, *Indian J. pure appl. Phys.*, **16** (1978), 968.
11. Valyashko N A & Rozum Y S, *Zh. Obshchei Khim.*, **17** (1947), 783.

12. Valyashko N A & Lutskii A E, *Zh. Obshchei Khim.*, **21** (1951), 1091.
13. Eneback C, *Acta. Chem. Scand.*, **11** (1957), 895.
14. Lavruskin V F & Trukerman S V, *Zh. Obshchei Khim.*, 33 (1963), 3971.
15. Pariser R & Parr R G, *J. chem. Phys.*, **21** (1953), 466; 767.
16. Pople J A, *Trans. Faraday Soc.*, **49** (1953), 1375.
17. Pariser R, *J. chem. Phys.*, **21** (1953), 568.
18. Mataga N & Nishimoto K, *Z. phys. chem.*, **13** (1957), 140.
19. Mulliken R S, Rieke C A, Orloff D & Orloff H, *J. chem. Phys.*, **12** (1949), 1248.
20. *Interatomic distances and configurations in molecules and ions*, edited by Sutton L E (Chemical Society, London), Special Publication, No. 18, 1965.
21. Nishimoto K & Forster L S, *Theoret. chim. Acta*, (*Berl.*), 4 (1966), 155.
22. Ray N K & Narasimhan P T, *Chem. Phys. Lett.*, **2** (1968), 101, 634.
23. Weltin E, Weker J P & Heilbronner E, *Theoret. chim. Acta*, **2** (1964), 114.
24. Pukànic G W, Forshey D R, Dr Jerome D Wegener & Greenshields J B, *Theoret. chim. Acta*, 9 (1967), 38.
25. Ahuja V K, Kapoor K L & Ray N K, *Indian J. Chem.*, **11** (1973), 143.
26. Jaffe H H & Orchin M, *Theory and application of ultraviolet spectroscopy* (John Wiley, New York), 1962.
27. West W, *Chemical applications of spectroscopy* (John Wiley, New York), 1968.
28. Scott A I, Interpretation of ultraviolet spectra of natural products, (Pergamon Press, London), 1964.
29. Kimura K & Nagakura S, *Molec. Phys.*, 9 (1965), 117.
30. Pimentel G C & McClellan A L, *The hydrogen bond* (Freeman, San Francisco & London), 1960.
31. Burawoy A & Chamberlain J T, *J. chem. Soc.*, (1952), 2310.
32. Gray G W, *Steric effects in conjugated systems* (Butterworths London), 1958.

Indian Journal of Pure & Applied Physics
Vol. 18, May 1980, pp. 337-341

EPR Studies on N, N′-Ethylenebis (Salicylaldiminato) Copper (II)-Thiourea & N, N′-*o*-Phenylenebis (Salicylaldiminato) Copper (II)-Thiourea

B A Sastry, S Md Asadullah & Anita Deb
Department of Physics, Osmania University, Hyderabad 500 007
and
C Pelizzi
Istituto di Chemica Generale ed Inorganica, Universita di Parma
Centro di Studio per la Structuristica Diffrattometria del C N R
Parma, Italy

Received 25 *July* 1978; *revised received* 7 *December* 1979

EPR studies at room and liquid nitrogen temperatures (LNT) have been carried out on the title compounds in N, N′-dimethylformamide (DMF) and pyridine solutions. Two species of copper (II) are detected in the second complex in DMF at LNT which correspond to the two molecules in the unit cell. The approximate strengths of the σ- and π-bonds have been estimated for both the complexes in the above solvents. Copper (II) hyperfine linewidth of the first complex in pyridine at room temperature, which is less complicated than the second complex, is analyzed using the theory of R Wilson and D Kivelson [*J. chem. Phys.*, 44 (1968), 150, 4440, 4445].

1. Introduction

Relatively few copper complexes with CuN_2O_2 chromophore have been studied by the EPR technique.[1,2] The copper complexes under investigation, viz. N, N′-ethylenebis (salicylaldiminato) copper (II)-thiourea [Cu(salen)tu] and, N, N′-*o*-phenylenebis (salicylaldiminato) copper (II)-thiourea [Cu (salof) tu] belong to the above type with metal-oxygen and metal-nitrogen distances shorter than most of the complexes in this category. A rare feature associated with Cu(salof)tu is that it contains two crystallographically independent molecules[3] of both Cu(salof) and thiourea, unlike Cu(salen)tu. The difference in metal-ligand bond lengths in the two molecules of Cu(salof)tu varies only from 0·01 Å to 0·004 Å and the bond angle difference varies from 0·1° to a maximum of 0·9°. The metal-oxygen and metal-nitrogen bond lengths in the case of Cu(salen)tu complex are slightly less than these found in Cu(salof)tu (Table 1).

In the absence of corresponding diamagnetic complexes for diluting the salts, the authors have taken up the EPR studies in solutions of DMF and pyridine to study the magnetic properties of these copper complexes for obtaining information about bond nature and relaxation mechanisms responsible for hyperfine linewidth of copper (II)

2. Experimental Details

The complexes under investigation are prepared by the methods described earlier.[3] Cu(salof)tu is found to dissolve in DMF and pyridine whereas Cu(salen)tu could only dissolve in pyridine. The EPR absorption first derivative signals of the above complexes in approximately 5×10^{-3} M of pyridine and DMF both at room and liquid nitrogen temperatures are recorded with a Varian E-4 *X*-band spectrometer using E-231 type of cavity. DPPH is used as a field marker. The accuracies in *g*, hyperfine line separation and linewidth are about $\pm 0{\cdot}001$, ± 2 gauss and $\pm$ 3 gauss respectively. A Unicam SP 700 spectrophotometer is used to record optical absorption in the above solutions.

3. Results and Discussion

The EPR spectra of all the complexes at room temperature are found to show four spin-dependent linewidths. At liquid nitrogen temperature, the EPR spectrum of Cu(salof)tu in DMF is unusual as shown in Fig. 1A. From the spectrum it is evident that two rhombic copper(II) species are present. Since the hyperfine lines on the low field side are less intense than the lines on the high field side, the ground state of these species may be dominated by $d_{z^2-y^2}$ orbital with slight mixing from d_{z^2} orbital. The

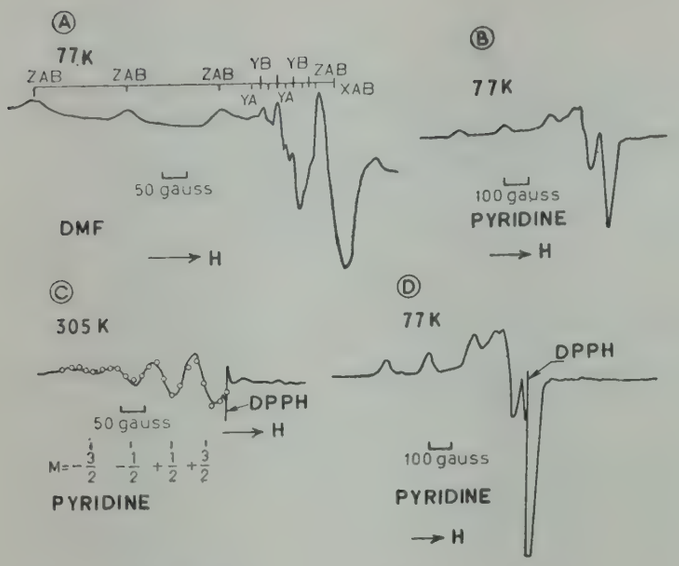

Fig. 1—EPR spectra of : (A) Cu(salof)tu in DMF at 77 K, (B) Cu(salof)tu in pyridine at 77 K, (C) Cu(salen)tu in pyridine at 305 K and (D) Cu(salen)tu in pyridine at 77 K [The circles on the room temperature spectrum (C) correspond to the absorption values obtained using Eq. (16) for the linewidths 42, 45, 62 and 88 gauss corresponding to the M values 3/2, 1/2, −1/2 and −3/2 respectively.]

hyperfine lines of both the species in the g_z direction are very close and are superposed on each other. Except the extreme left line ($M = -3/2$), which is clearly a doublet, all others are single lines, indicating that the g_z values of both the species are almost equal. But the hyperfine lines in the g_y direction of both the species are partially resolved. The single strong line on the extreme right must have resulted due to the superposition of two single unresolved lines due to g_x components of both the species. As shown in Fig. 1 A, the $M=3/2$ line of the g_z component is also superposed on this line. The EPR spectrum in the pyridine solution of this complex (Fig. 1B) is less complicated which may be due to the closeness of g and A values of both the species brought by the interaction of pyridine with both the species. Even though this spectrum also appears to be rhombic, due to the superposition of g_y component on g_x, it is not possible to evaluate the above values separately. The spectra of Cu(salen)tu in pyridine (Fig. 1D) is same as the above spectrum (Fig. 1B). But in this complex, only one type of species is existing.[3] Due to the difficulties involved in getting the values of g_x, g_y, A_x and A_y separately, we have calculated the values of $g_\perp \left[= \frac{(g_x + g_y)}{2}\right]$ and $A_\perp \left[= \frac{(A_x + A_y)}{2}\right]$ from the room temperature (g_0 and a) and low temperature spectra using the following equations :

$$g_0 = \frac{g_{\|} + 2\, g_\perp}{3} \qquad \ldots(1)$$

$$a = \frac{A_{\|} + 2\, A_\perp}{3} \qquad \ldots(2)$$

The $g_{\|}$ (g_z) and $A_{\|}$ (A_z) values can be obtained from the low temperature spectra using the methods of Sands[4] and Germann and Swallen.[5] The principal g, A and optical absorption values along with the corresponding values of other CuN_2O_2 systems are given in Table 1. In the case of Cu(salof)tu in pyridine solution, the higher values of $g_{\|}$ and smaller values of $A_{\|}$ compared to DMF solution indicate that the solvation in pyridine is more than in DMF. From the g and A values it is evident that in all complexes, the copper (II) ions have $d_{x^2-y^2}$ ground-state.

Since two types of atoms are bonded with the copper, in the absence of superhyperfine structure and detailed optical data in single crystals it is difficult to get all the molecular orbital coefficients constituting the bond parameters.

In the absence of the above details, the approximate relations between the spin-Hamiltonian constants, bond parameters and optical absorption data are given as follows :

$$g_{\|} = 2 - \frac{8\,\lambda\,\alpha^2\,\beta_1^2}{\Delta E_{xy}} \qquad \ldots(3)$$

$$g_\perp = 2 - \frac{2\,\lambda\,\alpha^2\beta^2}{\Delta E_{xz}} \qquad \ldots(4)$$

$$A_{\|} = P\,[-4/7\,\alpha^2 + (g_{\|} - 2) + 3/7\,(g_\perp - 2) - k + \text{small terms}] \qquad \ldots(5)$$

$$A_\perp = P\,[2/7\,\alpha^2 + 11/14\,(g_\perp - 2) - k + \text{small terms}] \qquad \ldots(6)$$

$$a = P\,[g_0 - 2 - k + \text{small terms}] \qquad \ldots(7)$$

where the constants have their usual meanings.[6]

From Eqs. (3), (4) and (5), an expression for α^2 can be obtained as follows :

$$\alpha^2 = \frac{7}{4}\left[\frac{|\,A_{\|}\,|}{P} - \frac{|\,a\,|}{P} + \frac{2}{3}\,g_{\|} - \frac{5}{21}\,g_\perp - \frac{6}{7}\right] \qquad \ldots(8)$$

Only one broad optical absorption peak for both the complexes in pyridine and DMF is obtained, the values of which are given in Table 1. It is assumed that this value corresponds to ΔE_{xy} and ΔE_{xy}, ΔE_{xz}, and ΔE_{yz} are degenerate. Using these values, the values of in- and out-of-plane π-bondings and orbital reduction factors $r_{\|}$ ($\alpha\beta$) and $r_\perp$ ($\alpha\beta$) are estimated. The g and ΔE values of the present two complexes in solutions are comparable to the corresponding values in Cu(N-n-Prsalim)$_2$ and Cu(N-Mesalim)$_2$.[1] It is surprising to note that the $g_{\|}$ values of Cu(Et$_2$ − α − Al)$_2$ (Ref. 1) are smaller and ΔE values are larger than those for all the members in Table 1, even though the Cu—O and Cu—N bond lengths are larger

Table 1—Spin-Hamiltonian and Bond Parameters of Some Copper (II) Complexes with CuN_2O_2 Chromophores

Substance	g_z	g_y	g_x	$A_z\times10^4$ cm^{-1}	$A_y\times10^4$ cm^{-1}	$A_x\times10^4$ cm^{-1}	ΔE_{xy} (kK)	ΔE_{xz} (kK)	ΔE_{yz} (kK)	α^2	β_1^2	β^2	$r_{\|\|}$	$r_\perp$	Cu—O distance (Å)	Cu—N distance (Å)
Bis (N-n-propylsalicylal† diminato) copper (II) Cu (-N-n-propalim)$_2$ (Ref. 1)	2·2254	2·0648	2·0425				14-17 (assumed)§	14·8	16·4				0·69 −0·76 (assumed)	0·71	1·86	1·99
Bis (N-methylsalicylaldiminato) copper (II)* Cu (N-Mesalim)$_2$ (Ref. 1)	2·2157	2·0386	2·0561				14-17 (assumed)§	15·2	17·0				0·67 −0·74	0·71	1·901	1·989
Cu [(±)-NN-diethyl-α-alamine]$_2$† Cu (Et$_2$-α-Al)$_2$ (Ref. 1)	2·1967	2·0507	2·0390				17-21 (assumed)§	17·4	20·8				0·71 to 0·79 (assumed)	0·71	1·911	2·031
Copper (II) Glycinate‡ (Ref. 2)	2·2674	2·055	2·055	141·0	10	10	15·75			0·89	0·71		0·795			1·984 2·021
N, N-ethylenebis (salicylal diminato) copper (II) thiourea Cu(Salen)tu (a) pyridine	2·228	2·049	2·049	186·5	31·4@	31·4@	17560			0·781	·774	0·665	0·77	0·72	1·890 1·891	1·945 1·918
N, N-*o*-phenylene bis (salicylal diminato) copper (II) thiourea Cu(salof)tu (a) DMF Species A	2·218	2·059	2·031	196·0	28·7@	—	17·0			0·814	0·687	0·743	0·748		1·893 1·902	1·942 1·960
Species B	2·218	2·069	2·031	196·0	33·7@	—	17·0			0·810	0·690	0·870	0·748		1·889 1·902	1·946 1·970
(b) Pyridine	2·232	2·0505C	2·0505C	192·0	27·6@	27·6@	16·44			0·807	0·713	0·621	0·758	0·710		

† ESR studies in undiluted single crystal studies; ‡ Studies in solution; * Copper complex diluted in isomorphous zinc salt. @ Calculated using Eqs. (1) & (2); § Assumed by Dudly *et al.* (Ref. 1).

than those for other members. It is reasonable to get larger $g_{\|}$ and smaller $A_{\|}$ values in the case of copper (II) glycinate[2] because of larger metal-ligand bond lengths compared to the other complexes. The value of $r_{\|}$ of the complexes mentioned in Table 1 is of the same order indicating that the in-plane (both σ and π) bond strengths are of comparable magnitudes in all the complexes. In the case of Cu(salen)tu dissolved in pyridine, $r_{\perp}$ is more than those for the other complexes, indicating a relatively weak out-of-plane π-bonding in the above complex. But it should be remembered that unambiguous data of ΔE_{xz} in the complexes under investigation are not available to correctly estimate the out-of-plane π-bond.

For dilute solutions where dipolar and exchange interactions are negligible, Wilson and Kivelson[7] developed a theory of hyperfine linewidth, considering motional modulation of the anisotropic g and A tensors on the linewidth. Assuming Lorentz shape, the linewidth for different M values is given as

$$T_2^{-1} = A + BM + CM^2 + DM^3 \qquad ...(9)$$

The expressions for the linewidth parameters A, B, C and D are given from their theory as :

$$\frac{A}{\tau_R} = \frac{1}{45}\left[(\Delta\gamma H_0)^2 + 3(\delta r H_0)^2\right](4+3u) + \frac{1}{40} b^2 I(I+1)(3+7u) + \frac{2}{15} C^2 I(I+1)(3+7u) - \frac{1}{8} b^2 I(I+1)\frac{a}{\omega_0} uf - \frac{1}{30}\Delta\gamma H_0 bI(I+1)\frac{a}{\omega_0}(1+u) \qquad ...(10)$$

$$\frac{B}{\tau_R} = \frac{1}{15}(b\Delta\gamma H_0 + 4C\delta\gamma H_0)(4+3u) - \frac{2}{45}(\Delta\gamma H_0)^2(4+3u+3uf)\frac{a}{\omega_0} - \frac{1}{20} b^2 I(I+1)\frac{a}{\omega_0}(4+3u+7uf) + \frac{1}{40} b^2 \frac{a}{\omega_0}(3+2u)\left[2I(I+1)-1\right] \qquad ...(11)$$

$$\frac{C}{\tau_R} = \frac{b^2}{40}(5-u) + \frac{2}{15} C^2(5-u) + \frac{1}{8} b^2 \frac{a}{\omega_0} uf - \frac{1}{30}(\Delta r b H_0)\frac{a}{\omega_0}(7+5u+12uf) \qquad ...(12)$$

$$\frac{D}{\tau_R} = \frac{1}{20} b^2 \frac{a}{\omega_0}(1+u+uf) \qquad ...(13)$$

where

$$u = (1+\omega_0^2 \cdot T_R^2)^{-1};\ f = \omega_0^2\,\tau_R^2\,u$$

$$b = \frac{2}{3}(A_{\|} - A_{\perp}) \text{ rad/sec}$$

$$c = \frac{1}{4}(A_x - A_y) \text{ rad/sec}$$

$$\Delta\gamma = \beta_0 \Delta g/\hbar \qquad \Delta g = g_{\|} - g_{\perp}$$

$$\delta\gamma = \beta_0 \delta g/\hbar \qquad \delta g = \tfrac{1}{2}(g_x - g_y)\rho_0/\hbar$$

$$\tau_R = \frac{4}{3}\frac{\pi r^3 \eta}{kT}$$

In order to fit the experimental results, a factor A' is introduced in Eq. (9) and the modified equation is given as

$$\Delta H = (A + A') + BM + CM^2 + DM^3 \qquad ...(14)$$

The spin-rotational relaxation which contributes to the residual linewidth, as derived by Wilson and Kivelson,[7] is given as

$$\alpha_{RS} = \frac{2\hbar}{\sqrt{3}\,\beta_0 g_0}\ \frac{1}{12\pi r^3}(\Delta g_{\|}^2 + 2\Delta g_{\perp}^2)\frac{kT}{\eta} \qquad ...(15)$$

Relaxations due to electric field fluctuations from van Vleck[8] and Orbach[9] processes may also contribute to this residual linewidth. The EPR spectrum of Cu(salof)tu in both the solvents at room temperature is complicated due to the superposition of the spectra of two molecules. Due to this fact, we have taken up linewidth calculations for Cu(salen)tu complex in pyridine only. Since the hyperfine linewidths are broad and there is overlapping, the experimental absorption curve is fitted into the equations given below assuming the Lorentz shape to the lines, to get the correct linewidths for a best fit[10,11]

$$\frac{df(H)}{dH} = \frac{2A''}{2I+1}\sum_{\nu=1}^{2I+1}\frac{(\Delta H_{1/2\nu})\quad (H_0 - M_\nu a - H)}{[(\Delta H_{1/2\nu})^2 + (H_0 - M_\nu a - H)]^2} \qquad ...(16)$$

where the constants have their usual meanings.[10] For Lorentz lineshape, the half-width at half-power points is related to the peak-to-peak linewidth (ΔH) as $\Delta H_{1/2} = (\sqrt{3}/2)\,\Delta H$, which is substituted in Eq. (16). The calculated absorption values are shown in Fig. 1 as circles for the linewidths 42, 45, 62, 88 gauss for a best fit. Substituting these values in Eq. (14), the values obtained for $(A + A')$, B, C and D are, 52·06, −17·21, 5·75, −0·833 respectively.

Using Eqs. (11) and (12), the values of B and C are calculated adjusting hydrodynamic radius (r) in

such a way that these values are near to the experimental values obtained above. Using this value of r, the values of A and D are calculated. The values of A, B, C and D thus calculated come out to be 23·07, −17·08, 2·83, −0·0547 respectively. The residual linewidth is obtained by subtracting A from $(A + A')$. Using the experimentally obtained $(A + A')$ value and calculated values of B, C and D, the linewidths are calculated with the help of Eq. (14). The values thus obtained are 32·8, 44, 61·40 and 84 for M equal to 3/2, 1/2, −1/2 and −3/2 respectively.

The agreement between the experimental values and calculated values is fairly good except for the line $M = 3/2$. The contribution from spin-rotational relaxation is calculated using Eq. (15) and comes out be 3·28 gauss. As discussed earlier, the contribution to the residual linewidth from other sources may be more than that from the spin-rotational relaxation. This difference may arise due to the anisotropic tumbling motion of the molecule.[12]

Acknowledgement

The authors are thankful to Prof. K V Krishna Rao, Head of the Department for his constant encouragement and to Prof. Navneetha Rao, Head of the Department of Chemistry for giving facilities to take optical data. One of them (S Md A) is grateful to the University Grants Commission, New Delhi, for financial assistance.

References

1. Dudley R J, Fereday J, Hathaway B J & Hodgson, *J. chem. Soc. Dalton*, 6 (1972), 1341.
2. Kuska H A & Rogers M T, *J. chem. Phys.*, 43 (1965), 1744.
3. Ferrari M B, Fava G G & Pelizzi C, *Acta crystallogr.*, 32B (1976), 901.
4. Sands R H, *Phys. Rev.*, 99 (1955), 1222.
5. Gersmann H R & Swallen J D, *J. chem. Phys.*, 36 (1962), 3221.
6. Maki A H & McGarvey B A, *J. chem. Phys.*, 29 (1958), 31, 35.
7. Wilson R & Kivelson D, *J. chem. Phys.*, 44 (1966), 154, 4440, 4445.
8. van Vleck J H, *Phys. Rev.*, 57 (1940), 426.
9. Orbach R, *Proc. phys. Soc. Lond.*, A77 (1961), 821.
10. Noack M & Gordon G, *J. chem. Phys.*, 48 (1968), 2689.
11. Lewis W B, Alei M & Morgan L O, *J. chem. Phys.*, 44 (1966), 2409.
12. Hoel D & Kivelson D, *J. chem. Phys.*, 62 (1975), 4535.

Indian Journal of Pure & Applied Physics
Vol. 18, May 1980, pp. 342-347

Dispersion Effects in the FM Mode-Locked Laser

K P Jagannatha Reddy

Department of Industrial Research, Birla Institute of Technology, Mesra, Ranchi 835 215

Received 13 *September* 1978; *accepted* 13 *December* 1979

A theory of FM mode-locking in lasers with a phase modulator whose modulation frequency is slightly detuned from optimum frequency is presented, by taking dispersion effects into consideration. It is found that one of the main effects of the dispersion is to decrease the time taken by the system to reach the steady state. Dispersion causes pulse stretching for positive modes and pulse compression for negative modes. The condition for equalizing the pulse widths of the opposite modes is found.

1. Introduction

A good progress has been made in the generation of powerful coherent light pulses of picosecond duration by a process of mode-locking of lasers. Both active and passive mode-locking of lasers have proved to be reliable means for bandwidth limited pulses.

Prior to the work of Kuizenga and Siegman,[1] theoretical studies were confined to mode-locking of lasers with inhomogeneously broadened atomic lines. A linearized solution of such problems has been discussed by DiDomenico,[2] Yariv[3] and Crowell.[4] Detailed nonlinear calculations for the FM and AM type mode-locking have been given by Haris and Mcduff.[5] All the above analyses, where the coupled-mode-equations has been used, led to a good understanding of mode-locked gas lasers like He-Ne laser and argon laser.

Even though mode-locking of solid state lasers by intracavity active modulator has been experimentally observed by several workers,[6-9] there was no satisfactory theory till 1970.[1] In analyzing these homogeneously broadened lasers, the use of the coupled mode equations is complicated due to the fact that the axial modes do not saturate independently and also due to the fact that a very large number of coupled axial modes are usually generated.

In Ref. 1, the authors have followed a different approach to the above problem; working completely in the time domain. Their approach is similar to that used by Cutler[10] where it is assumed that there is a short pulse inside the laser cavity and it is followed once around the laser cavity, through active medium and the modulator. In steady state operation, the net change in the pulse in one round trip is zero. This self-consistency requirement gives the solutions for pulse parameters. A similar approach in the case of passive mode locking of lasers with a saturable absorber has recently been used by several workers.[11-14]

In Refs. 1 and 15, the authors have considered the problem of mode-locking of homogeneously broadened lasers by a intracavity modulator with modulation frequency slightly detuned from its optimum value. In the present paper, we consider the same problem taking the cavity dispersion into account. As in Ref. 1, we follow a Gaussian pulse through the amplifier and the modulator in the cavity where approximations to the atomic line shape and modullation function are made to keep the pulse Gaussian.

2. Properties of Gaussian Pulses, Active Medium and Phase Modulator

2.1 Gaussian Pulses

We will consider the most general Gaussian optical pulse given by

$$E(t) = \tfrac{1}{2} E_0 \exp(-\gamma t^2) \exp(j\omega_p t) \quad \ldots(1)$$

where

$$\gamma = \alpha - j\beta \quad \ldots(2)$$

In Eq. (1) the term α determines the Gaussian envelope of the pulse and the term $j\beta t$ is a chirp during the pulse.

The Fourier transform of Eq. (1) is

$$E(\omega) = \left(\frac{E_0}{2}\right)(\pi/\gamma)^{1/2} \exp\left[-(\omega-\omega_p)^2/4\gamma\right] \quad \ldots(3)$$

The pulse width (τ_p) defined as the time between half-intensity points is given by

$$\tau_p = \{(2 \ln 2)/\alpha\}^{1/2} \quad \ldots(4)$$

The pulse bandwidth (Δf_p) defined as the frequency between half-power points of the pulse spectrum is given by

$$\Delta f_p = (1/\pi)\{2 \ln 2 [(\alpha^2 + \beta^2)/\alpha]\}^{1/2} \quad \ldots(5)$$

The pulsewidth-bandwidth product is given by

$$\tau_p \cdot \Delta f_p = (2 \ln 2/\pi)\{1 + (\beta/\alpha)^2\}^{1/2} \quad ...(6)$$

Two important cases are $\beta = 0$ and $|\beta| = \alpha$. For these two cases $\tau_p \times \Delta f_p = 0{\cdot}440$ and $\tau_p \times \Delta f_p = 0{\cdot}626$. These cases apply to AM and FM modulation respectively.[1]

2.2 Active Medium

The amplitude gain for a homogeneously broadened laser is given by

$$g_a(\omega) = \exp[g/\{1 + 2j(\omega - \omega_a)/\Delta\omega\}] \quad ...(7)$$

where g is the saturated amplitude gain (at $\omega = \omega_a$) for one round trip in the cavity and $\Delta\omega$ is the amplifier linewidth.

If we consider a case where $(\omega - \omega_a) < \Delta\omega$, we can expand Eq. (7) about the frequency ω_p as follows:

$$g_a(\omega) = \exp\left[\frac{g}{x}\left\{1 - \left(\frac{2j}{x}\right)\left(\frac{\omega - \omega_p}{\Delta\omega}\right) - \frac{4}{x^2}\left(\frac{\omega - \omega_p}{\Delta\omega}\right)^2\right\}\right] \quad ...(8)$$

where $\omega_a = \omega_p + \nu$; $\eta = \dfrac{\nu}{\Delta\omega}$;

$$x = 1 + 2j\eta$$

and η is the shift of the spectrum centre frequency ω_p from gain centre frequency ω_a, normalized to the atomic linewidth $\Delta\omega$.

When we consider the modulator detuning we notice the shift of the pulse centre frequency from that of atomic linewidth, hence we should use the above equation for g.

2.3 Phase Modulator

The intracavity phase modulator introduces a sinusoidally varying phase perturbation $\delta(t)$ such that the round-trip transmission through the modulator is given by Yariv[16] as :

$$\exp[-j\delta(t)] = \exp(-j2\delta_c \cos \delta\omega_m t) \quad ...(9)$$

where $\omega_m = 2\pi f_m$ is the modulation frequency and δ_c is the effective single-pass phase retardation of the modulator.

We shall consider the most general case where the pulse goes through the modulator at a phase angle θ from the ideal case. Then with the assumption that the pulsewidth (τ_p) is smaller than the modulation period $(T_m = 1/f_m)$ we can expand Eq. (9) as

$$\exp[-j\delta(t)] = \exp[\mp j2\delta_c \cos\theta \pm j2\delta_c \sin\theta(\omega_m t) \pm j\delta_c \cos\theta(\omega_m t)^2] \quad ...(10)$$

Eq. (10) shows that there can exist two possible solutions. We shall call the mode of operation corresponding to the top sign in Eq. (10) as the +ve mode and the other as the −ve mode.

In Eq. (10), the first term is an additional phase shift that changes the optical length of the cavity, from L to L_0 where

$$L_0 = L \pm \left(\frac{\delta_c}{\pi}\right)\lambda_a \cos\theta \quad ...(11)$$

The second term is a Doppler frequency shift as reported by Kafiro *et al.*,[17] and gives a linear frequency chirp to the pulse. The last term causes the mode-locking.

3. Effect of Cavity Dispersion

In the region of negative-absorption frequencies, the change of the refractive index can be represented by

$$n(\omega) = n + n'(\omega - \omega_a) + \frac{n''}{2}(\omega - \omega_a)^2 + \ldots \quad ...(12)$$

where

$$n = n(\omega = \omega_a);\ n' = \frac{\partial n}{\partial\omega},\ n'' = \frac{\partial^2 n}{\partial\omega^2}.$$

Let us consider a Fabry-Perot cavity of length L containing an amplifying medium and a modulating crystal of lengths $l c_1$ and $l c_2$ respectively.

Then the total optical length of the cavity becomes

$$L_{opt} = L_0 + L_0'(\omega - \omega_a) + L_0''(\omega - \omega_a)^2 + \ldots \quad ...(13)$$

$$= L_0 + (\omega - \omega_p)M + (\omega - \omega_p)^2 L_0'' - \Delta\omega\,\eta N \quad ...(13a)$$

where

$$L_0 = lc_{av} + (n_1 - 1)\,l c_1 + (n_2 - 1)\,l c_2$$

$$= L \pm \left(\frac{\delta_c}{\pi}\right)\lambda_a \cos\theta$$

$$L_0' = n_1' l c_1 + n_2' l c_2$$

$$L_0'' = (n_1''/2) l c_1 + (n_2''/2) l c_2$$

$$M = L_0' - 2L_0''\eta\Delta\omega$$

$$N = L_0' - L_0''\eta\Delta\omega.$$

Let $L_{opt} = L_0 + L_d$

where

$$L_d = (\omega - \omega_p)M + (\omega - \omega_p)^2 L_0'' - \Delta\omega\,\eta N. \quad ...(13b)$$

L_0 is the optical length in absence of dispersion. The two extra terms in Eq. (13) due to the dispersion induce an additional phase shift per round-trip given by :

$$(\omega/c)\left[2L_0'(\omega - \omega_a) + 2L_0''(\omega - \omega_a)^2\right]. \quad ...(14)$$

We add this to the gain of active medium given by Eq. (8) and get the effective gain

$$g_e(\omega) = \exp\left[g_1\left\{1-2j\left(\frac{\omega-\omega_p}{\Delta\omega}\right)\frac{g_2}{g_1} - 4\left(\frac{\omega-\omega_p}{\Delta\omega}\right)^2\frac{g_3}{g_1}\right\}\right] \quad ...(15)$$

where

$$g_1 = \frac{g}{x} + 2j\left(\frac{\omega}{c}\right)\eta\,\Delta\omega\,N \quad ...(16a)$$

$$g_2 = \frac{g}{x^2} + \left(\frac{\omega}{c}\right)\Delta\omega\,M \quad ...(16b)$$

$$g_3 = \frac{g}{x^3} + jL_0''\Delta\omega^2\left(\frac{\omega}{2C}\right) \quad ...(16c)$$

We can write Eq. (15) as

$$g_e(\omega) = G\left[\exp\left\{-2jg_2\left(\frac{\omega-\omega_p}{\Delta\omega}\right) - g_3\left(\frac{\omega-\omega_p}{\Delta\omega}\right)^2\right\}\right] \quad ...(15a)$$

where $G = \exp(g_1)$. ...(15b)

Eq. (15 a) is the effective gain which contains the dispersion effects due to all components which are present in the cavity. Taking this as the starting gain we will proceed to seek self-consistent solutions when the modulator frequency is slightly detuned from the ideal modulation-frequency (f_{m0}).

4. Self-consistent Solution with Detuning

If we call f_{m0} as the ideal frequency of mode-locking then the detuning is defined as

$$\Delta f_m = f_{m0} - f_m \quad ...(17)$$

Note that Δf_m is negative for $f_m > f_{m0}$ and vice versa. Now let us assume that a pulse $E_1(\omega)$ with frequency spectrum given by Eq. (3) goes through the amplifier. When this pulse arrives at reference plane as shown in Fig. 1. It will have a frequency spectrum

$$E_2(\omega) = g_e(\omega)\,E_1(\omega) = \frac{E_0}{2}\,G(\pi/\gamma)^{1/2}\exp\left[-A(\omega-\omega_p)^2\right]\exp\left[-jB(\omega-\omega_p)\right] \quad ...(18)$$

where

$$A = \frac{1}{4\gamma} + \frac{4g_3}{\Delta\omega^2} \quad ...(18a)$$

$$B = \frac{2g_2}{\Delta\omega} \quad ...(18b)$$

Fourier transforming Eq. (18) we get

$$E_2(t) = \int_{-\infty}^{\infty} E_2(\omega)\,e^{j\omega t}\,d\omega$$

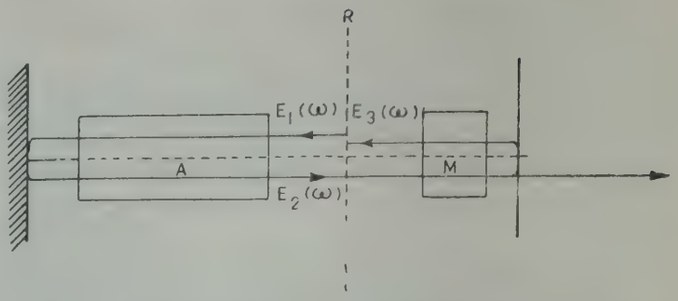

Fig. 1—Fabry-Perot Resonator containing the active medium (A) and the modulator (M). R is the reference plane

$$= \frac{E_0\,G}{4\sqrt{\gamma A}}\exp\left[-(t-B)^2/4A\right]\exp j\omega_p t \quad ...(19)$$

In Eq. (19), B is a complex quantity hence we can split it into real and imaginary parts. By doing this we can write

$$\frac{(t-B)^2}{4A} = \left[\left\{(t-\frac{2g}{\Delta\omega}y) - 2\left(\frac{\omega}{c}\right)N + \frac{K_1}{2}\right\}^2\Big/4A\right] - \frac{K_1^2}{16A} - \frac{64g^2\eta^2}{\Delta\omega^2(1+4\eta^2)^4\,4A} + jK_2\left[(t-\frac{2g}{\Delta\omega}y) - 2\left(\frac{\omega}{c}\right)N\right] \quad ...(20)$$

where $y = (1-4\eta^2)/(1+4\eta^2)^2$ ...(20a)

In the above equation we have used the expansion

$$\frac{16jg\eta}{\Delta\omega(1+4\eta^2)^2\,4A} = \frac{K_1}{4A} + jK_2 \quad ...(20b)$$

where

$$K_2 = \frac{16g(\alpha^2+\beta^2)(1+4\eta^2)}{10g(\alpha^2+\beta^2)(1-12\eta^2)+\alpha\Delta\omega^2(1+4\eta^2)^3} \quad ...(20c)$$

$$K_1 = K_2\left\{\frac{\beta}{\alpha^2+\beta^2} - \frac{16g}{\Delta\omega^2}\left[\frac{6\eta-8\eta^3}{(1+4\eta^2)^3}\right] + L_0''\Delta\omega^2\left(\frac{\omega}{2c}\right)\right\} \quad ...(20d)$$

By substituting Eq. (20) in Eq. (19) we get

$$E_2(t) = \frac{E_0\,G}{4\sqrt{\gamma A}}$$

where

$$M = \exp-\left[\left\{\left(t-\frac{2g}{\Delta\omega}y\right) - 2\left(\frac{\omega}{c}\right)N + \frac{K_1}{2}\right\}^2\Big/4A\right]\exp\left[j(\omega_p-K_2)t\right]\cdot\exp\left[\frac{K_1^2}{16A} + jK_2\left\{\frac{2g}{\Delta\omega}y - 2\left(\frac{\omega}{c}\right)N\right\} + \frac{64g^2\eta^2}{\Delta\omega^2(1+4\eta^2)^4\,4A}\right] \quad ...(21)$$

By inspecting Eq. (21) we notice some changes of the pulse due to the dispersive gain $[g_e(\omega)]$.

1. The pulse envelope has been delayed by a factor

$$\frac{2g}{\Delta\omega} y + 2\left(\frac{\omega}{c}\right) N + \frac{K_1}{2}$$

This change will compensate exactly for the change in modulation frequency.

By comparing with Ref. 1, we notice that the dispersion has delayed the pulse envelope by a factor $2(\omega/c)N$.

2. A frequency shift K_2 has been introduced.

3. An additional phase shift has been introduced by dispersion which is given by

$$\exp\left[-2K_2\left(\frac{\omega}{c}\right)N\right]$$

The output pulse from the modulator is given by $E_3(t) = [\exp -j\delta(t)]. E_2(t)$

$$= \frac{r E_0 G}{4\sqrt{\gamma A}} \cdot \exp -\left[\left(t - \frac{2g}{\Delta\omega} y\right) - 2\left(\frac{\omega}{c}\right)N + \frac{K_1}{2}\right]^2 \left(\frac{1}{4A} \mp j\omega_m^2 \cos\theta\right)$$

$$\exp\left\{\left[\left(t - \frac{2g}{\Delta\omega} y\right) - 2\left(\frac{\omega}{c}\right)N + \frac{K_1}{2}\right]\left[\omega_p - (K_2 \mp 2\delta_c \omega_m \sin\theta)\right]\right\}$$

$$\exp\left[\frac{K_1^2}{16A} + \frac{64 g^2 \eta^2}{\Delta\omega^2 (1+4\eta^2)^4 4A}\right]$$

$$\exp\left[\frac{2g}{\Delta\omega} y - 2\left(\frac{\omega}{c}\right)N\right] \qquad \ldots(22)$$

where r is the reflection coefficient of the mirror. For self-consistent solutions to exist, the pulse envelope should pass through the modulator at the same modulation phase every time. Hence, the total round-trip time for the envelope T_m is same as the modulation period ($T_m = 1/f_m$).

Therefore, the self-consistency requirement becomes

$$E_1(t - T_m) e^{-j\phi} = E_2\left(t - \frac{2L_{opt}}{c}\right) \qquad \ldots(23)$$

Putting Eq. (22) in Eq. (23) and equating the identical terms on both sides we get,

$$T_m = \frac{2L_{opt}}{c} + \frac{2g}{\Delta\omega} y + 2\left(\frac{\omega}{c}\right)N - \frac{K_1}{2} \qquad \ldots(24a)$$

$$K_2 = \pm 2\delta_c \omega_m^2 \sin\theta \qquad \ldots(24b)$$

$$\gamma = \frac{1}{4A} \mp j\delta_c \omega_m^2 \cos\theta \qquad \ldots(24c)$$

and

$$\left|\frac{rG}{2\sqrt{\gamma A}}\right| \cdot \left|\exp\left[\frac{K_1^2}{16A} + \frac{16 g^2 \eta^2}{\Delta\omega^2 (1+4\eta^2)^4 A}\right]\right| = 1 \qquad \ldots(24d)$$

In Eq. (24 d), we have equated only magnitude because the phase part has no importance in our discussion. By putting the value of A from Eq. (18 a) in Eq. (24 a) and assuming $\Delta\omega^2/4\ \omega_m^2\ \delta_c >> 1$, we get

$$\gamma = \left(\omega_m \frac{\Delta\omega}{4}\right)\left[\mp j \frac{\delta_c \cos\theta\, x^3}{g \mp j L_0'' \frac{\Delta\omega^2}{2}\left(\frac{\omega}{c}\right) x^3}\right]^{1/2} \qquad \ldots(25)$$

This equation can be written as

$$\gamma = \alpha - j\beta$$

$$= \left(\frac{\omega_m \Delta\omega}{4}\right)\left(\frac{\delta_c \cos\theta}{2g}\right)^{1/2} P\left[(1 \mp Q) \mp j(1 \pm Q)\right] \qquad \ldots(26)$$

where

$$P = \frac{(1+4\eta^2)^{3/2}}{(1-12\eta^2)^{1/2}} \qquad \ldots(26a)$$

and

$$Q = \frac{1}{2(1-12\eta^2)}\left[L_0''\left(\frac{\omega}{c}\right)\frac{\Delta\omega^2}{2g}(1+4\eta^2)^3 - (6\eta - 8\eta^3)\right] \qquad \ldots(26b)$$

while deriving the above equation we have assumed that

$$g > L_0''\left(\frac{\omega}{c}\right)\frac{\Delta\omega^2}{2}.$$

Equating real and imaginary parts we get

$$\alpha = \pi^2 (f_m \Delta f)\left(\frac{\delta_c \cos\theta}{2g}\right)^{1/2} P(1 \mp Q) \qquad \ldots(27)$$

$$\beta = \pm \pi^2 (f_m \Delta f)\left(\frac{\delta_c \cos\theta}{2g}\right)^{1/2} P(1 \pm Q) \qquad \ldots(28)$$

α and β have got different values for positive and negative modes. By using Eqs. (27) and (28) in Eqs. (4) and (5) we get the following expressions for the pulsewidth (τ_p) and the pulse bandwidth (Δf_p);

$$\tau_p = \frac{(2\ln 2)^{1/2}}{\pi}\left(\frac{2g}{\delta_c \cos\theta}\right)^{1/4} P^{-1/2}\left(\frac{1}{f_m \Delta f}\right)^{1/2}\left(\frac{1}{1 \mp Q}\right)^{1/2} \qquad \ldots(29)$$

$$\Delta f_p = \sqrt{2}(2\ln 2)^{1/2}(f_m \Delta f)^{1/2}\left(\frac{\delta_c \cos\theta}{2g}\right)^{1/4} P^{1/2}\left(\frac{1+Q^2}{1 \mp Q}\right)^{1/2} \qquad \ldots(30)$$

The pulsewidth-bandwidth product is given by

$$\tau_p \cdot \Delta f_p = \sqrt{2}\left(\frac{2\ln 2}{\pi}\right)\left(\frac{\sqrt{1+Q^2}}{1 \mp Q}\right) \quad ...(31)$$

With the assumption that $\Delta\ \omega/\omega_m \gg 1$ we can show that

$$K_2 = \frac{26\, g\, \eta}{\alpha\, \Delta\, \omega\, (1+4\,\eta^2)^2} \quad ...(32)$$

and

$$K_1 = \frac{16\, g\, \eta}{\Delta\, \omega\, (1+4\,\eta^2)^2}\left[\left(\frac{\beta}{\alpha}\right) + \left(\frac{\alpha^2+\beta^2}{\alpha}\right) L_0'' \left(\frac{\omega}{2\,c}\right) \Delta\, \omega\right] \quad ...(33)$$

From Eqs. (24 a) and (23) we get the modulation frequency

$$f_m = \left\{\left(\frac{2\,L}{c}\right) \pm 2\left(\frac{\delta_c}{\pi}\right)\frac{\lambda_a}{c}\cos\theta + \left(\frac{2\,L_d}{c}\right) + \frac{2\,g}{\Delta\,\omega}\,y + \left(\frac{2\,\omega}{c}\right) N - \frac{16\, g\, \eta}{\Delta\,\omega\,(1+4\,\eta^2)^2}\left[\left(\frac{\beta}{\alpha}\right) + \left(\frac{\alpha^2+\beta^2}{\alpha}\right) L_0''\left(\frac{\omega}{2\,c}\right)\Delta\,\omega\right]\right\}^{-1} \quad ...(34)$$

From Eqs. (24 b) and (32) we get

$$\cos\theta = \left[4\,\delta_c^2\ \omega_m^2 - 64\ \frac{g^2\,\eta^2\,(\alpha^2+\beta^2)^2}{\alpha^2\,\Delta\,\omega^2\,(1+4\,\eta^2)^4}\right]^{1/2}\left(\frac{1}{\delta_c\,\omega_m}\right) \quad ...(35)$$

Finally, from Eq. (24 d) under the assumption

$$\Delta\, f_p \gg \sqrt{\delta_c\, f_m} \quad ...(36a)$$

We get $g \simeq \frac{1}{2}(1 + 4\,\eta^2)\ln\left(\frac{1}{R}\right)$ ...(36b)

We have now obtained all the necessary equations to discuss the effects of dispersion on mode-locking solutions of the FM mode-locked laser with detuned modulator.

5. Discussion

From Eqs. (27) and (28), α and β have different values for positive and negative modes. The dispersion has caused, pulse stretching for positive mode and pulse compression for negative mode. Therefore, the dispersion is one of the processes which lifts the degeneracy of the positive and negative modes.

The dispersion has also changed the modulation frequency f_m [Eq. (34)]. It has caused an additional delay. But, the delay caused by the dispersion does not discriminate between the two different modes. Hence the frequency discrimination of the two opposite modes solely depends upon δ_c for a given ideal frequency of mode-locking (f_{m0}).

From Eq. (10) we note that the pulses experience some Doppler shift and in consecutive passes through the modulator, the optical frequency (ω_p) of the pulses is shifted until some equilibrium is reached where the Doppler shift of the modulator is cancelled out by an equal and opposite frequency shift from the active medium. K_2 is the frequency shift introduced by the active medium and the equilibrium condition is given by the Eq. (24c). From Eq. (32) we have

$$K_2 = \frac{32\, g\, \eta\, \pi^2\, (f_m\, \Delta f)}{\Delta\, \omega\, (1+4\,\eta^2)^2}\left(\frac{\delta_c\cos\theta}{2\,g}\right)^{1/2} P\left(\frac{1+Q^2}{1 \mp Q}\right) \quad ...(37)$$

By substituting for P and Q from Eqs. (26a, b), we see from Eq. (37) that the frequency shift caused by the active medium is increased due to the dispersion. Therefore, from the equilibrium equation [Eq. (24 b)] it is clear that the equilibrium (steady state) is reached much before, compared to that in absence of the dispersion. Hence the dispersion in the FM mode-locking of a laser by a detuned modulator causes a decrease in the time taken by the system to reach the steady state.

The difference between the pulse-widths of positive and negative modes is given by [from Eq. (29)].

$$\tau_p{}^+ - \tau_p{}^- = \sqrt{2}\left(\frac{2\ln 2}{\pi}\right)^{1/2}\left(\frac{2\,g}{\delta_c\cos\theta}\right)^{1/2} P^{-1/2}\left(\frac{1}{f_m\,\Delta f}\right)^{1/2}\left[\frac{1}{1-Q^2} - \frac{1}{\sqrt{1-Q^2}}\right] \quad ...(38)$$

From Eq. (38), we see that the pulse-width difference of the positive and negative modes is increased due to the cavity dispersion

When the saturated gain of the active medium satisfies the relation

$$g = \left[\frac{(1+4\,\eta^2)^3}{2\,(6\,\eta - 8\,\eta^3)} L_0''\left(\frac{\omega}{c}\right)\Delta\,\omega^2\right] \quad ...(39)$$

the pulse-widths of the positive and negative modes become equal.

From Eq. (36 b) we note that the dispersion has not caused any change in the saturation gain coefficient of the medium under the assumption given by Eq. (36a).

To achieve the bandwidth limited pulses the dispersion effects due to the components in the cavity should be eliminated. This may be achieved by using supplementary substances whose dispersion has a sign opposite to that of the dispersion of the components in the resonator.[16] In principle, such a method can make the total dispersion to vanish in first order. In this case, only the dispersion of higher orders can cause the broadening of the pulses.

Acknowledgement

The author wishes to thank Dr H G Venkatesh for his guidance in preparing the paper and Dr H C Pande for providing the financial assistance.

References

1. Kuizenga, D J & Siegman A E, *IEEE J. quantum electron.*, QE-6 (1970), 694.
2. DiDomenico (Jr) M, *J. appl. Phys.*, 35 (1964), 2870.
3. Yariv A, *J. appl. Phys.*, 36 (1965), 388.
4. Crowell M H, *IEEE J. quantum electron.*, **QE-1** (1965), 12.
5. Harris S E & McDuff O P, *IEEE J. quantum electron.*, **QE-1** (1965), 245; **QE-3** (1967), 101.
6. DiDomenico (Jr) M, Geusic J E, Marcos H M & Smith R G, *Appl. Phys. Lett.*, 8 (1966), 180.
7. Osterint L M & Foster J D, *J. appl. Phys.*, 39 (1968), 4163.
8. Deutsch T, *Appl. Phys. Lett.*, 7 (1965), 80.
9. Pantell R H & Kohn R L, *IEEE J. quantum electron.*, QE-2 (1966), 306.
10. Cutler C G, *Proc. IRE*, 43 (1955), 140.
11. Haus H A, *J. appl. Phys.*, 46 (1975), 3049.
12. Haus H A, *IEEE J. quantum Electron.*, **QE-11** (1975), 736.
13. Hagelstein P L & Ausschnitt C P, *J. appl. Phys.*, 47 (1976), 224.
14. Ausschnitt C P, *IEEE J. quantum electron.*, **QE-13** (1977), 321.
15. Siegman A E & Kuizenga D J, *IEEE J. quantum electron.*, QE-6 (1970), 803.
16. Yariv A, *Quantum electronics* (John Wiley, New York), 1975.
17. Kafari O, Speiser S & Kimel S, *IEEE J. quantum electron.*, QE-7 (1971), 12.
18. Letokhov V S & Morozov V N, *Soviet Phys. JETP.*, 25 (1967), 862.

Indian Journal of Pure & Applied Physics
Vol. 18, May 1980, pp. 348-350

Effect of Field & Detector Temperatures on Photon Count Statistics

J P DUDEJA*

Optics Division, National Physical Laboratory, New Delhi 110 012

Received 12 *November* 1979

The effect of the temperatures of the incident thermal radiation and of the photodetector on the statistical distribution of photoelectrons has been studied. Expressions for excess photon counts are obtained in four different cases of high and low temperatures of fields and detector. Significant contribution to the excess photon counts is seen to come only from the fields with high temperature.

1. Introduction

The question of origin of excess photon counts in thermal light has recently been debated by several authors.[1-9] Webb[1] attributes it to high temperature of the field implying stimulated emission. This approach has been found to be fundamentally incorrect.[2] Mandel[3] relates it to the interference between stimulated and spontaneous emissions. Several authors[4-8] attribute it to the coupling between incident field and the spontaneously generated field. According to them, the stimulated emission coherently amplifies any initial field, with no change in the nature of photon statistics, apart from the addition of, and interference with spontaneous emission noise, and hence, the excess photon counts are attributed to the superposition of random independent fields from a chaotic source as in the case of spontaneous emission.[7] Rockower and Abraham[8] interpret Tataraskii's effect[9] of the thermal fluctuations in the detector when a coherent field is incident on it, as the sum of a coherent signal and Gaussian thermal noise. According to Selloni *et al.*,[10] the detector acts as a source of an intrinsic Gaussian field, which is superimposed by the incoming field.

2. Theory

Dudeja and Chopra[2] have shown that the excess photon correlation in thermal radiation is due to the high temperature of the field. The detector was assumed to be in thermal equilibrium with the incident field. It is usually not a practical assumption. In the present paper, a more realistic view is taken and different temperatures of the incident field and of the photodetector are considered. In conformity with Rockower *et al.*[8] and Selloni *et al.*,[10] we assume that at high temperatures the photodetector acts as a source of an intrinsic Gaussian field, whereas at low temperatures the harmonic-oscillator model[9] of the detector can be assumed when it acts as a source of intrinsic coherent field. Similarly the incident single-mode thermal radiation obeys Gaussian distribution in amplitude at high temperatures, and a Poisson distribution implying a δ-function distribution in amplitude at low temperatures. Thus we write the following expressions for the probability distribution $[P(\alpha)]$ for incident field and the photodetector:

For incident field (*temperature* T_1)

For high T_1 : P_1

$$(\alpha_1) = \frac{1}{\pi \langle n_1 \rangle} \exp\left(-\frac{|\alpha_1|^2}{\langle n_1 \rangle}\right) \quad \ldots(1)$$

For low T_1 : $P_1(\alpha_1) = \delta(\alpha_1 - \bar{\alpha}_1)$ ...(2)

For photodetector (*temperature* T_2)

For high T_2 :

$$P_2(\alpha_2) = \frac{1}{\pi \langle n_2 \rangle} \exp\left(-\frac{|\alpha_2|^2}{\langle n_2 \rangle}\right) \quad \ldots(3)$$

For low T_2 : $P_2(\alpha_2) = \delta(\alpha_2 - \bar{\alpha}_2)$ ...(4)

In Eqs. (1) and (3) $\langle n_1 \rangle$, $\langle n_2 \rangle$ are the average number of photons due to the incident field and the intrinsic field in the photodetector, respectively. So we have

$$\langle n_1 \rangle = \langle |\alpha_1|^2 \rangle \quad \ldots(5)$$

$$\langle n_2 \rangle = \langle |\alpha_2|^2 \rangle \quad \ldots(6)$$

Since the incident field and the photodetector-field are assumed to be independent of one another, we have

$$\langle n \rangle = \langle n_1 \rangle \langle n_2 \rangle \quad \ldots(7)$$

*Present address : Department of Physics, Punjab Agricultural University, Ludhiana (Punjab)

where $\langle n \rangle$ is the average number of photons in the output field, after the incident field has passed through the photodetector. The joint probability distribution $P(\alpha)$ due to the incident field and photodetector, is given by the convolution of their individual probability distributions $P_1(\alpha_1)$ and $P_2(\alpha_2)$. Thus

$$P(\alpha) = P_1(\alpha_1) \otimes P_2(\alpha_2) = \int P_1(\alpha-\alpha_1)\, P_2(\alpha_1)\, d^2\alpha_1 \quad ...(8)$$

where $\alpha = \alpha_1 + \alpha_2$ ...(9)

$P(\alpha)$ will be the distribution of the output field. Also we have

$$\langle n \rangle = \langle |\alpha|^2 \rangle = \int |\alpha|^2 P(\alpha)\, d^2\alpha \quad ...(10)$$

$$\langle n^2 \rangle = \langle n \rangle + \langle |\alpha|^4 \rangle \quad ...(11)$$

which gives the expression for variance

$$\langle (\Delta n)^2 \rangle = \langle n^2 \rangle - \langle n \rangle^2 \quad ...(12)$$

as

$$\langle (\Delta n)^2 \rangle = \langle n \rangle - \langle n \rangle^2 + \langle |\alpha|^4 \rangle \quad ...(13)$$

We now consider the following four eases :

Case (i) : High T_1, High T_2

When both the incident field and the detector are at high temperatures, they follow the distributions given by Eqs. (1) and (2), which when substituted in Eq. (8) gives

$$P(\alpha) = \frac{1}{\pi^2 \langle n_1 \rangle \langle n_2 \rangle} \int \exp\left(-\frac{|\alpha-\alpha_1|^2}{\langle n_1 \rangle}\right) \exp\left(-\frac{|\alpha_1|^2}{\langle n \rangle}\right) d^2\alpha_1 \quad ...(14)$$

If we substitute

$$\alpha = x + iy$$

$$\alpha_1 = x_1 + i y_1$$

in Eq. (14), we obtain

$$P(\alpha) = \frac{1}{\pi^2 \langle n_1 \rangle \langle n_2 \rangle} \left[\int_{-\infty}^{\infty} \exp\left(-\frac{(x-x_1)^2}{\langle n_1 \rangle}\right) \exp\left(-\frac{(x_1)^2}{\langle n_2 \rangle}\right) dx_1\right] \left[\int_{-\infty}^{\infty} \exp\left(\frac{(y-y_1)^2}{\langle n_1 \rangle}\right) \exp\left(-\frac{(y_1)^2}{\langle n_2 \rangle}\right) dy_1\right]$$

which, after simple calculations, yields

$$P(\alpha) = \frac{1}{\pi\left(\langle n_1 \rangle + \langle n_2 \rangle\right)} \exp\left(-\frac{|\alpha|^2}{\langle n_1 \rangle + \langle n_2 \rangle}\right) \quad ...(15)$$

Using Eq. (7), we get

$$P(\alpha) = \frac{1}{\pi \langle n \rangle} \exp\left(-\frac{|\alpha|^2}{\langle n \rangle}\right) \quad ...(16)$$

which is again a Gaussian distribution, as should be expected from the superposition of two independent Gaussian fields.

Now

$$\langle |\alpha|^4 \rangle = \int |\alpha|^4 P(\alpha)\, d^2\alpha$$

which, from Eq. (16) and a simple calculation, becomes

$$\langle |\alpha|^4 \rangle = 2 \langle n \rangle^2$$

which, when substituted in Eq. (13), gives

$$\langle (\Delta n)^2 \rangle = \langle n \rangle + \langle n \rangle^2 \quad ...(17)$$

The second term on the right-hand side of Eq. (17) is responsible for the excess photon counts.[2]

Case (ii) : Low T_1, Low T_2

In this case, the distributions given by Eqs. (2) and (4) are valid. On substituting these in Eq. (8), we get

$$P(\alpha) = \int \delta(\alpha-\alpha_1-\bar{\alpha}_1)\, \delta(\alpha_1-\bar{\alpha}_2)\, d^2\alpha_1 = \delta(\alpha-\bar{\alpha}) \quad ...(18)$$

where we have substituted

$$\bar{\alpha} = \bar{\alpha}_1 + \bar{\alpha}_2$$

since the two fields are completely independent of one another. From Eqs. (18), (10) and (13) we obtain

$$\langle (\Delta n)^2 \rangle = \langle n \rangle \quad ...(19)$$

which does not contribute to the excess photon counting, i.e. there is no photon-bunching in this case.

Case (iii) : High T_1, Low T_2

In this case, the distributions given by Eqs. (1) and (4) are applicable. With the help of Eqs. (1), (4) and (8), we get

$$P(\alpha) = \frac{1}{\pi \langle n_1 \rangle} \int \exp\left(-\frac{|\alpha-\alpha_1|^2}{\langle n_1 \rangle}\right) \times \delta(\alpha_1-\bar{\alpha}_2)\, d^2\alpha_1$$

$$= \frac{1}{\pi \langle n_1 \rangle} \exp\left(- \frac{|\alpha - \bar{\alpha}_2|^2}{\langle n_1 \rangle} \right) \quad ...(20)$$

Now

$$\langle |\alpha|^4 \rangle = \int |\alpha|^4 P(\alpha)\, d^2\alpha$$

$$= \frac{1}{\pi \langle n_1 \rangle} \int\int_{-\infty}^{\infty} (x^4 + y^4 + 2x^2 y^2) \exp\left(- \frac{(x-\bar{x}_2)^2}{\langle n_1 \rangle} \right) \exp\left(- \frac{(y-\bar{y}_2)^2}{\langle n_1 \rangle} \right) dx\, dy \quad ...(21)$$

where we have put

$$\alpha_2 = x_2 + i y_2$$

After simple calculations, we obtain

$$\langle |\alpha|^4 \rangle = \langle n \rangle^2 + \langle n \rangle \langle n_1 \rangle + \langle n_1 \rangle \langle n_2 \rangle$$

which, when substituted in Eq. (13), gives

$$\langle (\Delta n)^2 \rangle = \langle n \rangle \left(1 + \langle n_1 \rangle \right) + \langle n_1 \rangle \langle n_2 \rangle \quad ...(22)$$

From Eq. (22) we note that there is a departure in the variance due to the high temperature of the field. The excess counts term is given by

$$\langle n_1 \rangle \left(\langle n \rangle + \langle n_2 \rangle \right)$$

Since the temperature T_2 of the photodetector is very low, $\langle n_2 \rangle$ will be quite small, and in the approximation $\langle n_1 \rangle \simeq \langle n \rangle$, we have

$$\langle (\Delta n)^2 \rangle \simeq \langle n_1 \rangle + \langle n_1 \rangle^2 \quad ...(23)$$

the excess counts will be maily due to the incident field and negligibly due to the detector field.

Case (iv) : *Low* T_1, *High* T_2

Now the Eqs. (2) and (3) are valid. Thus we have, from Eq. (8)

$$P(\alpha) = \frac{1}{\pi \langle n_2 \rangle} \exp\left(- \frac{|\alpha - \bar{\alpha}_1|^2}{\langle n_2 \rangle} \right)$$

which, with the help of Eqs. (10) and (13), yields

$$\langle (\Delta n)^2 \rangle = \langle n \rangle \left(1 + \langle n_2 \rangle \right) + \langle n_1 \rangle \langle n_2 \rangle$$

contributing to the excess photon counts. Similar to the case (iii), since T_1 is low, $\langle n_1 \rangle$ is quite small and we have

$$\langle (\Delta n)^2 \rangle \simeq \langle n_2 \rangle + \langle n_2 \rangle^2 \quad ...(24)$$

Thus in this limit, the main contribution to the excess photon counts is from the detector field and negligibly from the incident field.

3. Conclusion

There will be maximum contribution to the excess photon counts when both the incident field and the detector are at high temperatures, whereas if the temperatures of both of these fields are very low, there will be negligible photon-bunching. When the temperature of only one of the two fields is high, the main contribution to the excesss photon counts will be from the field with the high temperature.

Acknowledgement

The paper is being published with the permission of the Director, National Physical Laboratory, New Delhi.

References

1. Web J H, *Am. J. Phys.*, 40 (1972), 850.
2. Dudeja J P & Chopra S, *Physics Lett.*, 64 (1977), A271.
3. Mandel L, *Phys. Rev.*, 14 (1976), A 2351.
4. Scarl D B & Smith S R, *Phys. Rev.*, 10 (1974), A709.
5. Scarl D B & Smith S R, *Phys. Rev.*, 14 (1976), A2355.
6. Abraham N B & Smith S R, *Phys. Rev.*, 15 (1977), A421.
7. Rockower E B, Abraham N B & Smith S R, *Phys. Rev.*, 17 (1978), A1100.
8. Rockower E B & Abraham N B, *J. Phys.*, A11 (1978), A1879.
9. Tataraskii V I, *Soviet Phys. JETP*, 39 (1974), 423.
10. Selloni A, Schwendimann P, Quattropani A & Baltes H P, *Phys. Rev.*, 18 (1978), A2234.

Indian Journal of Pure & Applied Physics
Vol. 18, May 1980, pp. 351-353

Sensor Design for an Electromagnetic Flow-Meter

S E Desa & E Desa

Instrumentation Division, National Institute of Oceanography, Dona Paula, Goa 403 004

Received 9 *April* 1979; *revised received* 18 *September* 1979

It is shown that in an electromagnetic flow meter the magnetic field strength, the number of turns and gauge of coil wire may be computed when the inductive and resistive effects in the coil are equal in magnitude.

1. Introduction

Several workers have published developments of electromagnetic flow-meters[1-3] in recent times. Aside from spar and discus shaped sensors, most instruments can be broadly classified either as single or double coil types, with excitation having the form of either ac or switched dc. It is noted from the published results that there is a wide range in coil power and sensor sensitivity. If the sensitivities are normalized to a coil power of 1W, ratios as disparate as 8·47 and 136·36 μV W/m/sec are obtained—the higher efficiency figure relating to the lower dissipation. The ratios are obtained considering that the sensor sensitivity increases as the square root of coil power and the difference in the obtained ratios is traceable, therefore, to the sensor design.

Our work has been largely on double-coil ac excited sensors and we intend to show here that for this mode of excitation, several different factors like wire gauge, number of turns, radius of coil, magnitude and frequency of coil current are interactive, and when other parameters are restricted, it is possible to obtain an increase in magnetic field by a correct choice of the gauge and number of turns—accounting for both the resistive and inductive effects of the coil. More efficient coils are especially attractive for field use as well as in situations demanding long-term unattended operation.

2. Theory

Consider a coil sensor consisting of two plane parallel coaxial coils, each of radius r and separated by a distance equal to r (Helmholtz coils). By Faraday's law of induction, the voltage V_i induced in a pair of electrodes lying in a plane parallel to and midway between the coils is given by:

$$V_i = uBl \qquad \ldots(1)$$

where l is the distance between the electrodes and u, the flow velocity of sea-water (say) is orthogonal to B, the magnetic flux density produced by the current flowing in the coils, and to V_i, the induced voltage.

The sensitivity V_i/u defined as the voltage induced at the electrodes per unit velocity flow is, therefore, directly dependent on B and l. Thus optimizing the flux density B, provides a method of increasing the sensitivity of the flow sensor.

The magnetic field (B) produced by two narrow Helmholtz coils carrying a current I, and each having N turns is well-known:

$$B \simeq \frac{0{\cdot}72}{r} \cdot \mu_0 \cdot NI \qquad \ldots(2)$$

In most coil sensors, N is usually large (200 to 500 turns) and it is necessary to consider inductive effects as important. A simple analysis of two series excited coils each having inductance L, and resistance R shows that the current I of frequency f lags the total applied voltage V_0 by the phase angle $\tan^{-1}(2\pi f L/R)$, and that the magnitude of the current I is[4]:

$$I = \frac{1}{2} \frac{V_0}{(4\pi^2 f^2 L^2 + R^2)^{1/2}} \qquad \ldots(3)$$

The value of L is obtained by substituting for the various terms in the expression $L = \phi_T/I$ where ϕ_T the total magnetic flux linkage is:

$$\phi_T = \mu_0 N^2 \pi r \cdot [(1/2) + (1/2)^{5/2}] \cdot I \qquad \ldots(4)$$

In Eq. (4), the first term in the square brackets is the self-inductive contribution whilst the second term is the contribution from the neighbouring coil.[5] The expression for R is straightforward and is given by

$$R = \frac{2\pi r p N}{A} \qquad \ldots(5)$$

where p is the resistivity of the coil wire (namely copper), A is the cross-sectional area of the wire, and $\mu_0 = 4\pi \times 10^{-7}$ H.m.$^{-1}$ is the permeability of

vacuum. Using Eq. (3)-(5) in Eq. (2) results in a modified expression for the flux density B

$$B = \frac{0{\cdot}72\ \mu_0 V_0}{4\ \pi\ r^2} \cdot \frac{N}{[f^2 \cdot (0{\cdot}677\ \mu_0\ \pi)^2 N^4 + p^2 N/A^2]^{1/2}} \quad ...(6)$$

Eq. (6) shows clearly that B is dependent on N, A, r, f, and V_0.

3. Design Analysis

In most electro-magnetic flow-meters, the parameters f, V_0, and r may have design constraints imposed on them. For example, f may be fixed by electronic design considerations, and V_0 (and consequently I) may be limited by the battery supply used. In a similar way, r could be restricted by the constructional details of the flow-meter. We need, therefore, consider only, the effect produced on B by changing N and A. The dependence of B on N for different cross-sectional areas (A) is shown in Fig. 1. These curves have been plotted using $r = 0{\cdot}92$ m, $f = 20{\cdot}8$ Hz, and $V_0 = 10$ V as representative values of a flow-meter developed by one of us (to be published). Also shown in Fig. 1 is the dependence of the current I on N for the same values of A. [see Eq. (3)]. The information presented in Fig. 1 allows us to investigate the dependence of magnetic flux density B on gauge cross-section A for a given rms value of current I. The latter dependence is shown in Fig. 2 for representative values of $I = 250$ mA, and 600 mA. It is also possible to extract the dependence of B on N at constant I from the curves given in Fig. 1, as shown in Fig. 3. The expected linear dependence is consistent with Eq. (2).

The behaviour in Fig. 2 shows that no appreciable change in B is obtained at large values of A in contrast to the linear change for small values of A, A close examination shows that the knee point on the graph at which the asymptotes to the two portions of the curves intersect, takes place at a value of B for which the two terms in the denominator of Eq. (7) are equal to each other. Making use of this fact, we have after rearrangement :

$$N = \frac{p}{0{\cdot}677\ \mu_0 f \pi\ A} \quad ...(7)$$

Similarly, equalizing the terms in the denominator of Eq. (3) and using Eq. (7), we have :

$$A^2 = \frac{4\sqrt{2}\, r p^2 I}{0{\cdot}667\ \mu_0 f V_0} \quad ...(8)$$

The formulae (7) and (8) enable one to calculate the number of turns N, and the wire gauge required in the design of the sensor when the magnitude and frequency of the maximum current allowable from a

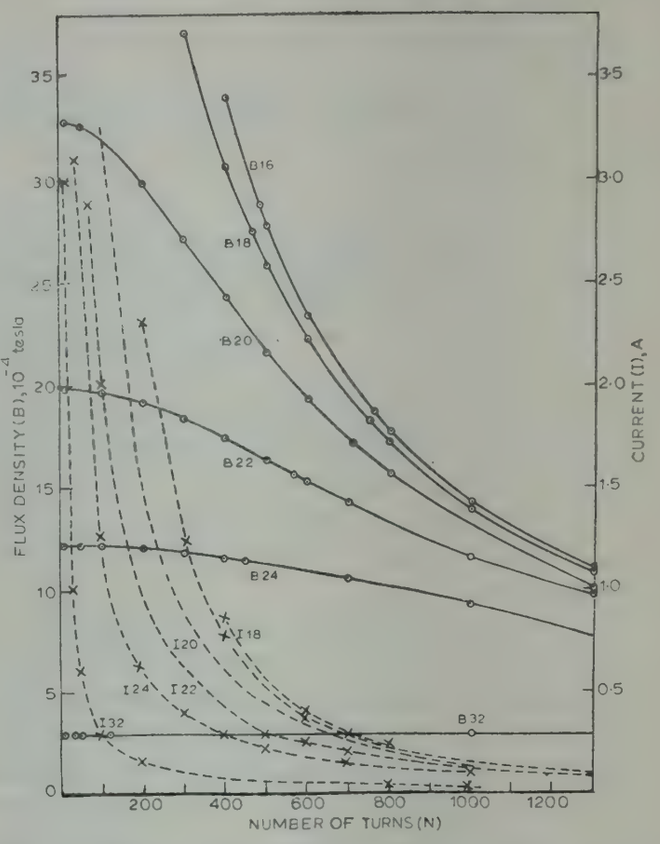

Fig. 1—Calculated dependence of magnetic flux density B and current I on the number of coil turns N for different gauges of coil wire (shown by numbers against each curve)

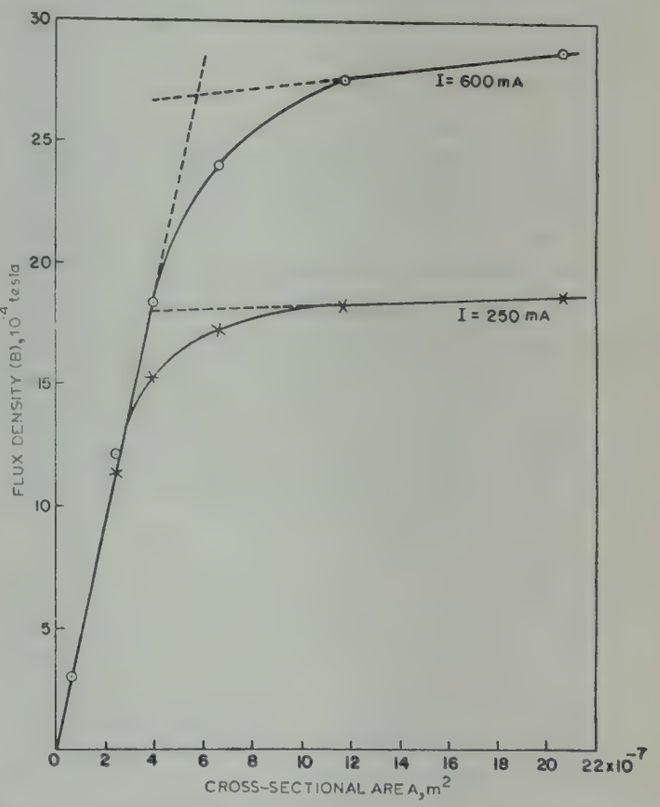

Fig. 2—Calculated curves of magnetic flux density (B) as a function of the cross-sectional area of coil wire (A) for constant rms values of the current (I) (The dotted lines are the asymptotes to the branches of each curve)

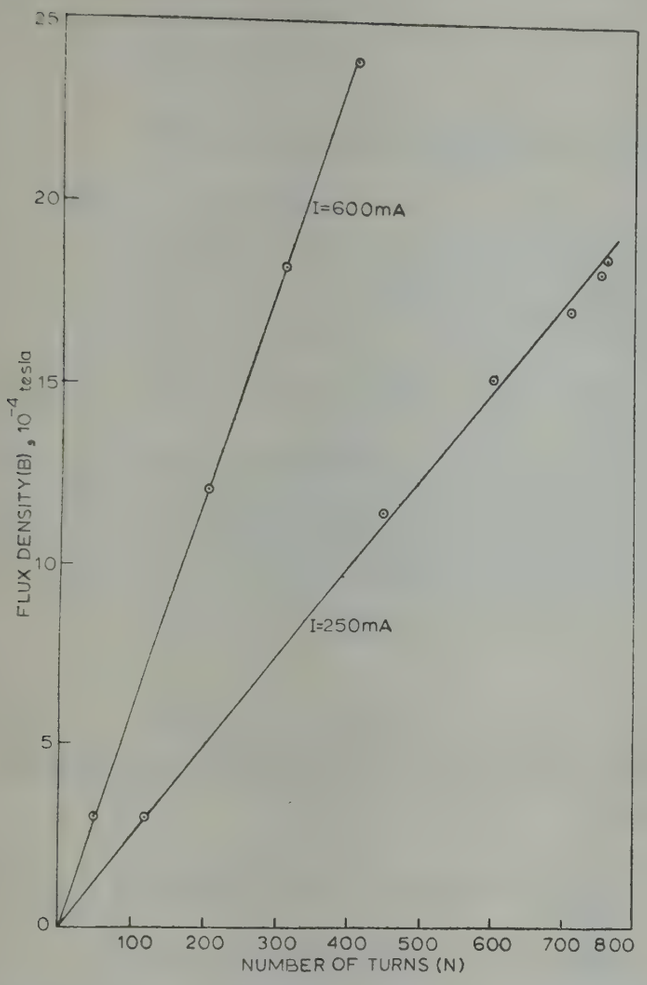

Fig. 3—Calculated dependence of magnetic flux density (B) on coil turns (N) at constant rms values of the current (I)

supply voltage V is known. As an example, using the values of r, f, and V_0 quoted above and also $I = 250$ mA, we have by substitution in Eq. (1), (2), (7) and (8) :

$N = 663$ turns. $A = 4{\cdot}6 \times 10^{-7}$ m^2 (SWG $\simeq$ 21), $B = 16{\cdot}3 \times 10^{-4}$ teslas, sensitivity = 190·7 μV/m/sec and 1·76 W for the power dissipated in the coils.

The physical picture of the origin of the 'knee' in Fig. 2, may be given as follows. It arises when the resistance and inductive reactance of the coil are equal in magnitude. When such a balance exists, the current I lags the applied voltage V_0 by 45°, and the power dissipated in the coils is $V_0 I/\sqrt{2}$ where V_0 and I are the rms values of voltage and current.

In the analysis above, it was assumed that the Helmholtz coils were of sufficiently narrow cross-section so as to justify the use of Eq. (2). In practice, the large number of turns used, results in typical coil cross-sections of the order of 10^{-4} m^2. If we consider a coil width equal to 10% of the coil radius, then a corresponding percentage change in flux density B is produced. The effect is small, and may be neglected in the treatment above.

If the constraints on parameters r, f, and I are removed, it would provide a means for increasing the field strength and sensitivity still further. This may be seen from Figs. 2 and 3 where large values of B correspond to higher values of I. In addition, it is seen from Eq. (6) that $B \propto 1/r^2 f$ when the expressions for N and A from Eqs.(7) and (8) are used. Hence, a low frequency current and a smaller coil are favoured, but the obvious advantages of a small coil are marked by the closer operation of the electrodes [see Eq. (1)], thus reducing the overall sensitivity. Also, at smaller coil radii, the effect of coil thickness is more marked and the allowance would have to be made in Eq. (1) for magnetic fields.

4. Conclusion

It has been shown that a proper choice of the gauge of wire and the number of coil turns can lead to the construction of an efficient sensor. The resulting improvement in the sensitivity of the sensor means that the power dissipated in the coils can be usefully conserved without having to pump current into the coils in order to increase its sensitivity. The saving of power is an important consideration for portable field instruments, and more so in oceanographic work where ocean current flows need to be monitored continuously.

Acknowledgement

The authors wish to thank Dr S Z Qasim, Director National Institute of Oceanography, Goa, for going through the manuscript.

References

1. Kanvisher J & Lawson K, *Limnology & Oceanography*, **20** (1975), 174.
2. Olson J R, *Two-component electromagnetic flow-meters*, *Marine Tech. Soc J.*, 6 (1972), 19.
3. Tucker M J, Smith N D, Pierce F E & Collins E P, *A two-component electromagnetic ship's log*, *J. Inst. Navig.*, 23 (1970), 302.
4. Nelkon M & Parker P, *Advanced level physics* (Heineman, London), 3rd Edn, 1969.
5. Carter G W, *The electromagnetic field in its engineering aspects*, Electrical Engineering Series (Longmans, London), 2nd Edn, 1967.

Indian Journal of Pure & Applied Physics
Vol. 18, May 1980, pp. 354-359

Injection Synchronization in the Face of Heavy Interference*

S K Ray, (Miss) K Pramanik & S Karmakar
Physics Department, Burdwan University, Burdwan 713 104

Received 7 *April* 1979; *revised received* 14 *December* 1979

The phenomenon of injection synchronization in an oscillator under the influence of strong interferences, hitherto unknown, has been studied. Starting with characterizing the effective synchronizing signal when the incoming wave is corrupted by a strong interfering tone, the effect of such a synchronizing signal on an injection synchronized oscillator (ISO) is then tackled on the basis of physical arguments. A new phenomenon called the 'frequency jump' in an ISO has been experimentally observed and explained in simple physical terms. A method has also been suggested to eliminate this confusing situation in an ISO.

1. Introduction

In these days of microminiaturization, the principle of injection synchronization is an indispensable technique for fabricating low noise amplifiers or filters at millimetre wave frequencies. The performance of such a device depends on its capability of being synchronized with the incoming signals, which in practice, are usually corrupted by cochannel interferences. The presence of these disturbances deteriorates the performance of the system in the sense that not only they introduce distortions at the output of the device but also induce a tendency of throwing the oscillator out of synchronism. Obviously, an understanding of the mechanism of interaction of the synchronized oscillators with the corrupted synchronizing signal is warranted for evolving the design criteria of such devices.

The conventional theoretical tools deal with cases in which a weak interfering tone accompanies an injecting signal.[1] But in the case of strong interference, which is a frequent occurrence in practice, it appears to the authors that no attempt has been made so far. It may be due to the fact that a rigorous analysis of the injection synchronized oscillator (ISO)—a highly nonlinear system, becomes formidable because of the very complex character of the system equations. This paper, therefore, examines the problem of synchronization in the face of heavy interference. It is quite interesting to note that the results of the investigation indicate that a new phenomenon, called 'frequency jump' sets in an injection synchronized oscillator. Moreover, the theoretical tools developed can be applied for a corrupted signal with about 70% strength of the interfering tone with respect to the synchronizing signal.

2. Characterization of an Interference Corrupted Signal

When a synchronizing signal ($E \sin \omega_1 t$) is corrupted with a cochannel interfering tone ($x\,E \sin \omega_i t$), it is perhaps informative to characterize the effective signal to be injected to the oscillator. Under this situation, the net input to the oscillator is given by

$$e_i(t) = E \sin \omega_1 t + x\,E \sin \omega_i t, \qquad \ldots(1)$$

$$= E_L(t) \sin\left[(\omega_1 t + \theta(t)\right],$$

where

$$E_L(t) = E(1 + x^2 + 2x \cos \Delta\omega_{i1} t)^{1/2}, \qquad \ldots(2)$$

$$\theta(t) = \arctan [x \sin \Delta\omega_{i1} t/(1 + x \cos \Delta\omega_{i1} t)], \qquad \ldots(3)$$

$$\Delta\omega_{i1} = \omega_i - \omega_1 \qquad \ldots(4)$$

In the above equations, $\theta(t)$ represents the phase difference between the resultant signal and the synchronizing signal. Let us now look into the character of the instantaneous amplitude and frequency of the net injecting signal. These are to be determined from the knowledge of the probability density distribution functions of $E_L(t)$ and $\dot{\theta}(t)$ respectively. Using Eqs. (2) and (3) one has the following relations :

$$p(E_L/E) = \frac{2E_L}{\pi E}[2(1 + x^2)(E_L/E)^2 - (E_L/E)^4 - (1 - x^2)^2]^{-1/2} \qquad \ldots(5)$$

*Presented at the 66th session of the Indian Science Congress held at Hyderabad during 3-7 January 1979.

$$p\,(\dot{\theta}/\Delta\,\omega_{i1}) = \pi\, x\,(2\,\frac{\dot{\theta}}{\Delta\,\omega_{i1}} - 1)^{-1}\left[\frac{1}{1-x^2}\right.$$

$$\left.\left(1-2\,\frac{\dot{\theta}}{\Delta\,\omega_{i1}}\right)-\left(\frac{\dot{\theta}}{2\,\Delta\,\omega_{i1}}\right)^2\right]^{-1/2} \quad ...(6)$$

Eqs. (5) and (6) are valid for $x < 1$. For $x = 1$, there is a transition in the frequency of the true injecting signal. For $x > 1$, the synchronizing signal interchanges its role with the interfering one.

The variations of $p\,(E_L/E)$ and $p\,(\dot{\theta}/\Delta\omega_{i1})$ with (E_L/E) and $(\dot{\theta}/\Delta\omega_{i1})$ respectively are shown in Figs. 1 and 2. Fig. 1 reveals that irrespective of the frequency difference between the synchronizing signal and the interference, the amplitude of the effective signal fluctuates around $E_L/E = 1$, and greater the value of x, larger is the deviation of the amplitude. Fig. 2 reveals that the instantaneous frequency difference between the net input signal and the true synchronizing signal spreads around $\dot{\theta} = 0$, depending upon the strength of the interfering tone. These facts indicate that in the presence of the interfering tone, the information, i.e. the spectral character of the synchronizing signal, is smeared out leading to an ambiguity in correctly assessing the character of the incoming signal. This definitely makes the synchronization problem difficult. Thus it appears that depending upon the strength of the interfering tone, the oscillator may or may not be synchronized. The details are discussed in the following sections.

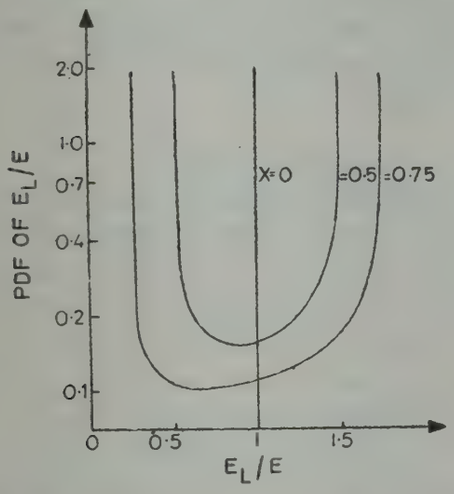

Fig. 1—Theoretical variation of the probability density distribution function of the amplitude $p\,(E_L/E)$ of an interference corrupted wave

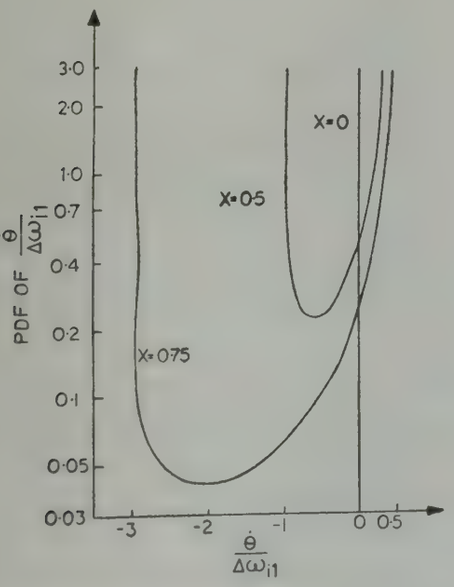

Fig. 2—Theoretical variation of the probability density distribution function of the instantaneous frequency $p\,(\dot{\theta}/\Delta\,\omega_{i1})$ of an interference corrupted wave

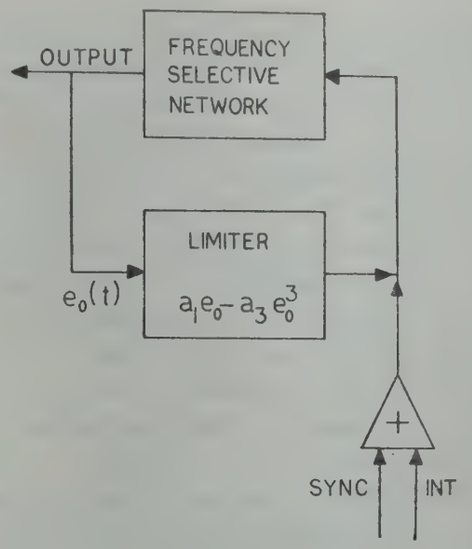

Fig. 3—Analytical equivalent representation of an ISO

3. Response to the Synchronizing Signal in the Presence of an Interfering Tone

Assuming the net input to the ISO in the form as in Eq. (1), one may take the output of the ISO in the following form :

$$e_0\,(t) = A\,(t)\,\sin\,(\omega_1 t - \psi) \quad ...(7)$$

With the help of Eq. (7) and Fig. 3, which is the analytical equivalent representation of an ISO, one may have the following equations governing the instantaneous amplitude and phase of the oscillator:[2]

$$\frac{dA}{dt} = \frac{\omega_0}{2\,Q}\left[\,(a_1\,G_0-1)-\frac{3}{4}\,a_3\,G_0\,A^2\,\right]A + \frac{\omega_0\,G_0}{2\,Q}\,E\,[\cos\,\psi + x\cos\,(\Delta\,\omega_{i1}\,t+\psi)] \quad ...(8)$$

$$\frac{d\psi}{dt} = \frac{\omega_0}{2}\left(\frac{\omega_1}{\omega_0}-\frac{\omega_0}{\omega_1}\right)-\frac{\omega_0}{2\,Q}\,\frac{E}{A}\,G_0\,[\sin\,\psi + x\,\sin\,(\Delta\,\omega_{i1}\,t+\psi)] \quad ...(9)$$

where a_1 and a_3 are the constants of the limiter, Q the quality factor of the tank circuit and G_0 is the gain of the oscillator at its free running frequency ω_0. An exact solution of Eqs. (8) and (9) will describe the effect of an interfering tone on the tracking behaviour of an ISO. But due to the highly nonlinear character of Eqs. (8) and (9), it is impossible to do so. On the other hand, an approximate solution may be presented with some judicious assumptions. The strength as well as the detuning of the interfering tone are assumed to be such that the oscillator is locked to the synchronizing signal whereas the presence of the interfering tone introduces perturbations in the instantaneous amplitude and phase of the oscillator. It is not difficult to conjecture that the amplitude of the ISO is modulated with a fundamental frequency equal to the difference between the frequency of the interfering tone and that of the synchronizing signal ($\Delta\omega_{i1}$). And the instantaneous phase of the oscillator fluctuates around a static phase error (say ψ_0) at a rate depending on $\Delta\omega_{i1}$. This static phase error ψ_0 is a measure of the detuning of the synchronizing signal (ω_1) with respect to the free running frequency (ω_0) of the oscillator. It may be mentioned that the mixing process provided by the nonlinearity of the oscillator is responsible for this phase modulation.

Eqs. (8) and (9) reveal that so long as the oscillator is operating in underdriven condition, i.e. $E/A<1$, its amplitude changes at a rapid rate in comparison with the phase process. That is to say, during a particular change of the oscillator phase, its amplitude attains the steady-state value. Therefore, in order to account for the phase variation of the oscillator, one may proceed without an appreciable error, taking the average value of the amplitude (say A_0) of the oscillator. And in the next step one can easily introduce the correction term due to the amplitude perturbation. This is what has been done in the following subsections.

3.1 Effect of Phase Perturbation

As discussed in Sec. 3, one may assume the solution of Eq. (9) in the form as given by

$$\psi = \psi_0 + m_\psi \sin(\Delta\omega_{i1}\, t + \psi_m) \qquad \ldots(10)$$

where m_ψ and ψ_m are the constants to be determined from Eqs. (9) and (10) respectively. Substituting this assumed value of ψ in Eq. (9), one arrives at the following equations by the method of harmonic balance

$$\frac{\Delta\omega_{10}}{K_0} = J_0(m_\psi)\sin\psi_0 + \frac{x^2 J_0(m_\psi) J_1(m_\psi)(\Delta\omega_{i1}/K_0)}{4\, J_1^2(m_\psi)\cos^2\psi_0 + m_\psi^2(\Delta\omega_{i1}/K_0)^2} \qquad \ldots(11)$$

$$\frac{\Delta\omega_{10}}{K_0} = \Delta\omega_{i0}/K_0 \mp \frac{1}{m_\psi}[x^3 J_0^2(m_\psi) - J_1^2(m_\psi)\cos^2\psi_0]^{1/2} \qquad \ldots(12)$$

where

$$\Delta\omega_{10} = \omega_1 - \omega_0 \text{ and } K_0 = \frac{\omega_0 G_0 E}{2 Q A_0}.$$

K_0 denotes the locking range of the ISO in response to the continuous wave (CW) synchronizing signal only.

The use of the plus or minus sign in Eq. (12) depends on whether $\Delta\omega_{10} < \Delta\omega_{i0}$ or $\Delta\omega_{10} > \Delta\omega_{i0}$ respectively. In deriving the above equations the symmetric frequency response characteristics of the tank circuit incorporated in the oscillator has been assumed so that $\frac{\omega_0}{2}\left(\frac{\omega_1}{\omega_0} - \frac{\omega_0}{\omega_1}\right)$ may be replaced by $\Delta\omega_{10}$. The value of ψ_0 on the verge of unlocking is $(\pi/2 - m_\psi)$ for the upper side and is $-(\pi/2 - m_\psi)$ for the lower side.

3.2 Effect of Amplitude Perturbation

The amplitude perturbation is a dominant factor in the determination of the locking range of an ISO, particularly when the interfering tone lies in the vicinity of the tracking zone of the ISO for the synchronizing signal. In order to have the effect of this amplitude perturbation of the ISO, it is sufficient to proceed with the average value of ψ which equals to ψ_0, and consider the amplitude governing Eq. (8) which may be rewritten in the normalized form as

$$\frac{da}{dt} = \frac{\omega_0}{q}(1-a^2)\,a + \frac{\omega_0}{q}E_0[\cos\psi + x\cos(\Delta\omega_{i1}\, t + \psi)] \qquad \ldots(13)$$

where

$$q = \frac{2Q}{a_1 G_0 - 1},\quad E_0 = \frac{E G_0}{(a_1 G_0 - 1) V_0},$$

$$V_0 = [4(G_0 a_1 - 1)/3 G_0 a_3]^{1/2},\quad a = A/V_0$$

Here, V_0 represents the free running amplitude of the ISO. As stated in Sec. 3, one may assume the solution of Eq. (13) to be of the form

$$a = a_0[1 + m_a \cos(\Delta\omega_{i1}\, t + \psi_a)] \qquad \ldots(14)$$

where a_0 ($= A_0/V_0$) is the average amplitude of the oscillator in the presence of interference corrupted synchronizing signal normalized with respect to its free running value (V_0), m_a and ψ_a are the constants to be determined from Eqs. (13) and (14) respectively. Applying the method of harmonic balance, it has been found that m_a statisfies the following relation

$$\frac{9}{16}a_0^6 m_a^6 + \left(\frac{9}{2}a_0^6 - \frac{3}{2}a_0^4\right)m_a^4 + a_0^2$$

$$\left[\left(\frac{\Delta\omega_{i1}}{\omega_0}\right)^2 q^2 + 1 + 9a_0^4 - 6a_0^4\right] m_a^2 - 2x^2 E_0^2 \cos^2\psi_0 = 0 \quad \ldots(15)$$

For an underdriven ISO having a large q, a_0 of Eq. (15) may be taken as unity particularly on the verge of unlocking. The magnitude of the quantity $\left(\frac{1}{2}\frac{\Delta\omega_{i1}}{\omega_0} q\right)$ is much smaller compared with unity within the range of interest. Then one may have the reduced form of Eq. (15) as

$$m_a^6 + \frac{16}{3} m_a^4 + \frac{64}{9} m_a^2 - \frac{32}{9} x^2 E_0^2 \cos^2\psi_0 = 0 \quad \ldots(16)$$

It is clear that the effect of the amplitude perturbation of the ISO is to modify the parameter K_0 appearing in Eqs. (11) and (12) respectively. K_0 is now to be replaced by K_s, where

$$K_s = \frac{K_0}{1+m_a} \quad \ldots(17)$$

With this modification, Eqs. (11) and (12) take respectively the modified forms as

$$\frac{\Delta\omega_{i0}}{K_0} = \frac{1}{1+m_a}\left[J_0(m_\psi)\sin\psi_0 + \frac{x^2 J_0(m_\psi) J_1(m_\psi) m_\psi \Delta\omega_{i1}/K_0}{\frac{4J_1^2(m_\psi)\cos^2\psi_0}{(1+m_a)^2} + m_\psi^2 (\Delta\omega_{i1}/K_0)^2}\right] \quad \ldots(18)$$

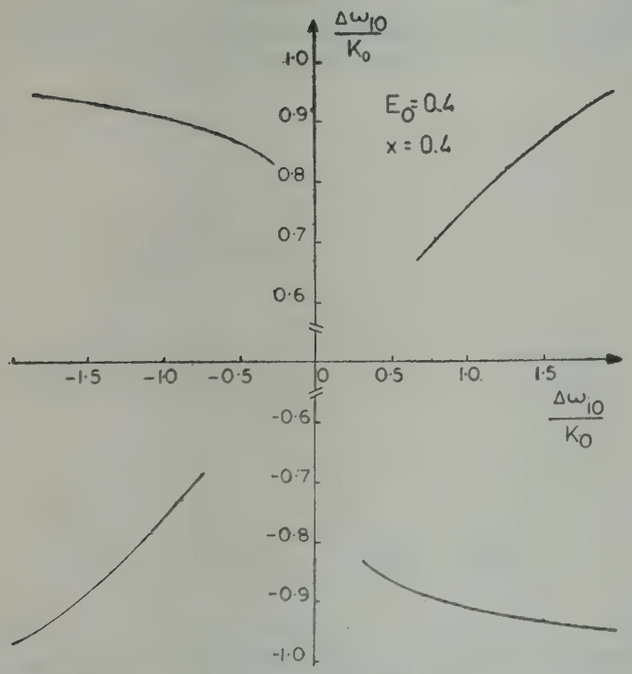

Fig. 4—Theoretical variation of the normalized locking range ($\Delta\omega_{i0}/K_0$) of an ISO in the presence of an interfering tone

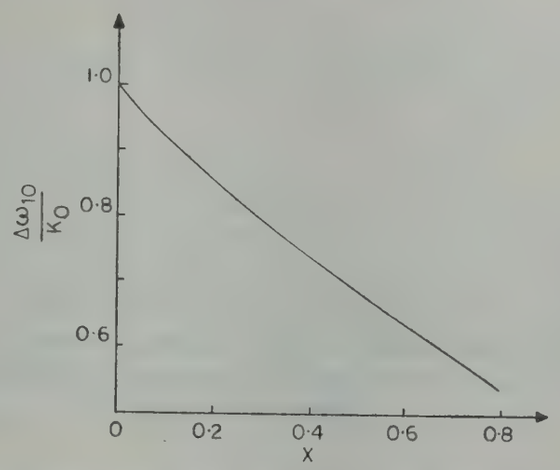

Fig. 5—Theoretical variation of the normalized locking range ($\Delta\omega_{i0}/K_0$) of an ISO in the presence of an interfering tone with the strength (x) of the interference

$$\frac{\Delta\omega_{i0}}{K_0} = \frac{\Delta\omega_{i0}}{K_0} \mp \frac{1}{m_\psi(1+m_a)}[x^2 J_0^2(m_\psi) - J_1^2(m_\psi)\cos^2\psi_0]^{1/2} \quad \ldots(19)$$

Theoretical variations of the normalized locking range of the ISO corresponding to Eqs. (18) and (19) are shown in Figs. 4 and 5 respectively. Fig. 4 indicates that as the frequency of the interfering tone approaches the free running frequency of the oscillator (ω_0), the locking range of the ISO decreases. And when it is very close to ω_0, its effect becomes so prominent that it throws the oscillator out of synchronism. When the interfering tone is away from ω_0, the single-sided locking range of the ISO in the direction of the interference frequency is increased while it is reduced on the other side of the interfering tone.

Fig. 5 depicts that the locking range of the ISO reduces with the increase in the strength of the interfering tone with a particular detuning. Fig. 6 represents the corresponding results obtained experimentally. It is to be noted that the theoretical results, in contrast to the earlier works, are in tune with the experimental findings up to 70% strength of the interfering tone with respect to the synchronizing signal.

4. Influence of a Strong Interfering Tone

The theoretical as well as the experimental findings discussed so far lead to the conclusion that depending upon the strength of the interfering tone the synchronization zone of an ISO may disappear. This leads to an explanation of the experimentally observed 'frequency jump' phenomenon in an ISO. Depending upon the detuning of the interfering tone with respect to the locking range of the ISO, the following two cases may arise : (i) the interfering tone lying out-side the locking range

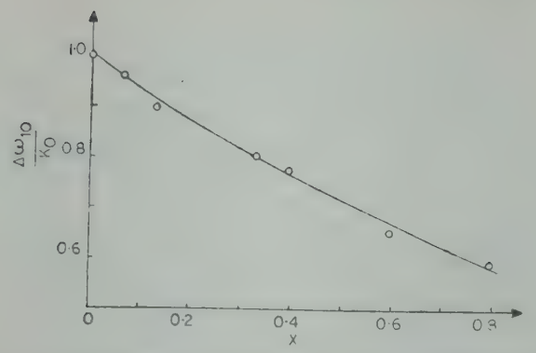

Fig. 6—Experimental variation of the locking range ($\Delta\omega_{i0}/K_0$) of an ISO with the strength (x) of the interfering tone

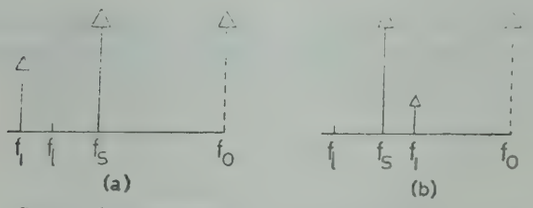

Fig. 7—Spectral representation of the two situations describing the frequency jump phenomenon in an ISO

of the ISO (Fig. 7a), and (ii) interfering tone lying inside the lockband of the ISO (Fig. 7b). Referring to Fig. 7a, one may consider that the oscillator is initially locked to the synchronizing signal at the frequency f_s. With this, if the strength of the interference is gradually increased from its original value, a stage is reached when the oscillator will be unlocked from the synchronizing signal and a further increase of the strength of the interfering tone may pull the oscillator to its own frequency (f_i) — the situation is such that the roles of the synchronizing signal and interfering tone are interchanged. In this case, it is to be noted that the strength of the interfering tone has to be greater than that of the synchronizing signal, and that f_0-f_i denotes the lower side locking range of the ISO for the synchronizing signal. A similar situation may also occur in the case shown in Fig. 7b. In this case, a condition will arise when, for a particular strength of the interfering tone, the oscillator will be de-entrained from the synchronizing signal and if this strength of the interfering tone is sufficient to hold the oscillator in lock, then the oscillator may jump to lock to the interfering tone, exhibiting a sort of frequency jump phenomenon. It is to be noted that the minimum strength required (x_{min}) by the interfering tone to pull in the oscillator from the synchronizing signal to its own frequency in the case (ii) is less than that required in the case (i).

In order to avoid such a confusing situation in an ISO under the influence of a strong interfering tone one may employ two ISOs connected in the manner as shown in Fig. 8. In this case, the output of ISO-I is fed to the input of the ISO-II, the output of which, in turn, is positively coupled to the input of the ISO-I. This system in which the two ISOs are coupled bilaterally may be called bilaterally coupled oscillator (BCO). Since the interference rejection capability of two ISOs connected in cascade is greater than that of a single ISO,[3] with the help of the method as diagrammatically represented in Fig. 8, it is seen that the strength of the synchronizing signal effectively increases. Hence the probability of a particular 'frequency jump' of a BCO from the synchronizing signal to the interfering tone is much poorer than that of a single ISO. It may be mentioned that the two ISOs comprising the BCO should have identical free running frequencies.

Experimental variations of the minimum strength (x_{min}) required to pull in the oscillator frequency from the synchronizing one to that of the interfering tone (f_i) are depicted in Fig. 9. It appears that for a particular detuning of the interfering tone, this minimum strength required by the interfering tone to pull the oscillator frequency to itself is greater for the curve II than that required for the curve I. This means that the probability of a frequency jump in a BCO is considerably reduced.

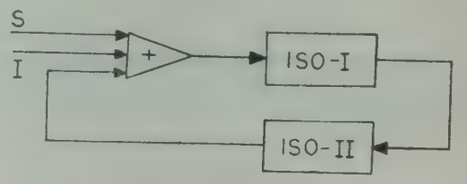

Fig. 8—Block diagram of an arrangement for reducing the probability of occurrence of frequency jump phenomenon in synchronized oscillators

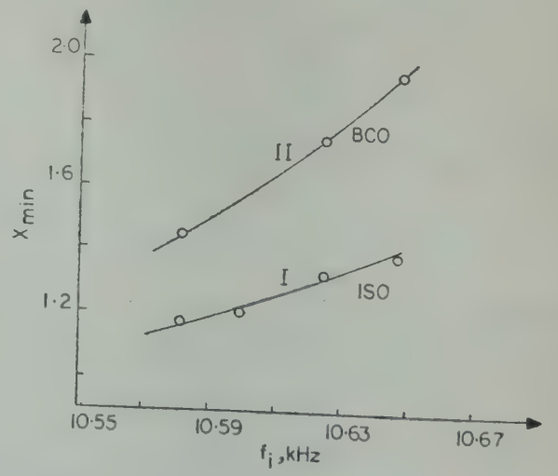

Fig. 9—variation of the minimum strength (x_{min}) required for pulling the frequency of the entrained oscillator from the frequency of the synchronizing signal to that of the interfering tone [Oscillator free running frequency, 10·547 kHz; frequency of the synchronizing signal, 10·552 kHz]

5. Conclusions

Theoretical and experimental findings of the present work lead to the following points. (1) Phase perturbation in an ISO in the face of an interference affects the tracking capability to a greater extent than the corresponding amplitude perturbation does. (2) When the interfering tone is away from the tracking zone of the oscillator for the synchronizing signal, it increases the one-sided locking range of the oscillator on the side of the interfering tone and reduces the same on the other side. This effect of the interference on an oscillator may also be visualized in another way. The interfering tone acts in such a manner so as to pull the free running frequency of the oscillator towards itself. (3) Depending on the detuning as well as the strength of the interfering tone, the frequency of the synchronized oscillator may jump to fall in synchronism with the interfering tone, exhibiting a sort of 'frequency jump' phenomenon in a synchronized oscillator. (4) The occurrence of the 'frequency jump' phenomenon in synchronized oscillators in the presence of a strong interfering tone may be reduced by using two oscillators coupled together in a particular manner so as to increase the effective strength of the synchronizing signal.

Acknowledgement

The authors are indebted to Prof. B N Biswas under whose supervision the material has been prepared. They are thankful to Mr A K Bhattacharya for his helpful suggestions and criticisms. They also thankfully acknowledge the financial assistance given by the University Grants Commission, New Delhi, for carrying out this work.

References

1. Spence R & Boothroyd A R, On the discrimination of a synchronized oscillator against interferences accompanying the synchronizing signal, *IEE monograph* 307 R, June 1958.
2. Ray S K, (Miss) Pramanik K, Banerjee P & Biswas B N, Locking characteristics of synchronized oscillators in the presence of interference, *IEEE Trans. Circuits and Syst.*, **27** (1) (1980).
3. Ray S K, (Miss) Pramanik K, Bhattacharya A K, Banerjee P, Majumdar T & Biswas B N, *Int. J. Electron.*, 43 (2) (1977), 169.

Notes

Crystal Field Stabilization Energies of Second-row Transition-Metal Oxides & Halides

LAMBODAR THAKUR* & B B SANDWAR

P G Department of Chemistry, Bhagalpur University
Bhagalpur 812 007

Received 21 *December* 1978; *revised received* 5 *November* 1979

The lattice energies and crystal-field-stabilization-energies of several second-row transition-metal oxides and halides have been estimated and their significance discussed.

It is well known that the d orbitals of transition-metal ions undergo splitting in an octahedron of ligands.[1] This splitting gives an extra stability to the crystal lattice known as the crystal-field stabilization energy. The factors which govern this energy are size, charge, dipole-moment and polarizability of the ligands and the d ions. The energy can be calculated by a tedious and lengthy procedure using the complete Hamiltonian and solving the requisite secular equation.[2] It is also experimentally determined from spectra of the aqueous solutions of complexes. For the solid state such spectral data are not available. Orgel[3] has pointed out that when the experimental (Born-Haber cycle) lattice energies of transition-metal compounds are plotted against their atomic numbers; a double-humped curve is obtained for a particular ligand series with minima at d^0, d^5 and d^{10} ions due to their orbital symmetries. Hush and Pryce[4] have regarded as a first approximation, the difference between the smooth line drawn through d^0, d^5 and d^{10} ions and the experimental points equal to the crystal-field-stabilization-energies, Δ_0.

We report in this note lattice energies and crystal-field-stabilization-energies of the second-row transition-metal oxides and halides and their significance has also been discussed.

Lattice energy (U_L) of a crystalline compound $M_m X_n$ (c), is related with the following thermochemical cycle which can be determined experimentally at 25°C

$$U_L + (n+1)\,RT = \Delta H_f^0\, M^{n+}(g) + n\,\Delta H_f^\circ\, X^{m-}(g) - \Delta H_f^0\, M_m X_n(c) \quad \ldots(1)$$

where the terms have their usual significance and $(n+1)\,RT$ is the PV correction to bring the ionic species from 0 K to 298 K. The experimental (cyclic) values for lattice energies of the second-row transition-metal oxides and halides have been calculated by compiling the thermal data from different sources.[5-8] On plotting the respective values against the increasing atomic number of the ions, a double humped curve is generated in each series of an anion (oxide or halide). Even though in several cases standard heats of formation values for crystals are not known, each curve has a trend similar to the earlier ones.[9,10] Some of the experimental values have been interpolated from the smoothened curves so drawn and they have been shown in Tables 1 and 2 (in parentheses). By drawing a curve joining $Sr^{2+}(d^0)$, Tc^{2+} (d^5) and Cd^{2+} (d^{10}) ions, Δ_0 (CFSE) for the crystals have been obtained as before.[10] We are presenting values for only five crystals (d^1 to d^5 ions) in each series in Tables 1 and 2. Calculated values for some more crystals are available with the authors and any interested worker can directly contact us for the needful. It has been found that Δ_0 values for the second-row transition-metal compounds are higher than those of the first-row transition-metal compounds. Lattice energies of the above compounds can also be computed from the Kapustinskii's equations[12]

$$U_L\ (\text{kJ mol}^{-1}) = \frac{1201{\cdot}6\,\Sigma n\,Z_1\,Z_2}{r_c + r_a}\left(1 - \frac{1}{m}\right) \quad \ldots(2)$$

$$= \frac{1201{\cdot}6\,\Sigma n\,Z_1 Z_2}{r_c + r_a}\left(1 - \frac{\rho}{r_c + r_a}\right) \quad \ldots(3)$$

where $m = 9$; $\rho = 0{\cdot}345$ Å; $\Sigma\, n$ is the total number of ions present in the gramme-molecular formula of the crystal; Z_1 and Z_2 are the formal ionic charges and $(r_c + r_a)$ the sum of six coordinated ionic radii in angstrom units. Another empirical equation recently suggested by us has been found to yield better agreement with experimental values in several cases[13]

$$U_L\ (\text{kJ mole}^{-1}) = \frac{1201{\cdot}6\,\Sigma\, n\,Z_1\,Z_2}{r_c + r_a}\left[1 - \log_{10}\left\{1 + p\,(r_c + r_a)^{-2}\right\}\right] + 10{\cdot}5\,\Sigma\, n\,Z_1\,Z_2 + (n+1)\,RT \quad \ldots(4)$$

* To whom correspondence is to be addressed

Table 1—Lattice Energies and Crystal-field Stabilization Energies of Some Second-row Transition-metal Oxides and Fluorides in their Bivalent States in kJ mole^{-1}

Element	Oxides				Fluorides			
	Cyclic	Δ_0	Eq. (4)+Δ_0	% error	Cyclic	Δ_0	Eq. (4)+Δ_0	% error
Y	(3515)	151	3616	2·8	(2761)	197	2827	2·3
Zr	(3791)	343	3990	5·2	3000	385	3155	5·1
Nb	4057	544	4225	4·1	(3046)	393	3188	4·6
Mo	(4042)	460	4186	3·5	(2979)	285	3113	4·4
Tc	(3498)	0	3750	7·2	(2657)	0	2848	7·2
Av. % error				4·6				4 7

r_c (in Å) = Y^{2+}, 1·10; Zr^{2+}, 0·93; Nb^{2+}, 0·90; Mo^{2+}, 0·86 and Tc^{2+}, 0·84 (Ref. 11 and estimated values)

r_a (in Å) = O^{2-}, 1·40; F^-, 1·36; Cl^-, 1·81; Br^-, 1·95 and I^-, 2·16 (Ref. 11).

Table 2—Lattice Energies and Crystal-field Stabilization Energies of Some Second-row Transition-metal Chlorides, Bromides and Iodides in their Bivalent States in kJ mole^{-1}

Element	Chlorides				Bromides				Iodides			
	Cyclic	Δ_0	Eq. (4)+Δ_0	% error	Cyclic	Δ_0	Eq. (4)+Δ_0	% error	Cyclic	Δ_0	Eq. (4)+Δ_0	% error
Y	(2360)	117	2429	2·9	(2410)	243	2470	3·0	(2301)	234	2343	3·3
Zr	2594	293	2715	2·7	2628	402	2732	2·9	2548	393	2597	3·1
Nb	2799	435	2880	2·7	(2711)	418	2769	2·8	(2611)	385	2605	3·1
Mo	2741	335	2807	2·7	2753	418	2795	2·8	2602	314	2557	3·0
Tc	(2369)	0	2487	5·4	(2301)	0	2390	3·9	(2218)	0	2257	1·7
Av. % error				3·3				3·1				2·8

with $p = 2$ Å^2 and the other terms have their usual significance.

As the crystal field effects make an appreciable contribution to the total lattice energy so that when Δ_0 values are added to the theoretical U_L values obtained from Eq. (4) a better agreement with the experimental cyclic values are quickly observed. Tables 1 and 2 include the effective lattice energy values ($U_L+\Delta_0$) computed from Eq. (4) along with the percentage errors. It can be seen that the average percentage errors yielded are within the narrow bands of 3-5% which is acceptable in such theoretical computations. In the case of technetium there is little thermodynamic data available and the discrepancies are higher with the observed values in some cases. Even then we may claim that in the absence of realiable experimental values for some of these crystals under consideration, our computed values may be used for any further studies.

References

1. Ilse F & Hartmann H, *Z. physik. Chem.*, **197** (1957), 239.
2. Griffith J S, *The theory of transition-metal ions* (Cambridge University Press, New York), 1961.
3. Orgel L E, *An introduction to transition metal chemistry* (Methuen, London), 1960.
4. Hush N S & Pryce M N L, *J. chem. Phys.*, **28** (1958), 244.
5. Weast, R C, *Handbook of physics & chemistry* (CRC Press, Florida), 59th edition, 1978.
6. Lange N A, *Handbook of chemistry* (McGraw-Hill, New York), 1974.
7. *Selected values of chemical thermodynamic properties*, N B S Technical notes 270-1; 270-4 & 270-5.
8. Franklin J L & Harland F W, *Ann. Rev. phys. chem.*, **24** (1975), 485.
9. Ladd M F C & Lee W H, *J. chem. Soc.*, (1962), 2837.
10. Thakur L, Sinha A K & Sandwar B B, *Indian J. Chem.*, 17A (1979), 1.
11. Greenwood N N, *Ionic crystals, lattice defects & non-stoichiometry*, (Butterworths, London), 1968, 40.
12. Kapustinskii A F, *Quart. Rev.*, 10 (1956), 283.
13. Thakur L & Sinha A K, *Indian J. pure appl. Phys.*, **15** (1977), 794.

Relation Between Microhardness & Atomic Vibration Frequency in Alkali Halides

B SUBRAMANIAM

School of Studies in Physics, Jiwaji University
Gwalior 474 002

Received 24 *January* 1979; *revised received* 27 *July* 1979

It has been found that microhardness (H_V) in alkali halides is affected not only by the addition of impurities but also by atomic vibration frequency (ν) and a linear relation exists between H_V and ν. Using this relation, values of H_V have been calculated from the known values of ν for all the alkali halides.

Hardness of a crystal is generally defined as its resistance to the structural breakdown when a stress is applied to it. In the past, attempts have been made to relate the hardness to many physical properties of the crystal. For example, Berzina *et al.*[1] have shown that with the increase in the surface energy of a crystal, the hardness also increases; Plendl and Gielesse[2] have shown that hardness is connected with the volumetric lattice energy. Experiments carried out by Chin *et al.*[3] have shown that crystals of NaCl, NaBr, KCl and KBr are strongly hardened by small additions of divalent ions (Ca^{2+}, Sr^{2+} and Ba^{2+}). They also found that the strengthening is proportional to $C^{1/2}$ where C is the atomic concentration. Young in 1845 proposed a relation between hardness and the frequency of vibration of the particles of a solid. In this note, an attempt has been made to relate hardness with atomic vibration frequency (ν); the study is confined only to alkali halides having fcc structure.

Several methods have been used to find ν which occurs in the Einstein equation for solids. The relation of ν with the deformation of a solid was calculated by Madelung for halide salt lattices and by Einstein for monatomic solids (Ref. 4). If M is the atomic weight, V_a the atomic volume, $K\left(=\frac{3}{C_{11}+2C_{12}}\right)$ compressibility, and N Avogadro number, then

$$\nu^2 = AN^{2/3} V_a^{1/3} M^{-1} K^{-1} \quad \ldots(1)$$

where A is a numerical factor called Madelung's coefficient which is of the order of magnitude unity. With $V_a = M/\rho$, where ρ is the density, Eq. (1) becomes

$$\nu = C M^{-1/3} K^{-1/2} \rho^{-1/6} \quad \ldots(2)$$

where C is a numerical constant including $N^{1/3}$. Eq. (2) can be derived as follows. Sutherland[4] assumed that the length of elastic waves in a solid is of the order of twice the mean distance between the atoms or ions (Ref. 4)

$$\lambda \simeq \text{Constant} \left(\frac{M}{N\rho}\right)^{1/3} \quad \ldots(3)$$

The velocity of the waves is

$$u = \nu\lambda = \text{Constant} \times \nu \times (M/N\rho)^{1/3} \quad \ldots(4)$$

and is also given by Newton's formula

$$u = \left(\frac{\epsilon}{\rho}\right)^{1/2} = \left(\frac{1}{K\rho}\right)^{1/2} \quad \ldots(5)$$

where $\epsilon\ (= 1/K)$ is the bulk modulus of elasticity. On equating Eqs. (4) and (5), we get

$$\text{constant} \times \nu \times (M/N\rho)^{1/3} = \left(\frac{1}{K\rho}\right)^{1/2} \quad \ldots(6)$$

$$\text{or } \nu = (\text{constant})^{-1} \left(\frac{1}{K\rho}\right)^{1/2} (N\rho/M)^{1/3}$$

$$= (\text{constant})^{-1} N^{1/3} M^{-1/3} K^{-1/2} \rho^{-1/6} \quad \ldots(7)$$

The value of $(\text{constant})^{-1}$ in Eq. (7) obviously depends [through Eq. (3)] on the type of lattice structure.

In an fcc lattice, e.g. NaCl, each Na^+ ion is surrounded by 6 Cl^- ions at a distance R (nearest neighbour distance). As a first approximation, all the ions can be regarded as distributed on a sphere of radius of R about the central atom, so that

$$\frac{4}{3}\pi R^3 = \frac{6V_a}{N} = \frac{6M}{N\rho}$$

$$\text{or} \qquad R = \left(\frac{6M}{N\rho} \cdot \frac{3}{4\pi}\right)^{1/3}$$

Since $\lambda = 2R$, it follows from Eq. (3) that

$$2.\left(\frac{9}{2\pi}\frac{M}{N\rho}\right)^{1/3} = \text{Constant}\left(\frac{M}{N\rho}\right)^{1/3}$$

By substituting this in Eq. (7) and taking $N = 6{\cdot}023 \times 10^{23}$, we obtain

$$\nu = 1/2\left(\frac{2\pi N}{9}\right)^{1/3} M^{-1/3} K^{-1/2} \rho^{-1/6} \quad \ldots(8)$$

For compounds or binary salts, M should be replaced by

$M' = 2M_1M_2/(M_1+M_2)$, where M_1 and M_2 are the masses of the individual ions. The atomic volume is also replaced by the mean atomic volume, $V_a' = M'/\rho = NR^3$, and Eq. (8) becomes

$$\nu = 1/2\left(\frac{2\pi N}{9}\right)^{1/3} M'^{-1/3} K^{-1/2} N^{1/6} R^{1/2} \quad \ldots(9)$$

Eq. (9) is used to calculate ν for all the twelve alkali halides. The values of K and R are taken from the literature.[5] A graph is plotted between the calculated values of ν and the observed values of Vickers microhardness (H_V) (Fig. 1). It is clear from Fig. 1

that ν is linearly related to H_V. The slope of the straight line is found to be $4{\cdot}30 \times 10^{-12}$ and its intercept on the Y-axis is $-4{\cdot}26$. The results can be represented by the following equation

$$H_V = 4{\cdot}30 \times 10^{-12}\,\nu - 4{\cdot}26 \qquad \ldots(10)$$

where H_V is expressed in kg/mm^2 and ν in sec^{-1}. The calculated values of H_V and ν for different alkali halides are given in Table 1.

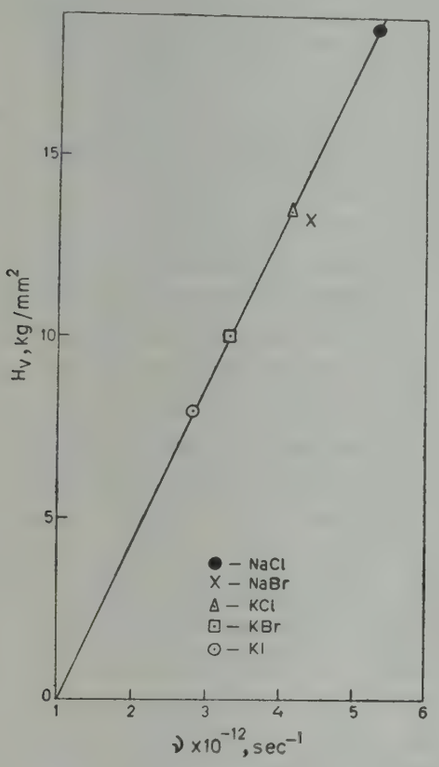

Fig. 1—Plot between the calculated values of ν and the observed values of H_V

Table 1—Values of R, K, ν and H_V (Calculated and Observed)

Crystal	R (from Ref. 5) Å	$K \times 10^{11}$ (from Ref. 5) cm^2/dyne	$\nu \times 10^{-12}$ [calculated using Eq. (9)] sec^{-1}	H_V [calculated using Eq. (10) kg/mm^2	H_V (Observed) kg/mm^2
LiF	2·014	0·1516	12·4616	49·32	
LiCl	2·570	0·3379	8·7951	35·56	
LiBr	2·751	0·4244	7·7405	29·03	
LiI	3·000	0·5792	6·8156	25.05	
NaF	2·317	0·2148	7·8228	29 38	
NaCl	2·820	0·4218	5·3186	18·61	18·5*, 21·3* 22·1*
NaBr	2·989	0·5141	4·3860	14·60	13·2
NaI	3·237	0·6705	3·8272	12·20	
KF	2·674	0·3309	6·1097	22·01	
KCl	3·147	0·5765	4·1636	13·64	13·1*, 13·5*
KBr	3·298	0·6832	3·2945	9·91	10·0*, 12·5*
KI	3·523	0·8603	2·8432	7·97	7·0*, 7·9†

* Madhu Shukla & Bansigir K G, *J. Phys.* D9 (1976), L 49.
† Subba Rao U V & Hari Babu V, *Pramana*, 11 (1978), 149.

To test the validity of Eq. (10), the calculated values of H_V are compared with the observed values reported by other workers (Table 1). It is evident that the values of H_V calculated using Eq. (10) are nearly equal to the values determined experimentally by other workers. Data in respect of observed values of H_V are available only for 5 alkali halides, and hence only these data are reported in Table 1.

In Fig. 1, the cross mark corresponding to NaBr is slightly away from the line. In this connection, it may be noted that the microhardness is a surface sensitive property and the experimental value of H_V that has been noted from the literature (cited in Table 1) does not indicate the surface conditions. As NaBr is very hygroscopic in nature, this property does affect the surface conditions and may change the value of H_V in this case.

The dependence of H_V on ν indicates that the microhardness is affected not only by the addition of impurities but also by lattice vibrations. It has been observed that as the lattice vibration frequency decreases, the microhardness also decreases.

The author is grateful to Prof. K G Bansigir for his guidance and also acknowledges with thanks the grant of a research fellowship by CSIR, New Delhi.

References

1. Berzina I G, Bermah I B & Savintsev P A, *Soviet Phys. Crystallogr.*, 9 (1965), 483.
2. Plendi J N & Gielesse P J, *Phys. Rev.*, 125 (1962), 829.
3. Chin G Y, Van Uitert L G, Green M L, Zydzik G J & Kometani G Y, *J. Am. ceram. Soc.*, 56 (1973), 369.
4. Partington J R, *An advanced treatise on physical chemistry*, Vol. 3, 1963, 360.
5. Garg V K, Puri D S & Verma M P, *Phys. Status Solidi B*, 80 (1977), 63.

Application of Hagemark's Theory to Multicomponent Systems ZnTe : Li, O & Na-implanted CdS

P D Ekbote & J K Zope*

Department of Physics, Nagpur University
Nagpur 440 010

Received 20 *April* 1978; *accepted* 4 *December* 1979

KI Hagemark's theory [*J. Phys. Chem. Solids*, 37 (1976), 461] has been applied to explain the modification of oxygen isoelectronic traps in a ZnTe : Li, O system and the anomalous intensity of I_1 line and green edge emmission of Na-implanted CdS annealed at a temperature where a considerable amount of lattice disorder is expected to remain.

Hagemark in his recent theory[1] stressed the importance of the thermal histo ry of a crystal in

* Present address : Department of Physics, Shivaji University, Kolhapur

which the component species have considerably different temperature dependence of component mobilities. The same is applicable to multicomponent systems. Further, he showed that for a semi-conductor of the type MX (due to the differences in the temperature dependence of the diffusion constants of M and X), M and X do not freeze in at the same temperature during a cooling from a high to low temperature. As a result of this, the following 3 temperature ranges have to be considered:

I. A high temperature range where both M and X are mobile. The system has been shown to have 2 degrees of freedom, i.e. P_M and T being variables where P_M is the partial pressure of species M and T is the temperature.

II. Intermediate temperature range where, in the case discussed by Hagemark, X is assumed to be frozen in. The system has now 3 degrees of freedom, i.e. P_M, T and $\Sigma [V_X]$ being variables, where $\Sigma [V_X]$ is the concentration of X vacancies.

III. A low temperature range where M and X are both immobile and the system has 3 degrees of freedom, i.e. $\Sigma [V_M]$, $\Sigma [V_X]$ and T being the variables.

It must, however, be emphasized that there in no sharp cut off point in mobility versus temperature curve for any component and hence the conclusions drawn are only qualitative in nature. In the present note, we have tried to explain the results of Marple and Aven[2] on ZnTe:Li, O system and of Tell *et al.*[3] on Na-implantation in CdS, making reasonable assumption regarding the relative mobilities of the species involved from the data available in literature.

ZnTe usually exhibits *p*-type conduction and its acceptor centres are doubly charged Zn vacancies due to excess Te.[4] The concentration of these vacancies depends on the partial pressure of the components. When the partial pressure of Te increases, the concentration of Zn vacancies usually increases. The lowest carrier density in *p*-type ZnTe has been reported for ZnTe crystals heated at 1000°C in molten Zn and is 10^{14} - 10^{15} cm^{-3}. The energy of formation for a Zn vacancy is 3·95 eV.[5] A successful synthesis of *n*-type ZnTe has been reported by Fischer *et al.*[6] This material has been prepared under an argon pressure of 30-50 atm from elements with 20% excess Zn. The melt was cooled by Bridgeman's method from 1280 to 1100°C in 5 hr and this was followed by quenching in oil. The crystals obtained in this way have a resistivity of 10^5 - 10^6 cm and an electron mobility up to 350 cm^2 V^{-1} sec^{-1}. In the samples prepared by Marple and Aven, the temperature was 850°C only and after several hours of heating were rapidly cooled to room temperature. It is thus apparent that the samples are still *p*-type, i.e. heating of ZnTe in Zn atmosphere alone cannot produce more Te vacancies than Zn vacancies.

In the Marple and Aven experiment, the conditions are slightly different than in the Hagemark's MX case. The species involved are saturated Zn vapour, saturated Li vapour; and oxygen and Te fixed in the lattice along with the excess Zn vacancies. It has been shown by Crowder[7] that lithium goes into the ZnTe structure at substitutional site, substituting for Zn^{2+}, thus giving a 0·04 eV deep acceptor level. The alkalies Li and Na are found to be both fast diffusing and highly soluble in II-VI compounds. Li will start diffusing into the crystal at much earlier stage (i.e. at much lower temperature) and diffusing by interstitial mechanism. During this time, Zn, Te or O will have negligible diffusion or movement. Owing to Li in-diffusion by interstitial mechanism under saturated Li vapour, it is obvious that a considerable quantity of Li has diffused in to ZnTe by the time the remaining species start moving. It may be argued that at lower temperature when Li alone was in-diffusing, it may transfer one of its (outer) electrons to the deep isoelectronic trap due to oxygen, thus forming a Coulombic pair Li^+- O^-. Some Li will of course occupy the Zn vacancies, thus trying to make the crystal *p*-type. As the temperature is raised and stabilized at 850°C there would be a balancing between Te out-diffusion and, Li and Zn in-diffusion, i.e. equilibrium is attained. There are chances that Li^+ in-diffusion (and subsequent substitution for Zn^{2+}) may facilitate Te out-diffusion if we take into account $[e^- h^+]$ the equilibria at a particular temperature. It is likely that Zn in-diffusion proceeds via vacancy mechanism. It is also possible that oxygen, due to its additional electrostatic bonding with Li^+ would not have much chance of leaving the crystal though it may change its position in the lattice by drifting through the anion lattice. Furthermore, the studies of Marple and Aven indicate that heating of ZnTe in the atmosphere of Zn alone does not remove oxygen. Hence even if the Li^+ - O^- pair dissociates at higher temperature, during the rapid cooling from higher to lower temperature due to its greater mobility as compared to Zn, Te and O, the chances of Li pairing up with O are quite formidable, thus modifying the oxygen centre and removing the brownish colour of ZnTe which is due to oxygen.

Na-*implanted* CdS—It is well known that the type conversion of *n*-CdS is not possible by equilibrium processes like diffusion due to lack of shallow acceptor and/or to the presence of compensating intrinsic defects. Ion implantation renewed the hope of obtaining type conversion in CdS by either

implanting a group V impurity or the alkalies Na or Li. It was found that Na and Li did give shallow acceptors of depth 0·17 eV and Tell[8] and Tell *et al.*[3] conclusively showed that the alkalies give at least one shallow acceptor in CdS which is responsible for the characteristic low temperature luminescence, the I_1 line (exciton bound to neutral acceptor) and the green edge emission (donor-acceptor pair recombination). It was found that for Na-implanted sample, a relatively sharp peak in the I_1 line intensity and the green edge emission are observed at annealing temperatures where a significant amount of lattice damage remains in the crystal. The alkalies are known to be both rapidly diffusing and highly soluble in CdS and it is known from studies of Tell that an increase in Cd vacancies (produced by heating in S atmosphere) favours the incorporation of the alkalies at the substitutional site. Application of Hagemark's theory would easily lead to the conclusion that the alkalies being fast diffusing (as compared to Cd) would capture the lattice sites more readily than could Cd. Also, the chalcogens are known to have a high mobility in all II-VI compounds as shown by Hall and Woodbury.[9] A large amount of Cd would, therefore, remain at the interstitial site where it would naturally behave as donor. Hence the low temperature annealing would result in a large number of Na acceptors at the substitutional site giving the high I_1 line intensity. Since the S sites are also captured by sulphur, the concentration of electrons would be lowered, thus some of the acceptors would be ionized to maintain the $e^- - h^+$ equilibria. This would naturally result in the increase in the intensity of I_2 line (donor-acceptor recombination) also. This situation is not observed in the Li implantation case, but studies of Tell show that under certain conditions Li behaves as an interstitial donor, and prefers the interstitial position.

The authors are thankful to Dr C Mande for his interest in the present work. One of them (PDE) acknowledges the financial assistance from the University Grants Commission, New Delhi.

References

1. Hagemark K I, *J. Phys. Chem. Solids*, 37 (1976), 461.
2. Marple D T F & Aven M, *International Conference on II-VI Semiconducting compounds*, (W A Benjamin, New York), 1967, 315.
3. Tell B, Gibson W M & Rogers J W, *Appl. Phys. Lett.*, 17 (1970), 312.
4. Hopfield J J, Thomas D G & Lynch R T, *Phys. Rev. Lett.*, 17 (1966), 312.
5. Thomas D G & Sadauski E A, *J. Phys. Chem. Solids*, 25 (1964), 395.
6. Fischer A G, Caridas J N & Dresner J, *Solid St. Commun.*, 2 (1964), 1577.
7. Crowder F A, *Phys. Rev.*, 177 (1969), 1235.
8. Tell B, *J. appl. Phys.*, 42 (1971), 2919.
9. Woodbury H H & Hall R B, *Phys. Rev.*, 157 (1967), 641.

Variation of Hardness with Load for Quenched KBr Single Crystals

R S Chaure

Department of Physics, Government Science, College Jabalpur

&

R N Shrivastava

Department of Physics, Government Science College, Rewa

Received 20 *January* 1979; *revised received* 24 *May* 1979

Meyer's analysis of the load (L) dependence of indentation given by $L = a\,d^n$ (d the diameter of indent and a and n are constants) has been extended to the study of variation of micro hardness with load for quenched single crystals of KBr. The coefficient a and the exponent n have been calculated and their dependence on crystal structure and quenching temperatures studied. An attempt has also been made to bring out the physical significance of a and n.

Indentation hardness testing at low loads reveals that recovered hardness number is not independent of load. In the case of Brinnell test, Meyer's[1] experimental investigations revealed that for a given diameter of ball, as the load is varied, the following relationship holds

$$L = a\,d^n \qquad \ldots(1)$$

where, L is the indenting load, d the diameter of indent and a and n are constants. Although dimensional analysis[2] indicates that the recovered hardness number for Vickers indenter, should be independent of load, actually variations have been observed experimentally. The present investigation extends Meyer's analysis to variation of Vickers hardness number H_v with load, for quenched single crystals of KBr. The coefficient a and exponent n have been calculated and their variation with the quenching temperature studied. The physical significance of a and n is brought out by the experimental data.

Single crystals of KBr were grown from the melt by Kyropoulos method. Specimens of 6 mm × 4 mm × 3 mm size (approximately) were prepared by cleaving. The specimens were heated at the predetermined temperature for about 2 hr and quenched in acetone (AnalaR grade). Reichert indenter, in conjunction with Reichert MEF metallurgical microscope were used to determine H_v. Indenting loads of 10, 15, 20, 25, 30 and 35 g were applied for a period of 30 sec. The experimental data are presented in Tables 1 and 2.

Fig. 1 is a plot of H_v versus indenting load for KBr single crystals quenched from various temperatures. For each quenching temperature, the hardness number increases as the indenting load is decreased. Increase in quenching temperature results in upward shift of the curve. All the curves, including the one for the unquenched specimen tend to become asymptotic to load axis, for indenting loads in excess of 35 g. The value of H_v remains practically constant, irrespective of load, in this region. As pointed out by Onitsch,[3,4] this can be referred to as the beginning of macrohardness region.

The Vickers hardness H_v can be put as

$$H_v = K \frac{L}{d^2} \qquad ...(2)$$

where, K is the constant depending on the type of indenter. Combining Eqs. (1) and (2) we have

$$H_v = K a d^{n-2} = K a^{2/n} L^{(n-2)/n} \qquad ...(3)$$

This shows that H_v can be independent of indenting load only when $n = 2$. Thus the "Macro hardness" range, i.e. the range for the indenting loads in excess of 35 g, may be characterized by logarithmic index having a value $n=2$.

The region for the indenting loads up to 35 g, constitutes what can be termed as the micro hardness, according to the concept of Onitsch. In this region, Meyer's relation, $L = a d^n$ holds.

Table 1—Variation of the Diagonal of indent (in μm) with Load (in g) for Quenched KBr Single Crystals

Quenching temp., °C	Diagonal of Indent (in μm) for Indenting load (in g)					
	10	15	20	25	30	35
50	43·84	55·20	64·80	73·92	80·80	88·48
100	43·36	54·40	63·84	72·96	79·68	87·20
150	42·88	53·76	62·88	72·16	78·72	86·08
200	42·40	53·28	62·08	71·20	77·76	84·96
250	42·24	52·96	61·76	70·40	77·12	84·16
300	42·08	52·96	61·44	70·40	77·12	83·84
350	42·24	53·12	61·44	70·24	77·12	83·84
400	42·08	52·96	61·28	70·08	76·48	83·52
450	41·76	52·16	61·44	69·92	76·80	83·68
500	40·96	51·52	60·00	68·16	75·04	81·28
550	39·68	49·60	58·40	66·56	72·96	78·88
600	37·92	47·84	56·16	64·16	70·24	76·16
Unquenched (40°C)	44·16	55·52	65·28	74·40	81·28	88·96

Table 2—Variation of Hardness (in kg/mm²) with Load (in g) for Quenched KBr Single Crystals

Quenching temp., °C	Hardness (in kg/mm²) for a load (in g)						
	10	15	20	25	30	35	Coefficient a
50	9·65	9·13	8 83	8·48	8·52	8·29	2·91
100	9·84	9·40	9·10	8·71	8·76	8·54	2·95
150	10·08	9·62	9·38	9·02	8·98	8·76	2·99
200	10·31	9·78	9·62	9·14	9·20	8·98	3·04
250	10·40	9·91	9·72	9·35	9·35	9·17	3·09
300	10·47	9·91	9·82	9·35	9·35	9·23	3·11
350	10·40	9·86	9·82	9·40	9·35	9·23	3·09
400	10·47	9·91	9·88	9·44	9·51	9·30	3·09
450	10·63	10·23	9·82	9·48	9·43	9·27	3·18
500	11·05	10·48	10·30	9·98	9·88	9·82	3·28
550	11·78	11·31	10·87	10·47	10·45	10·43	3·41
600	12·89	12·15	11·76	11·31	11·27	11·19	3·73
Unquenched (40°C)	9·52	9·02	8·70	8·37	8·42	8·19	2·90

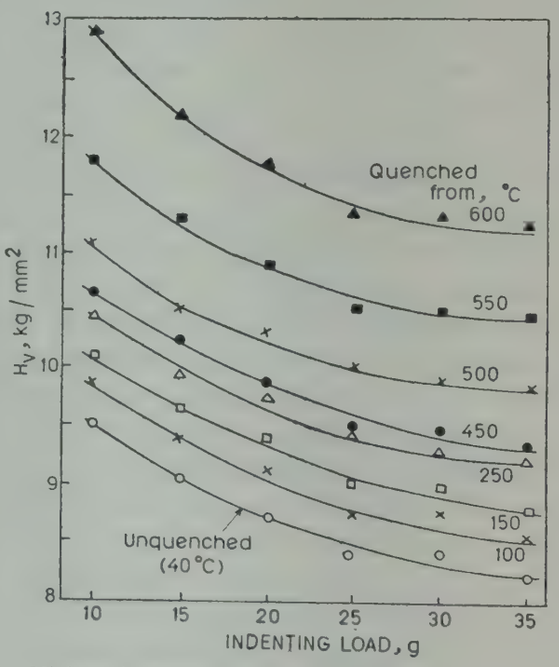

Fig. 1—Vickers hardness number H_v versus indenting load of quenched and unquenched KBr specimens

Fig. 2 shows the plot of log L versus log d for the specimens quenched from various temperatures. Irrespective of quenching temperature, a straight line is obtained in every case. Increase in quenching temperature causes a parallel shift of the straight line to the left. This is because, the value of n in Eq. (1) remains constant at 1·81 (as estimated by the method of best fit), and a varies in the manner shown in Fig. 3. The dislocation density also varies with the quenching temperature in an exactly similar

manner. The constant a is dependent on the dislocation content.

It is also observed that for equal increment of quenching temperature, the degree of lateral shift of the lines is different for different regions of the quenching range. For the quenching temperatures from nearly 250 to 450°C, practically no shift is observed. Calculated values of a for this set of straight lines are given in Table 2. The value of a is found to vary with the quenching temperature, indicating that a is a function of the quenching temperature.

The plot of log a versus quenching temperature (Fig. 3) can be divided into three portions AB, BC and CD. The straight line portion AB shows that log a is directly proportional to the quenching temperature up to nearly 250°C. While the portion BC indicates that between quenching temperatures 250 and 450°C (approximately), a remains practically constant, for quenching temperatures in excess of 450°C, a increases rather abruptly.

Fig. 4 is a plot of log H_v versus quenching temperature for different indenting loads. These curves indicate that decrease in indenting load results in an upward shift of the curves. These curves too, exhibit three distinct regions AB, BC and CD, similar to those of Fig. 3. The possible mechanisms, playing dominant role in each of these regions, have already been discussed by the authors.[5,6] The marked similarity between the variation of a and log H_v

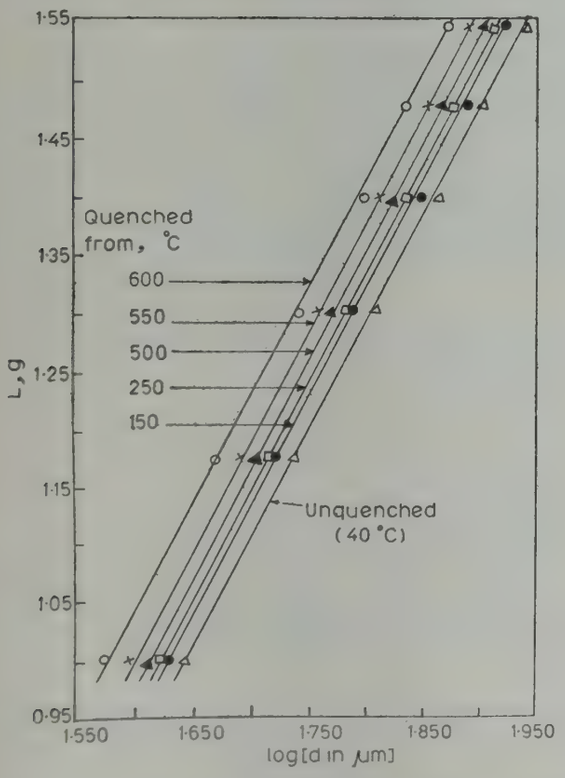

Fig. 2—Indenting load versus diagonal of indent of quenched and unquenched KBr specimens

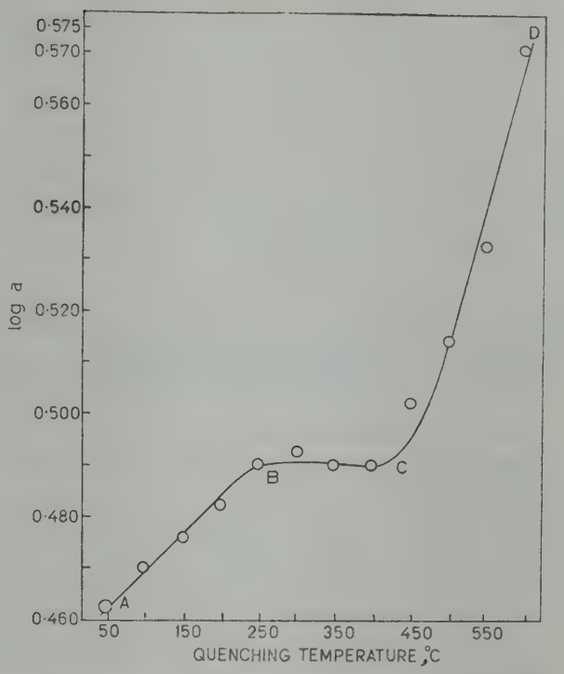

Fig. 3—The coefficient a versus quenching temperature of KBr specimen

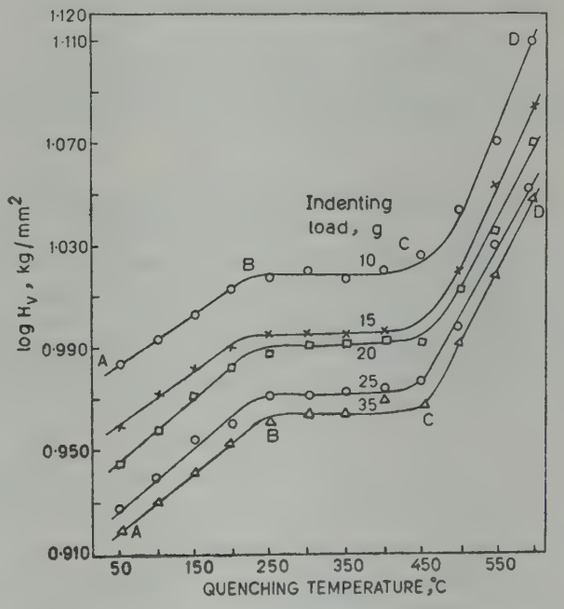

Fig. 4—Vickers hardness number H_v versus quenching temperature for different indenting loads

with quenching temperature, clearly indicates the possibility of dependence of a on the physical state of the specimens. The content and configuration of dislocations produced on quenching as well as the point defects retained, affect the variation of a in the manner of Fig. 3. Further experiments have revealed that the value of logarithmic index n remains constant (1·81) for other potassium halide crystals. This leads to the conclusion that n is a property depending upon the particular crystal structure.[7] On the other hand, the value of a was found to depend upon the material of the crystal as also upon the physical treatment given to the specimen.

The authors wish to thank Dr K C Jain, Principal, Prof. S K Mishra, Dr P S Agarkar of Government Science College, Jabalpur and Dr M C Sen of Government Engineering College, Jabalpur, for providing necessary laboratory facilities. Thanks are due to the University Grants Commission, New Delhi, for the financial assistance.

References

1. Meyer E, *Z. Ver. dt. Ing.*, **52** (1908), 645.
2. Wood Row J, *A E R E Harwell, Report ED/R-1*, (1954), 467.
3. Onitsch E M, *Microskopie*, **2** (1947), 131.
4. *Microhardness, its theory and practice with the Reichert microhardness tester*, Wien 1950.
5. Jain S K, Chaure R S & Shrivastava R N, *Indian J. pure appl. Phys.*, **15** (1977), 864.
6. Chaure R S, Jain S K & Shrivastava R N, *Indian J. pure appl. Phys.*, **16** (1978), 434.
7. Upit G P & Varchenya S A, *Phys. Status. Solidi*, 17 (1966), 831.

Elecrtochemically Deposited Schottky Contacts On *n*-Epitaxial Silicon

B K Singh, R N Mitra & A N Daw

Institute of Radio Physics & Electronics, Calcutta University
Calcutta 700 009

Received 21 *July* 1979; *revised received* 26 *September* 1979

Schottky diode has been fabricated by electrochemical deposition of copper on *n*-epitaxial silicon. The value of barrier height and ideality factor were found to be in good agreement with the results of D Kahng and M P Lepselter[6] [*Bell Syst. tech. J.*, 44 (1965), 1525] obtained by vacuum evaporation.

Generally, Schottky diodes are prepared by vacuum evaporation of the metal on semiconductors. While considerable work has been done on Schottky diodes fabricated by this method, this is not so in the case of Schottky diodes prepared by electrochemical process.[1,2,3] In this note, we report the results of some attempts made for the fabrication of diodes by depositing copper on *n*-epitaxial silicon wafers by an electrochemical method.

The silicon wafers used were of *n*-type having a substrate resistivity of 0·01 Ω-cm with an epitaxial film of 8 Ω-cm resistivity. Typical dimensions of the samples were 3 × 2 mm. The fabrication process basically consists of two steps. In the first step, after usual cleaning with organic solvents and acids, an ohmic contact was made on the rear (lapped) surface of the wafers by using the electroless plating technique.[4] The electrolessly plated samples were soldered on a nickel tab. The samples were then covered with an epoxy compound, keeping approximately 2 × 1 mm area of the sample open. The surface of the crystal was etched in a mixture of H_2O_2 and H_2SO_4 (Caro's etch[5]) in the ratio of 1 : 1 followed by dipping in 10% aqueous HF solution for oxide removal. The wafers were then dipped in a wetting solution consisting of sodium pyrophosphate (6 g), borax (6 g), sodium laurate (50 mg) and H_2O (200 ml) for 10 min. This treatment renders the polished surface completely hydrophilic. Immediately after this step, the wafer was brought under the glass jet for the deposition of metal as shown in Fig. 1. The experimental arrangement is based on Turner's work[2] for plating a metal dot on germanium and silicon. The silicon wafer was used as the cathode and a copper rod as the anode. A potential difference of 20-25 V was maintained between the cathode and the anode for a few seconds. The composition of the electroplating bath was typically as follows : $CuSO_4 \cdot 5H_2O$ (20 g), H_2SO_4 (2·7 ml) and H_2O (200 ml). After plating, a light etching was done for a well defined spot of the metal.

Typical area of the metal spot was $5{\cdot}023 \times 10^{-3}$ cm^2. Electrical contact to the plated metal spot was made by pressure contact with a loop of gold wire. All measurements were taken at room temperature. Barrier height was obtained by two methods : (i) by plotting the reciprocal square of the diode depletion capacitance ($1/C^2$) versus applied voltage (V) (Fig. 2) and (ii) by poltting the forward current (I) versus applied voltage (Fig. 3). The ideality factor (n) was obtained from the slope of the I-V characteristic.

Depletion capacitance of the diode as a function of applied voltage was measured at frequency of 20 MHz using a model 33A/1 Boonton capacitance bridge. The $1/C^2$ versus V plot (Fig. 2) is linear and the extrapolation of the plot gives a diffusion potential of $0{\cdot}32 \pm 0{\cdot}01$ eV. Taking into account the depth

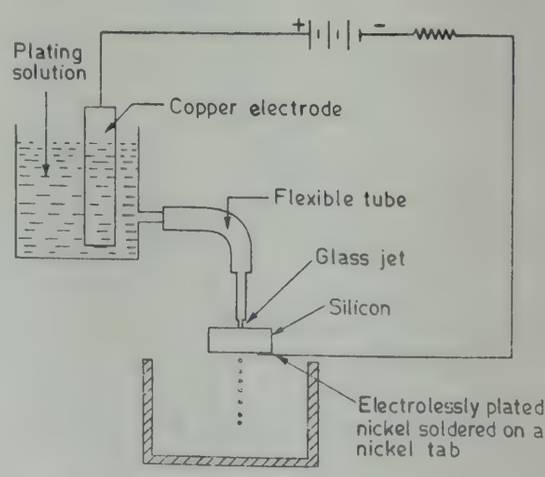

Fig. 1—Experimental arrangement for plating metal dot on silicon

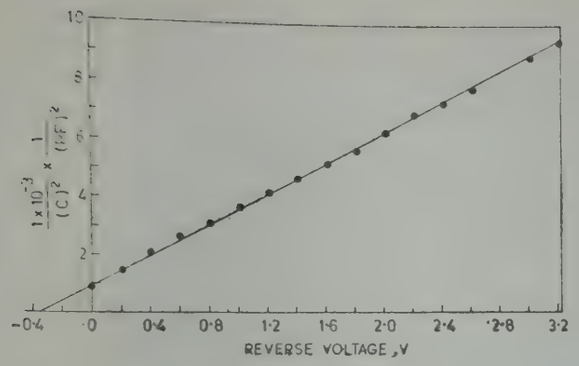

Fig. 2—Plot of the reciprocal square of the diode depletion capacitance versus applied voltage

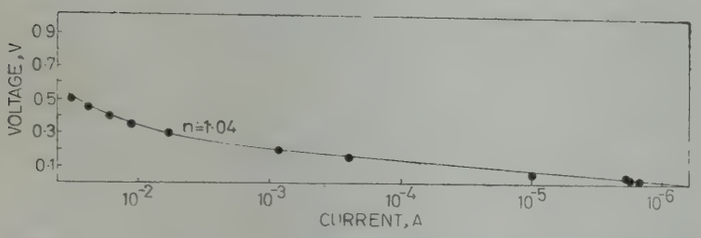

Fig. 3—Semilog plot of the forward current versus applied voltage of diode

of the Fermi level below the conduction band, the barrier height ϕ_B is obtained as 0·58 ± 0·01 eV. Doping density N_D was calculated to be $1{\cdot}192 \times 10^{14}$ atoms/cm³. From an analysis of *I-V* characteristic (Fig. 3) in the usual way, the values of barrier height and ideality factor n were found to be 0·58 ± 0·01 eV and 1·04 respectively. In calculating these values, the effective Richardson constant at room temperature was taken to be 96A/cm²/K². The above values of ϕ_B and n are in very good agreement with the result of Kahng and Lepselter[6] who reported $\phi_B = 0{\cdot}58$ eV and $n = 1{\cdot}03$ for Cu-*n* epitaxial silicon system by vacuum evaporation.

From the above study we conclude that the electrochemical process is a valid and easy method for the fabrication of Schottky diodes. Further studies on this topic are in progress.

The authors thank Prof. M K Das Gupta for his interest in this work. Thanks are also due to Mr K R Unni for his help.

References

1. Wurst E C & Borneman E J, *J. appl. Phys.*, 28 (1957), 235.
2. Turner D R, *J. electrochem. Soc.*, 106 (1959), 786.
3. Dorbeck F H, *Solid-St. Electron.*, 9 (1966), 1135.
4. Daw A N & Mitra R N, *J. scient. ind. Res.*, **33** (1973), 23.
5. Card H C, *Metal semiconductor contacts*, Proc. of Inst. of Physics, Conf. Series Number 22, Manchester, April 1974, p. 129.
6. Kahng D & Lepselter M P, *Bell Syst. tech. J.*, 44 (1965), 1525.

Electrical Properties of Vacuum-evaporated PbS-PbO Films

R Kumar, S K Agarwal & V C Sethi

Solid State Physics Laboratory, Lucknow Road, Delhi 110 007

Received 10 *January* 1979; *revised received* 3 *November* 1979

A mixture of pure PbS and PbO was vacuum evaporated in the atmosphere of H_2S on glass slides, held at 25 °C and 200 °C. Voltage and temperature dependences of electrical resistivity of these films were studied and compared with those of the chemically sprayed PbS films.

Photosensitive films of lead sulphide for the infrared detectors have been produced with the help of oxygen at different stages of fabrication. Various methods for introducing oxygen in the films have been used, e.g. evaporation of the mixture of PbO and the main compound or baking the final layer in a low pressure of oxygen. However, the work on the introduction of PbO in the starting materials is scarce.[1-3] Recently Zemel *et al.*[2,3] have studied the electrical and photoelectronic properties of PbS-PbO evaporated films. The present note describes some results of investigation by the authors for further understanding of the mechanism of photoconductivity in PbS films.

Powders of PbS and 25% PbO, (99·99% pure) were thoroughly mixed and evaporated from a deep narrow mouthed quartz crucible, plugged with quartz wool to prevent spitting during evaporation. The films were deposited on glass slides held at room temperature and 200°C, in vacuum of the order of 10^{-5} torr. In order to maintain the stoichiometry, evaporations were made in H_2S atmosphere.[4-6] H_2S was obtained from the thermal decomposition of thiourea at 150 °C, held in another crucible. This crucible was well separated from the PbS-PbO crucible, and covered on the top to avoid the escape of the decomposed material except H_2S. Thick films (1000 Å) were deposited at a rate of about 100Å/min.

The temperature dependence of electrical resistivity of two typical films grown in H_2S atmosphere on glass plate held at room temperature (25 °C) and 200 °C is shown in Fig. 1. All the electrical measurements were made in vacuum of $\sim 10^{-4}$ torr. It is found that films grown at 200 °C have low resistivity as compared to those grown at room temperature. The values of activation energy were obtained from the slope of the curves. For films deposited at 200°C, an activation energy of 0·4 eV is obtained, which is equal to the reported (room temperature) band gap values of PbS. X-ray analysis of these films also shows sharp diffraction rings of PbS only.

It is observed that the films deposited at 25 °C have high resistivity and high activation energy as compared to 200 °C films. The high value of resistivity and activation energy can be attributed to the presence of interparticle barriers.[7] At 200 °C, H_2S is reactive enough to convert all PbO into PbS, thus showing low resistivity and activation energy equal to the band gap of PbS. In addition to it, the *n*-type conductivity indicates the absence of oxygen content in these films. Contrary to the above, the room temperature films show *p*-type conductivity. In the case of the films of the mixture having a PbO content less than 25%, it was observed that the substrate temperature does not have any appreciable effect on their resistivity versus temperature characteristics. This may happen due to the fact that even at room temperature H_2S converts a part of PbO in the PbS.[1]

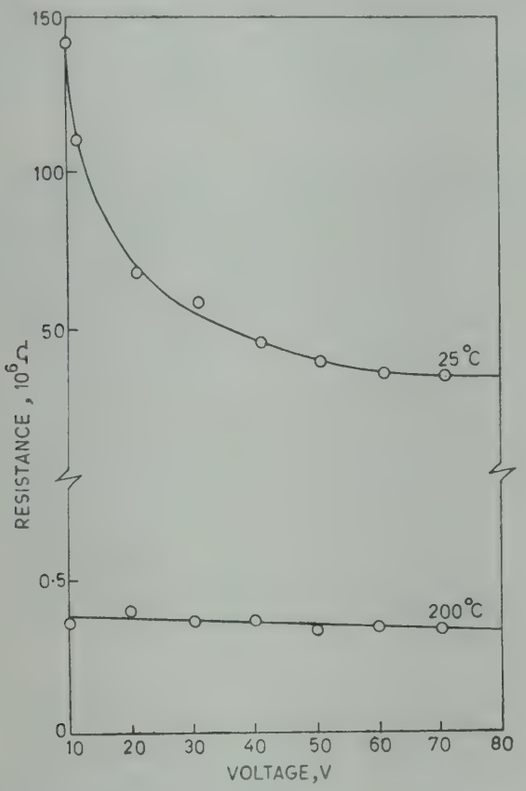

Fig. 2—Voltage dependence of electrical resistance of evaporated PbS-25% PbO films grown in H_2S atmosphere at 25 and 200 °C

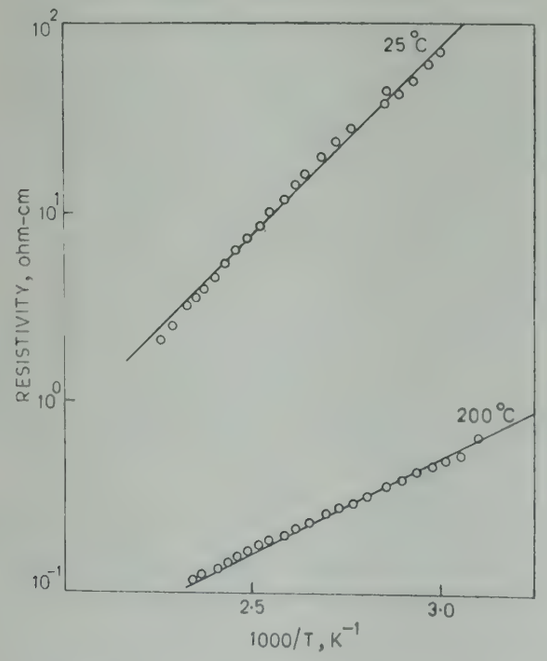

Fig. 1—Temperature dependence of electrical resistivity of PbS-25% PbO films grown in H_2S atmosphere at 25 and 200 °C

Fig. 2 shows the voltage dependence of electrical resistance. The films deposited at 200 °C do not show any electrical resistance variations. However, the films deposited at 25 °C show an exponential decrease in the resistance with voltage. Such diode characteristics could occur only due to the presence of interparticle barriers.[8] A similar trend has been reported for the chemically sprayed PbS films also.[7] The vacuum evaporated films at 25°C show good photoresponse like those of the sprayed films at low temperature (150 °C). Therefore, it may be concluded that the high concentration of oxygen in PbS films leads to the formation of interparticle barriers and the photoconductivity mechanism in such films is due to the barrier phenomenon rather than the bulk property.

References

1. Takao Ando, *Japan. J. appl. Phys.*, 13 (1974), 1301.
2. Sameh Said M & Zemel J N, *J. appl. Phys.*, 47 (1976), 866.
3. Sameh Said M & Zemel J N, *J. appl. Phys.*, 47 (1976), 871.
4. Tyagi R C & Kumar R, *Thin-Solid Films*, 25 (1975), S 21.
5. Tyagi R C, Kumar R, Sethi V C & Mall R P, *Indian J. pure appl. Phys.*, 15 (1977), 390.
6. Sethi V C, Kumar R & Agarwal S K, *Indian J. pure appl. Phys.*, 16 (1978), 481.
7. Tyagi R C, Agarwal S K & Sethi V C, *Indian J. pure appl. Phys.*, 15 (1977), 670.
8. Slater J C, *Phys. Rev.*, 103 (1956), 1631.

Rotational Analysis of the (2, 0) Band of $^{13}C\,^{16}O^+$ Molecule of Comet-tail System

B R Vujisic, D S Pesic, S Weniger* & D Rakotorijimy*
Boris Kidric Institute of Nuclear Sciences, Vinca Belgrade Yugoslavia

Received 31 *July* 1979

The red degraded $A^2\Pi X^2\Sigma^+$ system of $^{13}C\,^{16}O^+$ molecule (using water-cooled hollow discharge tube as a light source) has been photographed at high resolution. Rotational analysis has been carried out for the intense (2, 0) band. Molecular constants of lower and upper states have been calculated. Good agreement between observed and calculated rotational line values has been obtained.

* Observatoire de Paris, Section d'Astrophysique, Meudon, France

Emission spectra of the CO^+ molecule were subject of the comprehensive studies by many workers.[1-3] Comparatively very few spectral studies of isotopic CO^+ species are known.[4,5] In view of this it was considered worthwhile to give rotational analysis of the most intense band of this system.

The emission spectrum of the (2, 0) band (the double headed sub-band are situated at 23469·05, 23454·65, 23342·54 and 23329·73 cm^{-1} for ${}^SR_{21}$, R_2, R_1 and Q_1, respectively) of $^{13}C\ ^{16}O^+$ molecule was excited in a water-cooled hollow cathode discharge lamp with iron electrodes and filled with 1mm Hg $^{13}C\ ^{16}O_2$ (90% enriched). Spectra were photographed in the 9th order of a 2·2 m plane grating spectrograph (reciprocal dispersion 0·8 Å/mm) on Ilford HP4 film with 30 min exposure. The lines were measured on a photoelectric comparator using iron arc lines as wavelength standard. The measurements were reduced by the computer program which fits the iron arc lines to a 3rd power curve using least-squares method. The relative accuracy of individual unblended line is 0·04 cm^{-1}.

From the analysis of Coster *et al.*[6] it is known that this system belongs to a ${}^2\Pi - {}^2\Sigma^+$ transition with ${}^2\Pi$ inverted state. In the present case, lines were observed in seven of the twelve branches predicted in a ${}^2\Pi - {}^2\Sigma$ transition. The large doublet splitting in the upper state, gives rise to two completely separated sub-bands. Due to small value of the spin-rotational constant of ground state,[5] satellite branches are not resolved. The P_{12} branch is not found due to poor intensity. The observed wave numbers of the lines, together with the rotational assignments are listed in Table 1. It was found that in the analyzed region, this band is not

Table 2—Rotational Constants of (2, 0) Band Commet-tail System of $^{13}C\ ^{16}O^+$ Molecule $\nu_0 = 23390·65\ (10)$*

	$A^2\Pi$	$X^2\Sigma^+$
B	1·4783 (2)	1·8860 (2)
$D \times 10^5$	2·0 (6)	2·3 (8)
A_0	−122·02 (2)	—
γ_0	0·03 (1)	0·0092 (1)
p	−0·0101 (8)	—
$q \times 10'$	1·6 (8)	—
RMS	0·089	

*The number in parentheses is the uncertainty in the last digit that corresponds to two standard deviations

Table 1—Vacuum Wavenumbers and Line Assignments for the (2, 0) Band of $^{13}C\ ^{16}O^+$ $A^2\Pi - X^2\Sigma^+$ Transition

J	${}^SR_{21}$	$R_2+{}^RQ_{21}$	$Q_2+{}^QP_{21}$	P_2	R_1	$Q_1+{}^QR_{12}$	$P_1+{}^PQ_{12}$
0·5	23458·45		23450·20				
1·5	462·15	23454·65	447·17	23442·62	23337·07	23329·73	
2·5	465·01	453·79	443·35		339·67	329·57	
3·5	467·14	452·16	438·71		341·54	328·43	23318·26
4·5	468·47	449·77	433·33		342·54	326·48	313·38
5·5	469·05	446·59			342·54	323·68	307·71
6·5	468·84	442·62	420·23	400·98	341·90	320·04	301·13
7·5	467·85	437·90	412·52	390·29	340·28	315·56	293·73
8·5	466·00	432·36	404·00	378·76	337·84	310·23	285·51
9·5	463·46	426·06	394·72	366·47	334·58	304·08	276·43
10·5	460·11		384·63	353·48	330·48	297·06	266·46
11·5	455·96	411·06	373·77	339·67	325·50	289·13	255·57
12·5	451·12	402·39	362·10	325·06	319·70	280·40	244·03
13·5	445 32		349·71	309·68	313·02	270·82	231·67
14·5		382·64		293·56	305·50	260·44	218·23
15·5		371·67			297·06	249·16	
16·5		369·86			287·91	237·09	
17·5		357·26			277·89	224·12	
18·5						210·31	

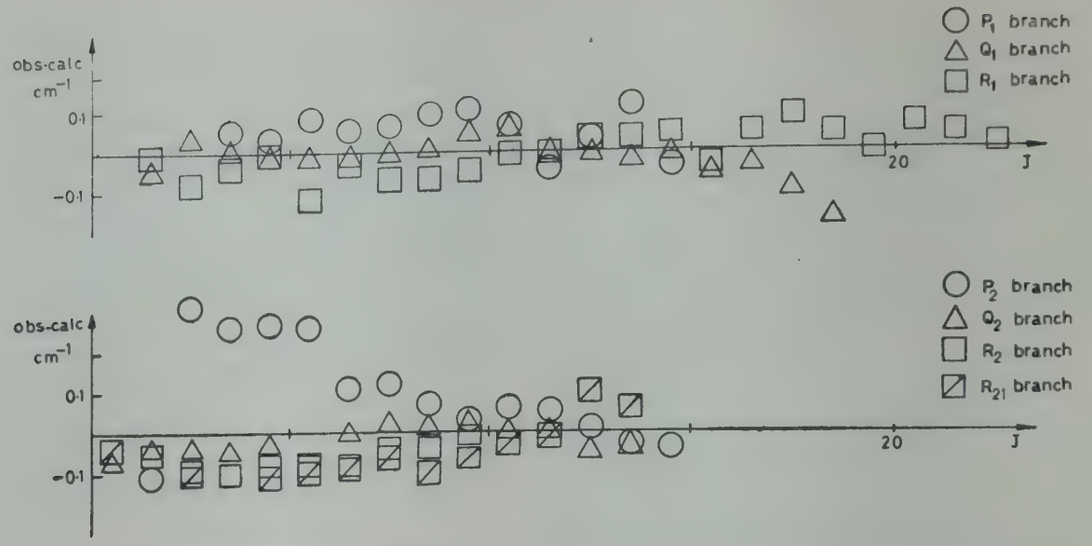

Fig. 1—Differences between the observed and calculated values of the rotational lines of (2, 0) band of $^{13}C\ ^{16}O^+$ molecule

perturbed. This made possible, using isotopic relations, and data for $^{12}C\ ^{16}O^+$ to calculate preliminary rotational constants of $^{13}C\ ^{16}O^+$ molecule. By using these values as a starting point, and employing computer program developed by Zare *et al.*[7] we obtained rotational constants (Table 2) for $^{13}C\ ^{16}O^+$ molecule. In this direct method the measured line position is fitted to the difference of two term values between which the transition occurs. Due to the fact that the observed J values are small the second centrifugal term of rotation, has not been taken into account. In this case the RMS error is 0·089 cm^{-1}. Differences between observed and calculated line values are shown in Fig. 1.

The present results show that differences in the constants of the spin-orbit interaction of the $A^2\Pi$ state between isotopic molecules $^{12}C^{16}O^+$, $^{12}C\ ^{18}O^+$ and $^{13}C\ ^{16}O^+$ are only in the limits of the experimental errors. The rotational constants obtained in this work are in good agreement with those calculated by isotopic relations and data for ordinary molecule.

This work was supported by the Serbian Fund for financing of Scientific Activities.

References

1. Krupenie H P, *Nat. Stand. Ref. Data Ser.* (US Natl. Bur. Standard, Washington) 5 (1966).
2. Rosen B, *Selected constants spectroscopic data relative to diatomic molecules* (Prgamon Press, Oxford), 1970.
3. Pearse R W B & Gaydon A G, *The identification of molecular spectra* (Chapman & Hall, London) 4th Edn, 1976.
4. Asundi R K, Dhumwad R K & Patwardhan A B, *J. molec. Spectrosc.*, 34 (1970), 528.
5. Vujisic R B, D Sc. thesis University of Beograd, 1977.
6. Coster D, Brons H H & Bulthuis H, *Z. Phys.*, 79 (1932), 787.
7. Zare R N, Schmeltekopf A L, Harrop W J & Albritton D L, *J. molec. Spectrosc.*, 46 (1973), 37.

Influence of Vibration Rotation Interaction On Franck Condon Factors

R Tripathi & S B Rai

Department of Physics, Banaras Hindu University
Varanasi 221 005

Received 5 *October* 1978; *revised received* 7 *December* 1978

The effect of vibration-rotation interaction (VRI) on Franck-Condon factors (FCF) has been studied for a large number of diatomic molecules using Murthy and Gowda's criterion. It is found that this criterion reproduces the VRI effect on FCF very well and also gives some idea about the nature of the potential energy curve of the states participating in the electronic transition.

The effective internuclear distance in a vibrating rotator at a particular J, according to Shumaker[1] can be given as

$$r_0\ (J) = r_e \left[1 + \frac{4\ B_e^2\ J(J+1)}{\omega_e^2} \right] \qquad ...(1)$$

where all the spectroscopic constants have their usual meaning. The Franck-Condon factor (FCF), neglecting rotation, depends on Δr_e value, the difference of the minima of the two potential energy curves. If one considers the molecule as a vibrating rotator and represents its energy by the relation

$$V(r)_J = V(r)_0 + \frac{h}{(8\ \pi^2\ \mu c)} \frac{J(J+1)}{r^2} \qquad ...(2)$$

the minimum of the potential energy curve will be different for different J values. This change in r_0—value with J in the two potential energy curves affects the FCF in a similar manner as Δr_e and gives an idea of the influence of vibration-rotation interaction (VRI) on FCF. Therefore, the term

$|\Delta r_0 - \Delta r_e|$ can be utilized as an indicator to represent the effect of VRI on FCF. Murthy and Gowda[2-4] utilizing this idea calculated the Δr_0 value corresponding to different J-values in the (0, 0) band of the (A-X) system of OH. These workers[2,3] showed that Δr_0 value in this system changes rapidly as we go from $J = 1\frac{1}{2}$ to $J = 40\frac{1}{2}$ indicating that FCF for the (0, 0) band of the A-X system of this molecule should vary rapidly which is in good agreement with the conclusions of Chakraborty and Pan.[5] The Δr_0 value is given by the relation

$$\Delta r_0 = |r'_0 - r''_0| = r'_e\left[\frac{1+4B'^2_e J'(J'+1)}{\omega'^2_e}\right] - r''_e\left[\frac{1+4B''^2_e J''(J''+1)}{\omega''^2_e}\right] \quad \ldots(3)$$

Thus in a transition, if the B'_e and ω'_e values are known the variation of FCF with J-value can be studied. If the variation of Δr_0 with J-value is appreciable, the variation in FCF will also be appreciable.

Murthy and Gowda[4] calculated the variation of Δr_0 with J for a large number of diatomic molecules. In the present note, we have extended this calculation to some other diatomic molecules of astrophysical importance. The Δr_0 values corresponding to different J-values in the (0, 0) band of different band systems of the various molecules, have been calculated. The results thus obtained are given in Table 1. The molecular constants used have been taken from Suchard.[6] We have calculated the Δr_0 value for two J-values, $J = 50$ and 100.

It is evident from the results that in some cases the Δr_0 value changes very rapidly as we go from $J = 0$ to 100. Thus in the case of (A-X) system of BH, AlH, GaH, MgH^+, BaH (A-X, E-X), CH (B-X), NH (C-X)..., the change in Δr_0 is large and therefore, in such cases the FCF will vary rapidly with J, whereas in the cases CO (a-x, a'-x), BO (B-X), AlO (B-X), GaO (B-X), BO (C-X), etc. the variation is negligibly small.

A study of variation of Δr_0 with J also gives an idea about the electronic states participating in the transition. A rapid change in Δr_0 value indicates that one of the two participating states in the transition is having a shallow minimum. The reason for this is that the r_0 value in the state which is more flat will change rapidly with J than that in a state which is deep; therefore, the difference of the two will also increase rapidly. Secondly, if the Δr_0 value after reaching a maximum starts decreasing with increasing J-value, the particular J will be very close to the convergence limit of the upper state. Using that

Table 1—Values of Δr_0, Δr_e and $|\Delta r_0 - \Delta r_e|$ of Different Diatomic Molecules of Astrophysical Importance

Band system	J	Δr_0 Å	Δr_e Å	$\lvert\Delta r_0 - \Delta r_e\rvert$ 10^{-3} Å
BH (A-X)	0		0·013	
	50	0·0460		33·0
	100	0·2321		219·1
AlH (A-X)	0		0·0001	
	50	0·3447		344·6
	100	1·3653		1365·2
GaH (A-X)	0		0·071	
	50	0·0394		31·6
	100	0·0546		16·4
GaH ($a\,^3\pi_0 - X\,^1\Sigma^+$)	0		0·033	
	50	0·0254		7·6
	100	0·0030		30·0
InH (A-X)	0		0·112	
	50	0·0905		21·5
	100	0·0271		84·9
MgH^+ (A-X)	0		0·357	
	50	0·4139		56·9
	100	0·5828		225·8
BaH ($A^2\,\pi_{1/2} - X\,^2\Sigma$)	0		0·0355	
	50	0·0453		9·8
	100	0·0750		39·5
BaH ($A\,^2\pi_{3/2} - X\,^2\Sigma$)	0		0·0205	
	50	0·0341		13·6
	100	0·0820		61·5
BaH ($E\,^2\pi_{1/2} - X\,^2\Sigma$)	0		0·0325	
	50	4·8825		4850·0
	100	19·4345		19402·0
CH (A-X)	0		0·0183	
	50	0·0218		3·5
	100	0·032		13·7
CH (C-X)	0		0·007	
	50	0·0003		6·7
	100	0·0715		64·5
CH (B-X)	0		0·0659	
	50	0·1683		102·4
	100	0·4716		405·7
NH (C-X)	0		0·067	
	50	0·1695		102·5
	100	0·4728		405·8
CO (a-X)	0		0·0775	
	50	0·0793		1·8
	100	0·0849		7·4
BO (A-X)	0		0·1481	
	50	0·1496		1·5
	100	0·1540		5·9
BO (C-X)	0		0·1153	
	50	0·1206		5·3
	100	0·1359		20·6
AlO (B-X)	0		0·0492	
	50	0·0511		1·9
	100	0·0567		7·5
GaO (B-X)	0		0·053	
	50	0·0526		0·4
	100	0·0513		1·7

J-value, an approximate value of the dissociation energy of the molecule in that state can be estimated.

The authors are thankful to Prof. D K Rai for his interest in the problem. One of the authors (RT) is grateful to CSIR, New Delhi, for the award of a junior research fellowship.

References

1. Shumaker J B, *J. quant. spectrosc. radiat. Transfer*, 9 (1969), 153.
2. Gowda L S & Murthy N S, *Indian J. pure appl. Phys.*, 14 (1976), 238.
3. Murthy N S & Gowda L S, *Curr. Sci.*, 45 (1976), 448.
4. Murthy N S & Gowda L S, *J. Phys.*, B10 (1977), 491.
5. Chakraborty B & Pan Y K, *J. chem. Phys.*, 55 (1971), 5147.
6. Suchard S N, *Spectroscopic data* (*Internuclear diatomic molecule*), Vol. 1 (IFI Plenum, New York), 1975.

Dielectric Dispersion in Certain Binary Mixtures & Solutions

B S Rajyam

Department of Physics, National Defence Academy
Pune 411 023

C V Rama Sastry

Department of Physics, Andhra University, Waltair
and
C R K Murty

Department of Physics, Nagarjuna University, Guntur

Received 4 *January* 1979; *revised received* 20 *June* 1979

From measurements of dielectric constant and dielectric loss at different frequencies, the dielectric dispersion characteristics of two binary mixtures, viz. 1,2-propane diol+dipropylene glycol (I) and propyl acetate+propyl alcohol (II) and of solutions of dihydroxy benzenes and dihydroxy toluene in ethyl alcohol (III) were examined at 30°C. The system I exhibited a single region of dispersion while II showed, unexpectedly, a single dispersion region which indicates a possible hydrogen-bonding between the carbonyl oxygen of the ester and the hydroxyl hydrogen of the alcohol. The alcohol solutions, i.e. III were examined for asymmetric dispersion of the Cole-Davidson type, but they showed only Debye behaviour. The relaxation times and distribution/dispersion parameters of the mixtures and solutions are reported and the results are discussed with reference to earlier studies on binary mixtures.

The study of the dielectric behaviour of several binary mixtures was carried out by Schallamach[1] and was followed by Denney and his associates[2-4] and later by McDuffie and his coworkers.[5,6] The latter studies yielded results which were in conformity with Schallamach's findings. Certain deviations from Schallamach's pioneering findings on the dielectric behaviour of several associated and non-associated binary mixtures were subsequently reported in binary mixtures of two non-associated liquids. Kadaba and Garg,[7] Forest and Smyth[8] and Kilp *et al.*,[9] noticed two dispersion regions and they explained that the relaxation processes in the particular two-component systems were those of molecules rather than larger of liquid regions.

In the present note, results of studies on three different systems, viz. 1,2-propane diol + dipropylene glycol (I), propyl acetate + propyl alcohol (II) and solutions of dihydroxy benzenes and toluhydroquinone in ethyl alcohol (III) are reported. The system I is a binary mixture of two associated liquids with each of them known to exhibit asymmetric dielectric behaviour of the Cole-Davidson type.[10,11] The glycols were mixed with 25,50 and 75% by volume of 1,2-propane diol which corresponds to 0·374, 0·641 and 0·843 mole concentrations of the propane diol in the mixture. The system II is a simple binary mixture of a non-associated and an associated liquid. This mixture was studied for two proportions of mixing, viz. 1 : 2 and 1 : 1 by weight of the ester and the alcohol. The corresponding mole concentrations of the acetate in the mixture are 0·227 and 0·370. In the system III, catechol, resorcinol and hydroquinone which have the two OH groups in the *ortho*, *meta* and *para* positions respectively, and toluhydroquinone, were dissolved in ethyl alcohol and the solutions were examined for asymmetric distribution of relaxation times, a feature characteristic of polyhydroxy compounds. All these measurements were made at 30°C.

1,2-Propane diol was supplied by Fluka and dipropylene glycol by Fisher & Co. Propyl acetate, dihydroxy benzenes and toluhydroquinone were BDH samples and were of AnalaR grade. Propyl alcohol was an E Merck product with a high degree of purity. Ethyl alcohol was supplied by M/s Hyderabad Chemicals & Pharmaceutical Works Ltd., and was 99·4 % pure. All these chemicals were used without any further purification.

The methods of measurement of dielectric constant (ϵ') and loss (ϵ'') at different frequencies were described earlier.[12] The static dielectric constant of the liquids and solutions was measured at 1 MHz employing a Franklin oscillator-wavemeter combination. Complex permittivity of the liquid systems was measured at UHF with the help of a coaxial line set-up. Microwave test bench employing standing wave method was used for determining ϵ' and ϵ'' at 3 cm wavelength. The frequencies of measurement are 353 to 2000 MHz in the UHF and 9·6 GHz in the microwave region.

The dispersion loci, were obtained by plotting ϵ'' versus ϵ' of the liquids in the Cole-Cole complex plane and were found to be semicircles in some cases (Debye behaviour), circular arcs in some other cases [Cole-Cole (C-C) behaviour] and skewed-arcs in certain others [Cole-Davidson (C-D) behaviour]. The data were analyzed and the relaxation times and distribution/dispersion parameters (α or β) were determined according to methods previously described by the authors.[12,13] The results are summarized in Table 1.

Table 1—Values of Dielectric Constants (ϵ_s), Distribution/Dispersion Parameters (α or β) and Relaxation Times (τ) of a Few Systems

Mole fraction of first component	ϵ_s	ϵ_∞	α or β	$\tau \times 10^{10}$, sec.
1,2-Propane diol + Dipropylene glycol (I)				
0	19·90	2·8	0·63	12·3
0·374	21·40	2·8	0·62	6·31
0·641	23·81	2·9	0·62	4·17
0·843	26·69	2·9	0·61	3·02
1	31·00	2.9	0·61	2·40
Propyl acetate + Propyl alcohol (II)				
0	19·90	3·20	0·03	3·20
0·227	13·86	2·87	0·22	1·66
0·370	10·51	2·45	0·30	0·716
1	5·76	2·08	0·08	0·072
Catechol + Ethyl alcohol (III)				
0	23·56	4·2	0	1·41
0·095	23·74	4·2	0	1·38
0·295	25·25	4·2	0	2·07
Resorcinol + Ethyl alcohol (III)				
0·095	23·92	4·2	0	1·61
0·295	23·56	4·2	0	2·07
Hydroquinone + Ethyl alcohol (III)				
0·077	23·54	4·2	0	1·51
0·173	24·00	4·2	0	2·30
Toluhydroquinone + Ethyl alcohol (III)				
0·069	23·40	4·2	0	1·60
0·271	21·97	4·2	0	3·48

1,2-Propane diol + dipropylene glycol—1,2-Propane diol and dipropylene glycol are both associated liquids; each of them containing two hydroxyl groups shows asymmetric dispersion of the C-D type. The values of β and τ_0 (limiting relaxation time) determined by the authors and reported in Table 1 agree well with standard values available in literature.[14,15] Values of ϵ' and ϵ'' of the binary mixture of these two liquids were plotted in the C-C complex plane and the dispersion loci obtained were skewed-arcs for all proportions of mixing. A single dispersion region in this mixture is in conformity with results of previous investigations on similar mixtures of two associated liquids. From Table 1, it can be seen that τ_0 of I decreases as the mole concentration of 1,2-propanediol is increased, finally approaching its τ_0 value. The variation of τ with the mole concentration of I is shown in Fig. 1 along with the variation of static dielectric constant (ϵ_s) with concentration. Value of ϵ_s increases with concentration for this system. In both the curves, the variation is smooth which suggests that the two glycols are homogeneously mixed up inside the groups as postulated by McDuffie and Litovitz.[16] The β values of the two glycols do not differ much and the β of the mixture lies in between those of the individual glycols. The variation of β is not graphically shown since it is not appreciable.

Propyl acetate + propyl alcohol—Propyl acetate is a non-associated liquid and its dispersion behaviour was reported by the authors elsewhere.[17] The dispersion locus of this ester is a circular arc[18] with $\alpha = 0{\cdot}08$ and $\tau = 7{\cdot}2 \times 10^{-12}$ sec. Propyl alcohol is an associated liquid with almost a Debye type[19] dispersion behaviour ($\alpha = 0{\cdot}03$) and $\tau = 3{\cdot}2 \times 10^{-10}$ sec. These two liquids were mixed in two different proportions, with mole fractions of propyl acetate equal to 0·227 and 0·370. Values of ϵ' and ϵ'' of the mixture measured at different frequencies, were plotted in the C-C plane and the dispersion loci were observed to be circular arcs with large α values, 0·22 and 0·30 respectively, for the two mole fractions. The dispersion characteristics of the mixture and the components are given in Table 1.

The dispersion loci obtained for the binary mixture showed clearly a single region of dispersion and attempts to resolve it into two overlapping discrete regions were futile. This result is unexpected since in a similar mixture of propyl alcohol and isoamyl bromide, Denney[3] observed that the β and τ values of the bromide were retained in the mixture and the τ value of the alcohol was influenced by the presence of the bromide in the mixture.

In the present binary mixture, if the characteristic dispersion of the ester and the alcohol are retained, these two should occur at different frequency regions due to the widely differing τ values of the components. But whether the viscosity of the

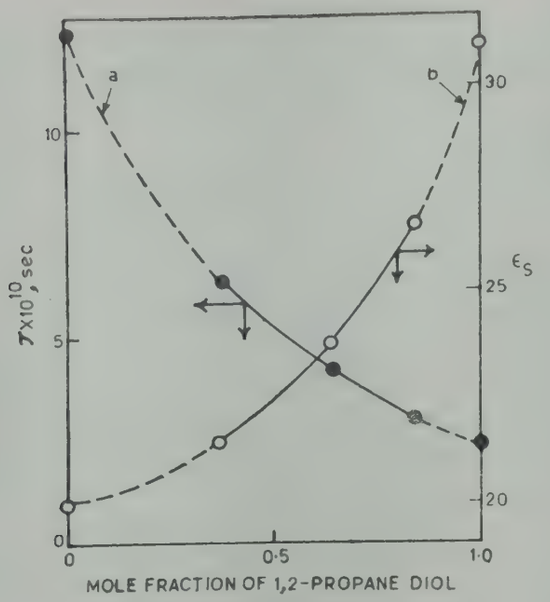

Fig. 1—Variation of (a) relaxation time (τ) and (b) static dielectric constant (ϵ_s) with mole concentration of the system I, i.e. 1,2-propane diol + dipropylene glycol

mixture will have some effect to shift the dispersion region of one component into that of the other is not clearly known. Even if such a shift is possible, the viscosity of the alcohol is only four times that of the ester and, therefore, the viscosity of the mixture cannot be high enough to shift the dispersion region of the ester into that of the alcohol. Thus a single dispersion region observed in the binary mixture cannot be attributed to the viscosity influence.

The α of the mixture is about 0·3 which is quite high compared to the almost zero α values of the components. It is probable that in the mixture, the carbonyl oxygen of the ester enters into hydrogen-bond formation with the hydroxyl hydrogen of propyl alcohol, thereby reducing the self-association of the alcohol. This kind of bonding can result in homogeneous mixing of the component liquids and an increase in the α value.

Solutions of dihydroxy benzenes and toluhydro quinone in ethyl alcohol—The three dihydroxy benzenes, catechol, resorcinol and hydroquinone with the two hydroxyl groups in the *ortho*, *meta* and *para* positions respectively and toluhydroquinone (*para*-dihydroxy toluene) are all solids at room temperature with a high melting point. The dispersion characteristics of these solids have not been reported. The values of ϵ_s* for these substances were reported by the authors previously.[20] These solids are not soluble in non-polar solvents (only slightly soluble in *dioxan*) while they dissolve in large quantities in ethyl alcohol. Catechol and resorcinol were dissolved in the alcohol at 0·095 and 0·295 mole concentrations of the solute, hydroquinone at 0·077 and 0·173 and toluhydroquinone at 0·069 and 0·271. Values of ϵ' and ϵ'' of the solutions were measured and the data plotted in the complex plane gave semicircular dispersion loci for all the solutions. Values of ϵ_s, ϵ_∞ and τ of the solutions are presented in Table 1.

Binary mixtures of glycols and glycerol with alcohols are known to show asymmetric dispersion. Some examples of such mixtures are glycerol-propyl alcohol and 1,3-butane diol-propyl alcohol mixtures studied by McDuffie *et al.*[5] and dipropylene glycol-ethyl alcohol mixture examined by Haranadh and Murty.[21] The absence of asymmetry in the present solutions is interesting to note.

From the results, it is obvious that catechol which is known to be an internally hydrogen-bonded compound behaves no differently from the other two isomers in alcohol solutions. In the solutions, a strong hydrogen-bonding between the solute and the solvent molecules, in preference to any possible intramolecular bonding within the solute molecules themselves, might have occurred as the hydroxyl hydrogen of the alcohols can enter into the bond-formation with the phenolic oxygen of the solute molecules. This leads to greater dispersion between the solute and solvent molecules and the association product exhibits a Debye behaviour. However, it must be remembered that the asymmetric behaviour tends to Debye behaviour under favourable conditions such as increase in temperature or increase in dilution of the solution.

From Table 1, it can be seen that the τ values of the solutions are higher than that of the alcohol. Also comparing the τ's of the different solutions, the relaxation mechanism in the solution of *meta*-substituted compound (resorcinol) appears slower than that in the solution of catechol, the *ortho*-substituted compound.

One of the authors (BSR) is grateful to CSIR, New Delhi, for the award of a senior research fellowship during the tenure of which this work was carried out.

References

1. Schallamach A, *Trans. Faraday Soc.*, 42A (1946), 180.
2. Denney D J & Cole R H, *J. chem. Phys.*, 23 (1955), 1767.
3. Denney D J, *J. chem. Phys.*, 30 (1959), 1019.
4. Denney D J & Ring R W, *J. chem. Phys.*, 44 (1966), 4621.
5. McDuffie (Jr) G E, Lamacchia J T & Conord A E, *J. chem. Phys.*, 39 (1963), 1878.
6. Kono R, Litoviz T A & McDuffie (Jr) A E, *J. chem. Phys.*, 45 (1966), 1790.
7. Kadaba P K & Garg S K, *J. phys. Chem.*, 69 (1965), 674.
8. Forest E & Smyth C P, *J. phys. Chem.*, 69 (1965), 1302.

9. Kilp H, Garg S K & Smyth C P, *J. chem. Phys.*, **45** (1966), 2799.
10. Cole R H & Davidson D W, *J. chem. Phys.*, **18** (1950), 1417.
11. Cole R H & Davidson D W, *J. chem. Phys.*, **19** (1951), 1484.
12. Rajyam B S & Murty C R K, *Indian J. pure appl. Phys.*, **11** (1973), 23.
13. Rajyam B S, Rama Sastry C V & Murty C R K, *Z. Naturf.*, **32a** (1977), 1309.
14. Muralidhara Rao V, *Development of the 8 mm technique and measurements on the dielectric dispersion of certain liquids*, D Sc thesis, Andhra University, Waltair, 1962.
15. Haranadh C, *Trans. Faraday Soc.*, **59** (1963), 2728.
16. McDuffie (Jr) G E & Litovitz T A, *J. chem. Phys.*, **39** (1963), 729.
17. Rajyam B S & Murty C R K, *Indian J. pure appl. Phys.*, **11** (1973), 28.
18. Cole K S & Cole R H, *J. chem. Phys.*, **9** (1941), 341.
19. Debye P, *Polar molecules* (The Chemical Catalogue, New York), 1929.
20. Rajyam B S, Rama Sastry C V & Murty C R K, *Curr. Sci.*, **40** (1971), 62.
21. Haranadh C & Murty C R K, *Trans. Faraday Soc.*, **61** (1965), 1039.

Annealing Effects on dc Current Gain (β) of Silicon Planar Transistors

S C Sood, K L Jasuja & A Venkataramani

Solid State Devices Division
Central Electronics Engineering Research Institute, Pilani

Received 30 *January* 1978; *revised received* 29 *August* 1979

The dc gain of the planar transistors (*n-p-n*) was measured before and after subjecting them to heat treatment (500°C) in different ambients. The effect of various ambients did not depend upon whether or not the surfaces were metallized. It has been found that by annealing the devices in hydrogen ambient, the current gain (β) of the transistors increases remarkably. Results on *n*-type collector of resistivity 5 ohm-cm are reported.

At low collector currents, one of the factors limiting the dc current gain amplification factor (β) is the surface recombination velocity which itself is determined by the fast surface density and surface potential. Blum *et al.*[1] pointed out that surface properties of oxide passivated *n-p-n* transistors can be affected by various ambients and temperature. In this work, significant changes in β of *n-p-n* silicon planar transistors were observed after heating the devices at moderate temperature (500°C) in different ambients, with and without aluminium contacts being made to the base and emitter regions.

The transistors used were *n-p-n* devices of the structure shown in Fig. 1 and were prepared by standard planar processing techniques.[2,3] The starting material was n^+ silicon with 19 μm thick epitaxial layer of resistivity 5 ohm-cm as a collector. An oxide layer was grown on silicon at 1150°C for 1½ hr in dry, wet and dry oxygen cycle. Then the base areas were defined by standard photomasking and etching procedures. The diameter of the base was 330 μm. Boron was diffused in this region to a depth of 6 μm using B_2O_3 as an impurity source. The junction depth was determined by angle lapping and staining[4] and the sheet resistivity of the diffused layer was measured with a four-point probe. From these two values the surface concentration of the base region was calculated using Irvin curves.[5] The value obtained was $2{\cdot}5 \times 10^{18}$ atoms/cm³. Similarly phosphorus doped (*n*-type) emitters were formed using $POCl_3$ as an impurity source. The diameter of the emitter dot was 150 μm and the junction depth 4 μm. The surface concentration obtained for emitter region was 2×10^{20} atom/cm³. Now the oxide was removed from the base and emitter contact regions and the wafer was broken into four pieces in order to study the annealing effects in different ambients.

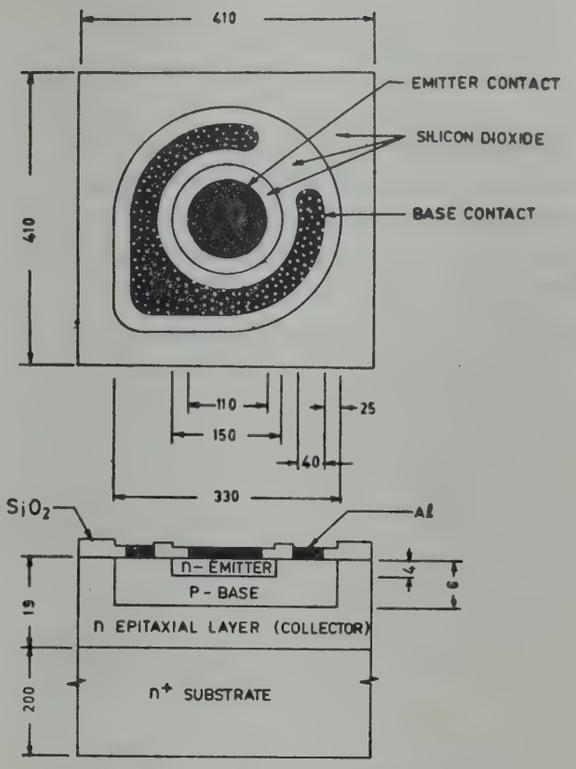

Fig. 1—Geometry of a typical *n-p-n* transistor (all dimensions in μm)

The series of devices on one piece were tested, i.e. β was measured and then heat treated in this form. The heat treatment was performed in nitrogen ambient in open tube furnace at 500°C for 30 min. The gas was dried using liquid nitrogen trap before passing into the furnace. Then the sample was cooled to room temperature and again β was measured. The

results are shown in Table 1. The effects on β for another sample were studied before and after heat treatment in the forming gas (H_2:N_2 as 1:4) and the results can be observed from Table 1. The remaining two pieces were also tested and then metallized, i.e. emitter and base metal contacts were made to the devices using aluminium metal. Now the effect on β of these devices was studied in different ambients and the results are summarized in Table 2.

As we know, a fraction of carriers injected into the base of a junction transistor will not reach the collector junction but will be lost by the recombination at the surface of the base region. This introduces an additional component of current to the total base current, thus reducing β significantly. Therefore, the semiconductor surface is characterized by the recombination velocity S_0, which depends upon the surface treatment during the fabrication of a transistor. Moreover,[6] due to the disruption of the periodicity of the lattice at a surface, a high density of states about 10^{15} cm^{-2} will be present near the surface. But the freshly etched or chemically clean silicon surfaces are always covered by a thin layer of oxide and shows fast surface state density of the order of 10^{11} to 10^{12} cm^{-2}. Thermally oxidized silicon surfaces have been found to have fast surface state density of the same order. Many workers like Terman,[7] Grove *et al.*[8] have verified these results from the *C-V* characteristics using MOS structure. Further, they have confirmed that if low temperature (500°C) annealing step is included, the density of fast surface states can be reduced by an order of magnitude. The relationship, $S_0 = \sigma v_{th} N_{st}$, where N_{st} is the single level surface generation recombination centres (i.e. fast surface states) per unit area, σ their capture cross-section and v_{th} is the thermal velocity of the carriers, is given by Grove and Fitzgerald.[9] The low temperature annealing reduces the recombination velocity to about 1/3 of its original value.

Table 1—Effects of Annealing in Dry Nitrogen and Forming Gas at 500°C for 30 min on β of the transistors Studied

In dry N_2		In forming gas	
Before heat treatment	After heat treatment	Before heat treatment	After heat treatment
25	30	20	160
20	25	20	150
20	20	25	200
25	25	20	175
25	25	20	150
20	20	25	160
		20	150

β has been measured of I_C = 1mA and V_{CE} = 10V

Table 2— Effects of Annealing in Dry Nitrogen and Forming Gas at 500°C for 15 min on β of transistors after Metallization

In dry N_2		In forming Gas	
Before metallization & heat treatment	After metallization & heat treatment	Before metallization & heat treatment	After metallization & heat treatment
25	60	25	100
25	50	25	80
25	75	25	80
20	40	25	150
20	30	20	100
20	25	20	80
25	50	25	200

In our experiments we have studied the effects of different ambients on the surface properties of thermally oxidized silicon surfaces, in the form of *n-p-n* transistors by measuring β before and after the heat treatments. Table 1 shows that annealing the devices in dry nitrogen at 500°C did not yield any appreciable change in β, which means that the number of active or fast surface states remains more or less of the same order of magnitude. But heating the devices in forming gas produces a remarkable improvement (Table 1 indicates that the current gain has increased six to seven times its original value). During[10] this annealing, hydrogen is able to react with unsaturated silicon atoms (which generally gives fast surface states) at the Si-SiO_2 interface, thus forming the covalent bond (Si—H) and hence makes the trapping centres inactive which means the disappearance of a large number of fast surface states.

After metallization, the annealing was done in dry nitrogen and again an improvement in β was observed as shown in Table 2. It seems that the role of nitrogen is similar to that of hydrogen when aluminium is present on the silicon surface. During the annealing of the aluminium alloy at 500°C, reaction of aluminium with the minute amounts of water contained in the oxide produces the active species of hydrogen (atomic H) which reduces the trapping centres of Si-SiO_2 interface.[11] The results of Table 2 can also be explained in a similar way, i.e. the disappearance of a large number of fast surface states in hydrogen ambients.

In conclusion, it can be said that β of *n-p-n* silicon planar transistor improves by annealing at 500°C in an atmosphere containing hydrogen. Hydrogen plays an active role in reducing the fast surface state density at the Si-SiO_2 interface.

The authors are thankful to Dr W S Khokle, Scientist, for his continuous encouragement and help during the course of this work.

References

1. Blum J *et al.*, *J. electrochem. Soc.*, Abstract No. 55 (1964), 59-C.
2. Warner (Jr) R M, *Integrated circuits-design principles and fabrication* (Mc Graw-Hill New York).
3. Balain K S *et al.*, *J. Inst. Telecommun. Engng.*, **12** (1966), 461.
4. Burger R M & Donovan R P, *Fundamentals of silicon integrated device technology* (Prentice Hall, New Jersey) 1967.
5. Irvin J C, *Bell Syst. tech. J.*, **41** (1962), 387.
6. Grove A S, *Physics and technology of semiconductor devices* (John Wiley, New York), 1967.
7. Terman L M, *Solid St. Electron.*, **5** (1962), 285.
8. Grove A S *et al.*, *Solid St. Electron.*, **8** (1965), 145.
9. Grove A S & Fitzgerald D J, *Solid St. Electron.*, **9** (1966), 783.
10. Kooi E, *Philips Res. Rep.*, **20** (1965), 568.
11. Kellner W, Goetzberger A, *Proc. IEEE*, **ED22** (1975), 531.

Spectral Studies of some Uranyl Complexes

V K Rastogi & A N Pandey*

Department of Physics, Lajpat Rai College, Sahibabad 201 005

and

S L Gupta & R C Saxena

Molecular Research Group, M M (P G) College
Modinagar 201 204

Received 21 *September* 1979

Stable uranyl complexes of β-α-naphthyl amino 2,4,6-trihydroxy propiophenone and β-benzidinyl, 2:4-dihydroxy propiophenone have been prepared, isolated and characterized on the basis of chemical analysis and IR spectral studies for the first time. Wilson's *F-G* matrix method has been followed to evaluate the U—O force constants. The complexation effect on U—O force constant and bond distance in these complexes have also been briefly discussed.

Recently, uranyl complexes having varying coordination number have been prepared with some nitrogen and oxygen donors like dithiophosphinic acid,[1] thiovanol,[2] 3,5-dinitro salicylic acid[3] and mono basic bidentate Schiff bases derived from salicyl aldehydes and alkylamines. These have been used to determine the stability constants of uranyl complexes using the Calvin Bjerrum[4,5] *p*H-titration technique as modified by Irving and Rossotti.[6] A survey of the literature shows that UO_2(VI) complexes of β-α-naphthyl amino 2, 4, 6-trihydroxy propiophenone and β-benzidinyl, 2:4-dihydroxy propiophenone have not been studied so far. This prompted us to prepare and characterize the UO_2(VI) complexes of mannich bases derived from substituted ketones, formaldehydes and amines.

Conn and Wu,[7] Lecomte and Freymann,[8] and Sevchenko and Stepanov[9] from their infrared studies confirmed the three fundamental frequencies of uranyl ion (ν_1 symmetric stretching, ν_2 bending and ν_3 antisymmetric stretching vibrations). Jones[10] recorded the infrared absorption spectrum of sodium uranyl acetate and identified the characteristic frequencies of acetate ion along with those of uranyl ion in the spectrum. Gatehouse and Comyns[11] found the nitrate ion frequencies from the IR spectra of uranyl nitrates. Thus it has been now confirmed that many of the bands in the infrared absorption spectra of uranyl compounds are caused by anions. Recently, a number of anion frequencies in infrared spectra of uranyl salts have also been reported by Garg and Narasimham[12] and Bist and Pant.[13]

In the present note, we report the preparation and characterization of two complexes of uranyl nitrate and two complexes of uranyl acetate with (i) β-α-naphthyl amino-2, 4, 6 trihydroxy propiophenone (NATP) and (ii) β-benzidinyl 2:4 dihydroxy propiophenone (BDP). The infrared spectra of all the complexes have been measured in the region from 400 cm^{-1} to 4000 cm^{-1}. The uranyl ion frequencies obtained from the infrared absorption spectra have been used to calculate the U—O force constant and U—O bond distance in these complexes, using Wilson's *F-G* matrix method[14] and Badger's formula.[15]

Experimental procedure—The ligands β-α-NATP and β-BDP were prepared by the general method for the synthesis of mannich bases given as below.

To a cold ethanolic solution of ketone[16,17] (0·02 mole), formaldehyde (2 ml, 40%) was added and left in ice mixture for ½ hr. To this cold solution, an amine (0·02 mole) solution in the same solvent, was added drop by drop with simultaneous constant stirring. The mixture on keeping for about 1½ hr gave coloured solids. The coloured precipitate thus obtained was washed successively with water containing a little amount of alcohol and recrystallized from ethanol. The composition of the ligands is as detailed below :

β-α-NATP

		m.p.,		C	H	N
$(C_{19}H_{17}NO_4)$	Dark yellow,	320 °C	Found	70·59	5·26	4·33
			Calc	70·62	5·30	4·16

* Molecular Spectroscopy Research Laboratory, Department of Physics, Meerut College, Meerut

			C	H	N
β-BDP					
($C_{21}H_{20}N_2O_3$)	Brick red	m.p. 149 °C, Found	72·20	5·73	7·92
		Calc	72·41	5·75	8·05

Isolation of complexes—The general method for the preparation and isolation of all the complexes is as follows.

$UO_2(OAC)_2 \cdot 2H_2O$ (BDH) and $UO_2(NO_3)_2 \cdot 6H_2O$ (BDH) solutions were prepared by dissolving them in a little amount of water and then adding excess of acetone/THF/alcohol. The ethanolic solution of the ligand was mixed with metallic ion solution in the ratio 1:1 and the *p*H was adjusted to 5 by the addition of ammonium hydroxide. The whole mixture was refluxed for about 3 hr. On cooling, the precipitate was separated, which was filtered and washed repeatedly with water, dried at 110°C and analyzed. Uranium was estimated as U_3O_8. Elemental analyses for C, H and N were performed microanalytically and analytical data are recorded in Table 1.

Spectral studies of complexes—IR spectra of uranyl acetate and uranyl nitrate complexes studied here are in agreement with those studied by other investigators in the complexes having the same group. The infared spectra of the ligands exhibit a number of bands in the region 1000-4000 cm^{-1}, which are assigned to ketonic $\rangle C=O$, phenolic—OH and secondary $\rangle N-H$ grouping. On comparing the spectra of the isolated uranyl nitrate and acetate complexes with the mannich bases it has been found that there is complete absence of —OH stretching frequency in the region 3600-3180 cm^{-1}, revealing thereby the release of protons from hydroxyl group by the metal atom and on complexation the frequency of ketonic group as well as secondary amino group is shifted to the lower regions 1600-1650 cm^{-1} and 3050-3130 cm^{-1}. The shift of these frequencies ($\rangle C=O$ and $\rangle N-H$) and complete disappearance of phenolic frequency indicate that these are three-coordinating sites to the uranyl ion.

Table 1—Analytical Data of Uranyl Complexes

Complex	Colour	Element, %			
			U	C	H	N
$[UO_2(C_{19}H_{16}NO_4).H_2O]NO_3$	Dark brown	F	35·00	33·80	2·55	4·00
		C	35·40	33·94	2·69	4·16
$[UO_2(C_{21}H_{19}N_2O_3)]NO_3$	Orange yellow	F	34·80	36·88	2·86	5·87
		C	35·03	37·12	2·81	6·18
$[UO_2(C_{19}H_{16}NO_4)(CH_3COO)](H_2O)_2$	Light brown	F	34·43	36·46	3·00	2·24
		C	34·62	36·69	2·93	2·03
$[UO_2(C_{21}H_{19}N_2O_3)(CH_3COO)](H_2O)_3$	Yellow	F	31·90	36·70	3·24	3·36
		C	32·58	37·81	3·86	3·83

F, found; C, calculated

The selection rules govern the appearance or non-appearance of a band in the spectrum. According to these rules, for the linear structure of UO_2, only symmetric stretching frequency ν_1 should appear in the Raman spectrum and symmetric bending frequency ν_2 and anti-symmetric frequency ν_3 in the IR spectrum. However, these selection rules are not strictly valid for ions under the influence of crystalline fields. In the present studies as well as in earlier studies, it has been observed that in uranyl complexes, the ν_1 mode of the uranyl ion appears as the weak intensity and ν_3 mode with the strong intensity in the IR spectra. The weak band at 835 cm^{-1} and a very strong band at 950 cm^{-1} have been assigned to ν_1 vibrations and ν_3 vibration of uranyl group in uranyl nitrate. Similarly a weak band at 855 cm^{-1} and a very strong band at 960 cm^{-1}, in case of uranyl acetate have been recorded. The band due to OUO bending mode, is expected to appear near 210 cm^{-1}, in the region which is not studied in the present work. The uranyl ion frequencies in these four complexes have been identified by compairing the spectra of these complexes with those of uranyl nitrate and uranyl acetate and are recorded in Table 2.

Force constants and bond distances—A group theoretical consideration shows that a linear and symmetrical triatomic UO_2^{2+} ion possessing $D_{\infty h}$ symmetry gives rise to three fundamental modes of vibrations which are distributed among different symmetry species as follows,

$$\Gamma_{vib} = \Sigma_g^+ + \Pi_u + \Sigma_u^+$$

Wilson's *G-F* matrix method[14] has been used to determine the stretching and interaction force constants. The results are in turn used to evaluate U—O bond distances following Badger's formula.[15] The force constants, bond distances and spectral data used in the present communication are included in Table 2.

Results and discussion—It is apparent from Table 2 that on complexation the symmetric stretching frequency (ν_1) of uranyl ion is affected to varying extents while anti-symmetric frequency (ν_3) is least affected. The increase and decrease in the symmetric stretching frequency on complexation may be attributed to the variation in U—O bond distance. The appearance of ν_3 fundamental (in the region 942-960 cm^{-1}) with strong intensity and ν_1 fundamental

Table 2—Various Force Constants (mdyne/Å), U—O Bond Distances (Å) and Frequencies (cm^{-1}) ν_1 and ν_3

Sample	U—O Force constant	Force constant due to interaction between bonds	U—O bond distance	ν_1	ν_3
Uranyl nitrate hexahydrate	7·036	−0·463	1·733	835	950
Mono-aquo (β-α-naphthyl amino 2,4,6-trihydroxy propiophenone) uranyl nitrato:	6 933	−0·439	1·736	830	942
(β-Benzidinyl 2:4-dihydroxy propiophenone) uranyl nitrato	7·059	−0·408	1·732	840	948
Uranyl acetate	7·274	−0·383	1·727	855	960
Di-aquo (β-α-naphthyl amino 2,4,6-trihydroxy propiophenone) uranyl acetato:	7·364	−0·229	1·725	870	956
Tri-aquo (β-Benzidinyl 2:4-dihydroxy propiophenone) uranyl acetato:	7·415	−0·115	1·723	880	952

with very weak intensity indicates that even in the complexes, ν_1 is IR inactive and the linearity of uranyl ion is maintained in all these complexes. The U—O bond distance decreases with the increase in the value of symmetric stretching frequency, thus confirming the observation of Garg *et al.*[17,18] Further, the U—O bond distance of uranyl salts generally varies from 1·60 to 1·92 Å depending on the equatorial ligands.[19,20] The calculated values of the U—O bond distances of the present complexes are well within the range 1·733-1·736 Å. It has also been observed that with the increase in the symmetric stretching vibration on complexation, the U—O force constant also increases.

The authors are thankful to Dr U P Varma, Physics Department, Meerut College, Meerut and Dr V Kumar, Physics Department, MM (PG) College, Modinagar, for helpful discussions during the course of this work. They are also thankful to Dr B S Tyagi, Principal, Lajpat Rai (PG) College, Sahibabad (Ghaziabad) for providing the necessary facilities in the College.

References

1. Dass Mohan P N, Diemert K & Kuchen W, *Indian J. Chem.*, 15A (1977), 29.
2. Nigam H L, Pandey K B & Kanth K M, *Indian J. Chem.*, **8** (1970), 454.
3. Santappa, M & Balkrishnan M S, *J. inorg. nucl. Chem.*, **38B** (1974), 36.
4. Wilson K W & Calvin M, *J. Am. Chem. Soc.*, **67** (1945), 2003.
5. Bjerrum J, *Metal ammine formation in aqueous solution* (Haus & Sons, Copenhagen), 1941.
6. Irving H & Rossotti H S, *J. chem. Soc.*, (1954), 2904.
7. Conn G K T & Wu C K, *Trans. Faraday Soc.*, **34** (1938), 1483.
8. Lecomte J & Freymann R, *Bull. Soc. Chim. Fr.*, **8** (1941), 622.
9. Sevchenko A I & Stepanov B I, *Zh. eksp. teor. Fiz.*, **19** (1949), 1113.
10. Jones L H, *J. chem. Phys.*, **23** (1955), 2105.
11. Gatehouse B M & Comyns A E, *J. chem. Soc.*, (1958), 3965.
12. Garg C L & Narasimham K V, *Spectrochim. Acta*, **26A** (1970), 627.
13. Bist H D & Pant D D, *Indian J. pure appl. Phys.*, **2** (1964), 107.
14. Wilson (Jr) E B, Decius J C & Cross P C, *Molecular vibrations* (McGraw-Hill, New York), 1955.
15. Badger R M, *J. chem. Phys.*, **2** (1934), 128.
16. Horning E C, *Organic synthesis*, (John Wiley, New York) Collective Volume 3, 1955, 761.
17. Vogel A I, *Practical organic chemistry* (Longmans, Green & Co., London), ELBS Edn, 1968, 677.
18. Garg C L, Gupta S D & Narasimham K V, *Indian J. pure appl. Phys.*, **8** (1970), 108.
19. Zachariasen W H, *Acta crystallogr.*, **8** (1954), 847.
20. Chernyaev II, *Complex compounds of uranium*, translated by L Mandal (Israel Programme for Scientific Translations, Jerusalem), 1966, 366.

Papers Accepted for Publication

The following papers have been accepted for publication in the *Indian Journal of Pure & Applied Physics* and will be published in the forthcoming issues

New Spectrum of NiCl Molecule in the Near Ultraviolet Region. A B DARJI & N R SHAH (Physics Department, M. S. University, Baroda 390 002).

Formation Energy of the Single Neutral Vacancy & the Vacancy-Interstitial Pair in Silicon. R K JAIN (Laboratorio de Electrónica, Instituto Venezolano de Investigaciones Cientificas, Apartado 1827, Caracas, Venezuela).

Application of Glueckauff's Model for the Lowering of Dielectric Constant to Activity Coefficient Data. V BRAHMAJI RAO (Department of Physics, Sri Venkateswara College, University of Delhi, Dhaula Kuan, New Delhi 110 021).

Controlled Nucleation & Growth of Cadmium Oxalate Trihydrate Crystals in Silica Hydrogel. S K ARORA & TONY ABRAHAM (Department of Physics, Sardar Patel University, Vallabh Vidyanagar 388 120).

Holographic Cylindrical Transmission Grating in Divergent Illumination. MAHIPAL SINGH, SHYAM SINGH & R S KASANA (Indian Institute of Astrophysics, Bangalore 560 034).

On the Bond Asymmetry Parameter of Polyatomic Molecules. J SAMUEL PERIANAYAGAM EBENEZER (Department of Physics, Bishop Heber College, Thiruchirapalli 620 017) and R SRINIVASAMOORTHY & G A SAVARIRAJ [Department of Physics, St Joseph's College (Autonomous), Thiruchirapalli 620 002].

A Composite Fluid Sphere with Two Density Distributions in General Relativity. P PAIRA & T ROY (Department of Physics, Jadavpur University, Calcutta 700 032).

Molecular Dynamics of Some Octahedral Hexahalide Anions. S MOHAN (Department of Physics, Presidency College, Madras 600 005) & K G RAVI KUMAR (Madras Christian College, Tambaram 600 059).

Radio Frequency Conductivity of Opalescent Binary Liquid Mixtures. S N SEN & A K GHOSH (Department of Physics, North Bengal University, Darjeeling 734 430).

Temperature & Frequency Dependence of Dielectric Properties of $CoSiF_6.6H_2O$ around Its Structural Phase Transition Temperature. S K DUTTAROY, S S MITRA & S K GHORAI (Cryogenic Engineering Centre, Indian Institute of Technology, Kharagpur 721 302).

Microtopographical Studies of n-Faces of Natural Analcite Crystals. M S JOSHI, P MOHAN RAO & A V ANTONY (Department of Physics, Sardar Patel University, Vallabh Vidyanagar 388 120).

Strong Coupling Harmonic Oscillator Potential with Weakly Coupled Linear Cubic Anharmonicities. JYOTI CHOUBEY & L K SHARMA (Department of Applied Physics, Government Engineering College, Jabalpur 482 011).

Dipole Pomeron & Neutron-Proton Elastic Scattering between 70-400 GeV/c. MOHAMMAD SALEEM & FAZAL-E-ALEEM (Department of Physics, Punjab University, Lahore, Pakistan).

Analysis of Proton-Proton Elastic Scattering at High Energies. Fazal-e-Aleem (Department of Physics, Punjab University, New Campus, Lahore, Pakistan).

Near Ultraviolet Absorption Spectra of 2,5-Dibromo & 2-Fluoro-5-Chloro-Toluenes in Vapour Phase. R K GOEL & S K SHARMA (Department of Physics, D N College, Meerut 250 002).

Temperature Dependence of ^{35}Cl NQR in Some Chloronitrotoluenes. J UCHIL& DLR SETTY (Department of Physics, University of Mysore, Mangalagangotri, Konaje 574 152) and A INDUMATHY & J RAMAKRISHNA (Department of Physics, Indian Institute of Science, Bangalore 560 012).

Infrared Absorption Spectra of 2-Amino-3-Methyl-& 6-Amino-2-Methyl-Pyridines. R K GOEL, S D SHARMA, K P KANSAL & S N SHARMA (Department of Physics, D N College, Meerut 250 002).

Thermal Conductivities of Binary Gas Mixtures. J D PANDEY (Department of Chemistry University of Allahabad Allahabad-2) and S R PRAJAPATI (Department of Chemistry, K N Government Postgraduate College, Gyanpur, Varanasi).

Green's Function Calculations on the Photoelectron Spectra of Some Small Heteroatomic M-Electron Systems. R GOPAL & PC MISHRA (Spectroscopic Laboratory, Department of Physics, Banaras Hindu University, Varanasi 221 005).

Thermoelectric Effect in Fe-Ni Films. M A ANGADI & A M KARGUPPIKAR (Thin Film Laboratory, Department of Physics, Karnatak University, Dharwad 580 003).

The Second Moment of Solid Hippuric Acid by Wide-Line NMR. N R JAGANNATHAN, S GANAPATHY & R SRINIVASAN [Department of Physics (Crystallography & Biophysics), University of Madras, Madras 600 025].

Effect of Frequency on Circuit-Gain of Transistor-Resistor Coupled Device. ANWAR A KHAN (University Department of Physics, Ranchi University, Ranchi 843 008) and Y ANAND DAS (Department of Physics, Magadh University, Bodh-Gaya 824 234).

Microwave Absorption & Internal Rotation in 1,5-, 1,6- & 1,7-Dicyanoalkanes in Benzene Solutions. PRADID BRAHMA & SUBIR KUMAR ROY (Optics Department, Indian Association for the Cultivation of Science, Jadavpur, Calcutta 700 032).

Evaluation of Dielectric Loss Factor in Magnetically Polarized Silicone Rubber Tubular Electrets by Thermally Stimulated Discharge Current. RUDRAKANT SHRIVASTAVA, M S QUFRESHI, M L KHARE & C S BHATNAGAR (Department of Physics, M A College of Technology, Bhopal 462 007).

INSTRUCTIONS TO CONTRIBUTORS

Manuscripts should be typewritten in double space and on *only one side* of good quality paper; the original and *one carbon copy are to be submitted.*

Papers must be written in clear and concise English. Good attention to spelling and grammar should be given. Long introductions should be avoided. Standard international nomenclature should be followed in giving names of chemical compounds. Standard abbreviations for units of measurement should be used in the text, tables and illustrations. The abbreviations should be used without fullstops.

Title—The title should be neither too brief/general nor unnecessarily long. It should reflect the content of the paper so as to derive the maximum advantage in indexing and information retrieval. A short title for use as running title should also be supplied. If a paper forms part of a series, a subtitle indicating the aspects of the work covered in the paper should be provided.

Abstract—The abstract should indicate the scope of the work and the principal findings of the paper. It should not exceed 3% of the length of the paper and, barring exceptional cases, it should not exceed 200 words. The abstract should be prepared in such a form that abstracting periodicals can use it without modification.

Data—Only such primary data as are essential for understanding the discussion and the main conclusions emerging from the study should be included. All such secondary data as are of interest to a specific category of readership may, if necessary, be deposited in the editorial office (or retained by the authors) for supply on demand. A footnote to this effect may be inserted at a suitable place in the paper.

Mathematical portions—Special attention should be given to the mathematical portions of the paper. Equations must be well separated from the text and written clearly with good separation between the successive lines. The usual norms of breaking long mathematical expressions may be adhered to. Equations should be numbered consecutively in Arabic numerals with the number in parentheses near the right hand margin. Superscripts and subscripts should be clearly indicated in pencil by $\vee$ and $\wedge$ sign respectively. Capital and small letters, particularly of the same letter when both occur, as well as letters or symbols likely to be confused one for the other, should be clearly distinguished. Special characters (e.g. Greek, script, vector, tensor, matrix, etc.) required must be indicated by marginal notes. Letters and symbols which should appear in bold face must be clearly indicated. To simplify typesetting: (i) long and complicated mathematical expressions which are frequently repeated should be replaced with single letter/symbol, without clashing with the others used in the paper; (ii) the "exp" form of complex exponential functions should be used: and (iii) to simplify fractions, the solidus (/) is to be used and fractional exponents are to be used instead of root signs, e.g.

write $\left(4\omega_{pl} K_{s\lambda}^2 \Big/ \tilde{\omega}\ K_D^2\right)^{1/2}$ and *not* $\sqrt{4 \frac{\omega_{pl} K_{s\lambda}^2}{\tilde{\omega} K_D^2}}$

write $\exp\{-i\omega_0 (t_1 - t_2)/2\}$ and *not* $e^{-i\omega_0 (t_1 - t_2)/2}$

Tables—Tables should be typed *on separate sheets* of paper without any text matter on the page. They should be numbered consecutively in Arabic numerals and should bear brief titles. *Column headings should be brief.* Units of measurements should be abbreviated and placed below the headings. Nil results should be indicated and distinguished clearly from absence of data. Graphs as well as tables, both representing the same set of data, must be strictly avoided. Inclusion of structural formulae inside the tables should be avoided as far as possible. Tables should be referred to in the text by numbers and not by terms like 'above', 'below', 'preceding' or 'following'.

Illustrations—All illustrations should be numbered consecutively in Arabic numerals. Captions and legends to the figures should be self-explanatory and should be typed on a separate sheet of paper and attached at the end of the manuscript. Line drawings should be made with Indian ink on white drawing paper (perferably Bristol board), cellophane sheet or tracing cloth. In addition to the originals, a set of blue-prints or photostat copies should be sent. For satisfactory reproduction, the graphs and line drawings should be drawn to approximately twice the printed size.

The lettering should be uniform, perferably in stencil, so as to be *not less than 2 mm after reduction* widthwise to 3" or 6" as required. The size of geometrical shapes (used to distinguish different graphs), dot, lines, etc. should be sufficiently large to permit the necessary reduction without loss of detail. In the case of *photographs*, prints *must be on glossy paper and contrasty.* If an illustration is taken from another publication, reference to the source should be given and prior permission secured. Illustrations should be protected by thick cardboard packing against creases, folds and broken corners during transit. Illustrations should be referred to in the text by numbers and not by terms like 'above', 'below', 'preceding' or 'following,.

Infrared, ultraviolet, NMR and other spectra, DTA curves, etc. should be included only if they pertain to new compounds and/or are essential to the discussion; otherwise only significant numerical data should be included in the text.

References—The list of references should be prepared strictly in accordance with the style followed

in the Journal. In the text, references to literatures should be numbered consecutively, in the order of their first occurence, and should be indicated by superscripts at the relevant places; as far as possible the placement of references on numerals of other symbols should be avoided; in such cases the reference may be given in parentheses in running text, e.g. "this yielded for n a value of 2·3 (Ref. 5)". Full bibliographic details for all the references mentioned in the text should be listed in serial order at the end of the paper.

In citing references to research papers, names and initials of authors should be followed, in order, by the title of the periodical in the abbreviated form (underlined), the volume number (two lines underneath), the year within circular brackets and the page reference [e.g. Venkatesh, H G & Guha Sarkar, G, *Indian J. pure appl. Phys.*, 12 (1974), 502]. For names of periodicals, the standard abbreviations listed in the *World list of scientific periodicals* edited by P Brown & G B Stratton (Butterworths & Co. Ltd, London), 4th Edition, 1963-65, should be used. If the reference is to an article published without any authorship in a periodical, the title of the article takes the place of the author in the citation [e.g. The content, influence and value of scientific conference papers and proceedings. *Unesco Bull. Libr.*, 16 (1952), 113-26.]. If a paper has been accepted for publication, the names of the authors and the journals should be given followed by the words "in press" within circular brackets [e.g. Sastry, B. A. & Sastry, G. S., *Physica*, (in press).].

In the list of references, unpublished work, accepted papers in press and personal communications should be clearly distinguished.

Even if a reference contains more than two authors, the names of all the authors with their respective initials should be given. The abbreviations *et al.*, *idem* and *ibid* should be avoided.

Reference to a book should include details in the following order: names and initials of authors, the title of the book (underlined), name of publisher and place of publication within circular brackets and year [e.g. Herzberg, G, *Spectra of diatomic molecules* (D Van Nostand & Co. Inc., New Jersey), 2nd Edn, 1950, 31.]. If the reference is to the work of an author published in a book by a different author or edited by a different person, the fact that it is cited from the source book should be clearly indicated [e.g. Garlick, G F J, cited in *Encyclopedia of Physics*, Vol. 26—*Light and matter* II, edited by S Flugge (Springer Verlag, Berlin), 1958, 1.].

Proceedings of conferences and symposia should be treated in the same manner as books. Reference to a paper presented at a conference, the proceedings of which are not published, should include, in the following order, names and initials of authors, title of the paper (underlined), name of the conference, place where the conference was held and date (Deekshitulu, B L. *Design and fabrication of drum scanner for picture processing*, paper presented in the Symposuim on Applied Optics, Indian Institute of Science, Bangalore, 28-30 Nov. 1974).

Reference to a thesis should include the name of the author, title of the thesis (underlined), university or institution to which it was submitted and year of submission (e.g. Chandrasekaran, K S., *Studies on crystal structure and absolute configuration of crystals*, Ph. D. thesis, Madras University, 1956).

Reference to a patent should include names of patentees, country of origin (underlined) and patent number, the organization to which the patent has been assigned within circular brackets, data of acceptance of the patent and reference to an abstracting periodical where available [Trepagnier, J H, *US Pat.* 2,463,219 (to E I du Pont de Nemours & Co.), 1 March 1949, *Chem. Abstr.*, 43 (1949). 7258.].

Abbreviations and symbols—Abbreviations used should conform to the style of the journals. The following prefixes to units of measurements may be used for expressing submultiples and multiples.

Submultiples	*Abbreviation*	*Multiples*	*Abbreviation*
Deci- ($=10^{-1}$)	deci	deca- ($=10^{1}$)	deca-
centi- ($=10^{-2}$)	c	hecto- (10^{2})	hecto
milli- (10^{-3})	m	kilo- ($=10^{3}$)	k
micro- ($=10^{-6}$)	μ	mega- ($=10^{6}$)	M
nano- ($=10^{-9}$)	n	giga- ($=10^{9}$)	G
pico- ($=10^{-12}$)	p	tera- ($=10^{12}$)	T
femto- ($=10^{-15}$)	f		
atto- ($=10^{-18}$)	at		

Frequently repeating combinations of words, e.g. electric field gradient (EFG), junction field effect transistor (JFET), stimulated Raman emission (SRE), should be abbreviated subsequently, indicating the abbreviated form in parentheses, as shown, at the place of their first occurrence,

Nomenclature—Where too many symbols are used in the text, a section entitled "Nomenclature", explaining the significance of the various symbols, may be given and placed just above the Acknowledgement section.

Acknowledgement—Acknowledgements should not be exuberant and must be made only to real assistance rendered in connection with the work reported in the paper.

Appendixes—Appendixes, typed on separate sheets, should be numbered consecutively, in Arabic numerals, in the order of their occurence in the text, and should be placed at the very end of the paper.

Printed and Published by Shri D S Sastry, Publications & Information Directorate, Council of Scientific & Industrial Research, New Delhi, at the Leipzig Press, D-52 South Extension Part I, New Delhi 110 049, India

Regd. D-(C)-540